Master's thesis

NTNU
Norwegian University of Science and Technology
Faculty of Natural Sciences
Department of Biology

Marte Opsahl Søreng

Mapping of *Zostera* Habitat in the Sublittoral Zone using Underwater Hyperspectral Imaging and Unmanned Surface Vehicle

Master's thesis in Ocean Resources
Supervisor: Geir Johnsen
Co-supervisor: Torkild Bakken, Aksel A. Mogstad, Kristoffer Gryte
May 2022

Geir Johnsen

NTNU
Kunnskap for en bedre verden

Marte Opsahl Søreng

Mapping of *Zostera* Habitat in the Sublittoral Zone using Underwater Hyperspectral Imaging and Unmanned Surface Vehicle

Master's thesis in Ocean Resources
Supervisor: Geir Johnsen
Co-supervisor: Torkild Bakken, Aksel Alstad Mogstad, Kristoffer Gryte
May 2022

Norwegian University of Science and Technology
Faculty of Natural Sciences
Department of Biology

NTNU
Norwegian University of
Science and Technology

Abstract

Seagrass meadows around the world are threatened by anthropogenic activity, causing habitat destruction and global warming. There is a need for better high-resolution mapping to increase monitoring abilities and fill knowledge gaps regarding these vulnerable shallow coastal ecosystems. In this study, an underwater hyperspectral imager (UHI) was deployed by an unmanned surface vehicle (USV) to map spatial and seasonal distribution of marine vegetation (seagrass and macroalgae) in a *Zostera* (eelgrass) habitat in Hopavågen, a semi-enclosed bay in Agdenes, Norway. The UHI enables species-specific identification based on characteristic pigment composition of the organism of interest (OOI), resulting in a spectral reflectance curve (i.e. optical signature) detected by the sensor, and obtained in each image pixel with spatial resolution of 1 cm^2 and spectral resolution of 2.2 nm. Three transect lines from September, December and February were recorded with an altitude of ~1.6 m above the area of interest on the seafloor.

After the georeferencing, radiometric processing and radiance conversion of the UHI data, the marine vegetation was identified using the supervised classification algorithm Support Vector Machine (SVM) in order to create distribution maps and estimate percent areal coverage of the OOIs. Additionally, the SVM-classifier was compared to Band Ratio and Decision Tree classifications. The efficiency and reliability of this mapping technique were assessed by looking at the classification accuracy, time use and the ability to revisit the same location. Since turf algae (filamentous epiphytic algae) is a major threat to seagrass health and grows rapidly due to eutrophication, the study also investigated the potential for detection and quantification of turf algae growth, but further work is needed to separate specific brown macroalgae species with confidence.

The SVM classification successfully separated seagrass from macroalgae, but performed differently according to the pre-processing and quality of the UHI data. Downwelling spectral irradiance and inherent optical properties of the seawater play an essential role in the signal-to-noise ratio, influencing correct classification. Thus, the Band Ratio classification is considered to be the most reliable and time efficient classifier for seagrass mapping in different seasons, under the conditions outlined by this thesis, using the characteristic reflectance maximum at 550 nm and reflectance minimum at 665 nm to extract information of the distribution of photosynthesizing biomass absorbing wavelengths corresponding to Chlorophyll *a* and *b*. However, withered seagrass was found to have a similar optical signature as brown algae, and this must be kept in mind when interpreting the classification results. Turf algae of small sizes were also difficult to classify with confidence.

By demonstrating USV-based UHI mapping, the study is a contribution to establish and validate different methods for acquiring and translating UHI data into ecologically important information, which can be applied to seagrass research and aid ecosystem management and conservation in the upcoming years.

Sammendrag

Sjøgressenger over hele verden trues av menneskeskapte habitatødeleggelser og global oppvarming. Det er et behov for kartlegging med høy oppløsning for å øke overvåkningsevnene våre og fylle kunnskapshull knyttet til disse sårbare og grunne kystøkosystemene. I denne studien blir en undervanns-hyperspektral avbilder (UHI) båret av et ubemannet overflatefartøy (USV) for å kartlegge sesongvariasjoner av romlig fordeling av marin vegetasjon (sjøgress og makroalger) i et *Zostera* habitat i Hopavågen, en nesten lukket våg i Agdenes, Norge. UHI-en muliggjør en artsspesifikk identifisering basert på den karakteristiske pigmentsammensetningen til en organisme av interesse (OOI). Dette innebærer at en spektral reflektanskurve (også kalt optisk signatur) blir registrert av sensoren og tilegnet hver bildepiksel med en rommlig oppløsning på 1 cm^2, og en spektral oppløsning på 2.2 nm. Tre transektlinjer fra september, desember og februar ble kjørt med UHI-en ~1.6 m over området av interesse på havbunnen.

Etter georeferering, radiometrisk prosessering og radians-konvertering av UHI-dataen, ble den marine vegetasjonen identifisert ved hjelp av Support Vector Machine (SVM), som er en veiledet klassifiseringsalgoritme. På denne måten ble utbredelseskart over OOIene lagd og dekningsgrad i prosent ble beregnet. I tillegg ble SVM-klassifiseringen sammenlignet med Band Ratio- og Decision Tree-klassifiseringer. Effektiviteten og påliteligheten til denne kartleggingsteknikken ble vurdert ved hjelp av klassifiseringsnøyaktigheten, tidsbruk og evnen til å gjenbesøke samme område. Trådalger (trådlignende epifyttiske alger) er en stor trussel mot sjøgresshelse og vokser raskt hvis det er eutrofiering i et område. Derfor undersøkte denne studien også potensialet for å oppdage og kvantifisere trådalgevekst, men mer arbeid trengs for å kunne separere brune makroalgearter med sikkerhet.

SVM-klassifiseringen klarte å skille sjøgress fra makroalger, men i varierende grad avhengig av pre-prosesseringen og kvaliteten til UHI-dataen. Innfallende spektral irradians (innstrålingstetthet) og sjøvannets iboende optiske egenskaper spiller en essensiell rolle i signal-til-støy-forholdet i dataen, og påvirker korrekt klassifisering. På grunn av dette blir Band Ratio-klassifiseringen vurdert som den mest pålitelige og tidseffektive klassifiseringsalgoritmen for sjøgresskartlegging i ulike sesonger, gitt forholdene som var til stede her. Ved å bruke det karakteristiske reflektansmaksimumet ved 550 nm og reflektansminimumet ved 665 nm var det mulig å trekke ut informasjon om fordelingen av fotosyntetiserende biomasse som absorberer bølgelengder av lys som sammenfaller med klorofyll *a* og *b*. Vissent sjøgress hadde lignende optisk signatur som brunalger, og dette må tas høyde for under tolkning av klassifiseringsresultatene. Små trådalger var også vanskelig å klassifisere med sikkerhet.

Ved å demonstrere USV-UHI-basert kartlegging er studien et bidrag til å etablere og validere ulike metoder for å samle og ekstrahere viktig økologisk informasjon fra UHI-data. Denne informasjonen kan videre brukes i sjøgressforskningen og være nyttig for økosystemforvaltning og konservering de neste årene.

Preface and Acknowledgements

Ongoing rapid technological development is important for addressing and solving challenges the environment is facing in an era of climate change, global warming and mass extinction. In order to resolve these problems, we need to utilize technology to extract important ecological information about the world's ecosystems in an effective and accurate manner, covering large areas. Thereupon we can keep track of changes to the climate and aid policy makers in initiating good knowledge-based ecosystem management strategies and mitigation measures. We need to know what we have in order to know what to protect and decide what should be prioritized. This is one of the main objectives for environmental research.

The work for this thesis took place at the Norwegian University of Science and Technology (NTNU) between January 2021 and May 2022. Most of the work has been performed at Trondhjem Biologiske Stasjon (TBS) and Sealab, at the Department of Biology, where data analysis and writing have taken place. The fieldwork and data collection were conducted in Hopavågen, next to Sletvik field station in Agdenes, Trøndelag. This study is a part of the SeaBee infrastructure project (funded by the Norwegian Research Council) and work package 5: Drone Data Product Validation, with the focus on developing protocols for coastal habitat mapping along the Norwegian coast, including seagrass meadows and other species relevant for management purposes, like opportunistic turf algae. This thesis is funded by NTNU AMOS and SeaBee, and conducted in collaboration with Mikkel Bjerkvoll, fellow student at MSc Ocean Resources, who is looking further into hyperspectral imagery from drone compared to the USV-based underwater hyperspectral imagery acquired from the *Zostera* habitat investigated here. Thus, his thesis will be referred to in this thesis.

I would like to express my gratitude to everyone who has helped me with this thesis. The work has been dependent on many people at TBS, as it is difficult to deploy an Otter with only two hands! I especially want to send a huge thanks to my supervisor Geir Johnsen for all the support, enthusiasm, cheering and guidance through the tedious prosess of writing this master thesis. I´m glad you gave me the advice on choosing seagrass meadows, giving me the opportunity to combine technology, ecology and marine botany. I would not have been able to do this work without you.

Further, I also want to thank my co-supervisors Aksel A. Mogstad, Torkild Bakken and Kristoffer Gryte. Aksel has been my UHI mentor, teaching me everything I know about ENVI and UHI data analysis. He has a great gift of keeping things realistic and practical, very useful when manouvering through many ideas and when things needs to get done. Torkild has been a great support in the writing process, allways giving good advice and thorough answers. Also, it has been valuable to have a taxonomist joining the team, providing a solid knowledge base for for the ecological topics. Last, but not least, Kristoffer has been the Otter-expert and tech-support. Without him, this thesis would not have been possible (even though he knew nothing about biology, hopefully this have changed). He is a patient teacher, and always with an idea on how to solve whatever went wrong.

A big thanks goes to my master group: Annecken Nøland, Camilla Marnor, Malin Bø Nevstad, Maren Thu and Mikkel Bjerkvoll. Without you, this process would have lacked a substantial amount of laughter, good vibes, memes, helpful discussions and data sampling.

Finally, thanks to all my friends and family supporting me though these last two years, it has been highly appreciated.

Marte Opsahl Søreng, Trondheim, May 2022

Table of Content

Abbreviations

AMOS	Centre for Autonomous Marine Operations and Systems
AOPs	Apparent optical properties
AUV	Autonomous underwater vehicle
BR	Band ratio
cDOM	Colored dissolved organic matter
Chl *a*	Chlorophyll *a*
DT	Decision Tree
$E_d(\lambda)$	Downwelling spectral irradiance
ENVI	Environment for Visualizing Images
FFR	Flat field reflectance
FOV	Field of view
GT	Ground truth
HI	Hyperspectral imager
IOPs	Inherent optical properties
LAI	Leaf area index
LiDAR	Light Detection and Ranging
$L_u(\lambda)$	Spectral upwelling radiance
NTNU	Norwegian University of Science and Technology
OOI	Object of interest
PAR	Photosynthetically active radiation
$R(\lambda)$	Spectral reflectance
RBF	Radial bias function
RGB	Red, green, blue
ROV	Remotely operated vehicle
RTK-GNSS	Real-time Kinematic Global Navigation Satellite Systems
SAM	Spectral Angle Mapper
SVM	Support Vector Machine
TBS	Trondhjem Biologiske Stasjon
TSM	Total suspended matter
UHI	Underwater hyperspectral imager
USV	Unmanned surface vehicle

1 Introduction

1.1 Global Perspective

Coastal areas are hotspots for human settlement, and many of the largest cities in the world are located on the coast (Kummu *et al.*, 2016). Human population growth increases land use and the pressure on coastal habitats like mangrove forests, kelp forests, coral reefs, salt marshes and seagrass meadows (Orth *et al.*, 2006; Gumusay *et al.*, 2019). Shallow coastal ecosystems contribute greatly to mitigating global warming. More than 50% of carbon stored in the ocean is sequestered by ecosystems with rooted vegetation in the coastal zone, also called blue carbon ecosystems (IPCC, 2022), but they only account for 0.5% of total ocean area, making them the most efficient carbon sinks in the ocean (UNEP, 2009). Unfortunately, blue carbon ecosystems have an estimated reduction rate of 2-7% per year, and 14% of all seagrass species have elevated extinction risk, with three species being endangered (*Phyllospadix japonicus, Zostera chilensis* and *Zostera geojeensis*) (Short *et al.*, 2011; UNEP, 2009). Habitat destruction from anthropogenic activity in terms of pollution, physical disturbance, and rising seawater temperature due to global warming are only some of the threats these coastal habitats are facing (Orth *et al.*, 2006; Grech *et al.*, 2012; Hori, Bayne and Kuwae, 2019; Short *et al.*, 2011; Han and Liu, 2014; Erftemeijer and Robin Lewis III, 2006; Moore and Short, 2006).

Seagrass meadows are a shallow coastal water ecosystem consisting of salt tolerant monocotyledons (flowering plants; Green and Short, 2003; Unsworth *et al.*, 2019; Unsworth *et al.*, 2018) belonging to the phylum Tracheophyta (WoRMS, 2022). They have a good anchoring system consisting of roots and rhizomes, hydrophile pollination and characters aiding dispersal in the marine environment (Ackerman, 2006). In total, there exist six families, 13 genera and 63 species (Green and Short, 2003; Kuo and den Hartog, 2006), with a global distribution estimated to cover ~165 000 m^2 (Jayathilake and Costello, 2018; McKenzie *et al.*, 2020) and are important biogeochemical and structural components of coastal ecosystems (Hemminga and Duarte, 2000). The highest seagrass diversity is located in Indonesia, see Figure 1.1. Seagrass extent range from mean sea level down to 90 m, limited by the water attenuation coefficient (Duarte, 1991), defined as the sum of absorption and scattering of light as it passes the water column (Cohen *et al.*, 2020).

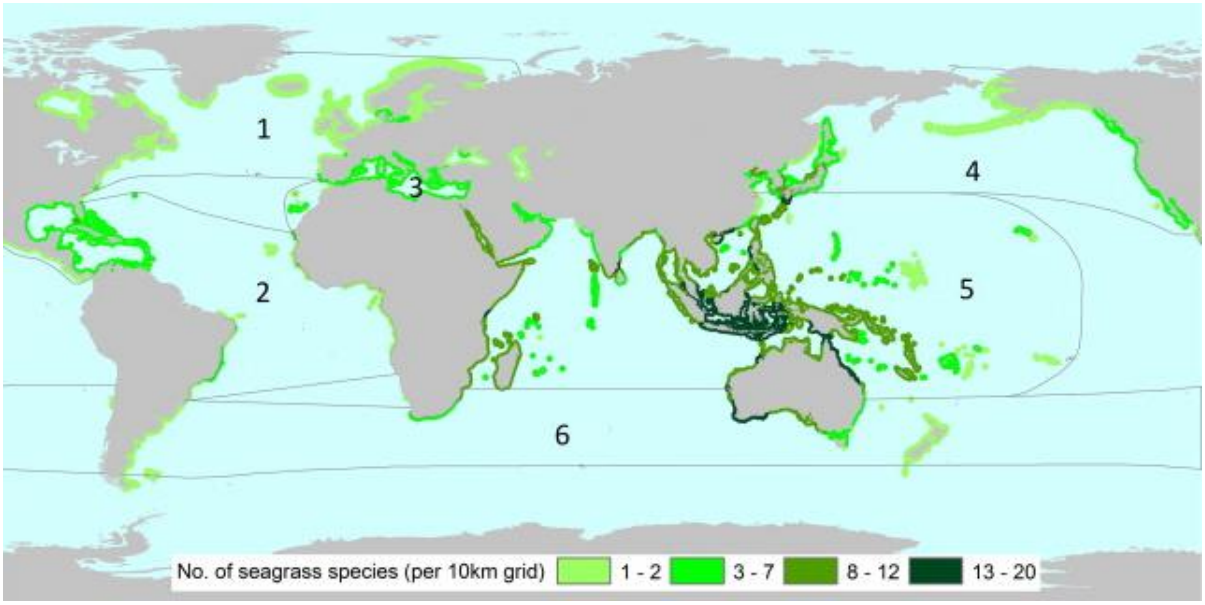

Figure 1.1: Estimation of global distribution of seagrass and species diversity. Light green color represents lowest number of species recorded, and dark green represents the highest number. Geographic bioregions: 1. Temperate North Atlantic, 2. Tropical Atlantic, 3. Mediterranean, 4. Temperate North Pacific, 5. Tropical Indo-Pacific, 6. Temperate Southern Oceans (Short *et al.*, 2007). Illustration: Short *et al.* (2011).

1.2 Zosteraceae - Eelgrass

The most species rich seagrass family is Zosteraceae, where *Zostera marina* Linnaeus, 1753 is the most abundant species in Europe and Norway (Moore and Short, 2006; Short *et al.*, 2007; Lid *et al.*, 2005). *Zostera* species are characterized as plants without visible upright stem but have strap-shaped leaves emerging from the rhizome nodes (Lid *et al.*, 2005; Kuo and den Hartog, 2006). *Zostera* can have two lifecycles (Figure 1.2), the annual is dominated by flower and seed production (sexual reproduction), and the perennial is dominated by vegetative propagation (asexual reproduction) (Hori, Bayne and Kuwae, 2019; Ackerman, 2006). The annual life cycle is believed to dominate in harsh environment and the perennial cycle in suitable environments (Hemminga and Duarte, 2000), e.g. in the littoral and sublittoral zone, respectively (Kuo and den Hartog, 2006).

Zostera marina, Zostera angustifolia (Hornemann) Reichenbach, 1845 and the more uncommon *Zostera noltei* Hornemann, 1832 grow along the Norwegian coast (Lid *et al.*, 2005; Moore and Short, 2006). *Zostera noltei* has status as Endangered due to a limited geographical distribution in Norway (Solstad *et al.*, 2021). *Z. marina* has (3)5-9(11) veins, grows from 0-10 m depth, 3-12 mm wide leaves, seeds are 3-4 mm long and a stigma-to-style ratio of 2:1. *Z. angustifolia* has 3-5 veins, 1-3 mm wide leaves, 15-40 cm long, emarginated leaf apex and a stigma-to-style ratio ~1:1. *Z. noltei* has 0.5-1.5 mm wide leaves, 1 longitudinal vein with emarginated leaf apex, up to 5-20 cm long leaves and seeds 1.5-2 mm long (Moore and Short, 2006; Lid *et al.*, 2005). The morphology varies greatly according to sediment type, temperature, location, light and nutrient availability, tides and wave regimes (Moore and Short, 2006). Typically, an increase of leaf width, length and above-to-belowground biomass with depth is seen. There is an ongoing debate whether *Z. angustifolia* is a distinct species or a morphological adaptation of *Z. marina* to the environment (D'Avack *et al.*, 2019). Olsen *et al.* (2013) found no microsatellite loci that separate them, in agreement with Coyer et. al (2013) that found no genetic differences between the *Z. angustifolia* ecotype and *Z. marina*. *Zostera angustifolia* is not accepted as

a taxonomic name, and is still regarded a synonym of *Zostera marina* (Guiry and Guiry, 2022). Nevertheless, *Zostera angustifolia* is referred to as a species by the Norwegian Biodiversity Information Centre to date. Depending on environmental factors influencing the development of characteristic traits, correct identification of the specimen is difficult.

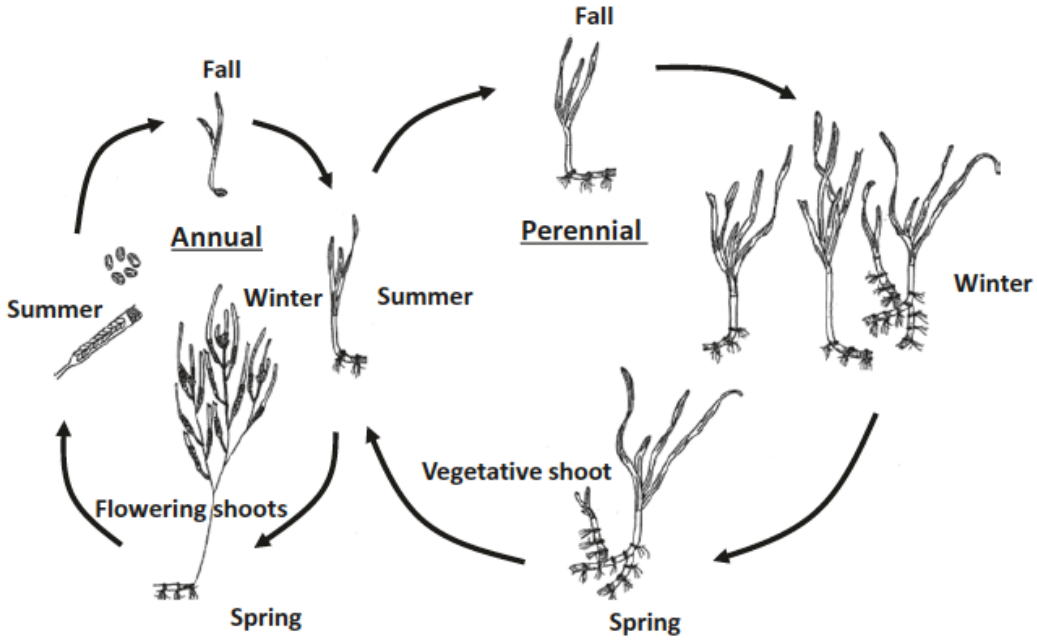

Figure 1.2: The life cycles of eelgrass (*Zostera marina* L.), with the annual life cycle to the left with flower production and perennial life cycle to the right dominated by vegetative growth. Reprinted from Hori, Bayne and Kuwae, (2019).

As a marine aquatic plant, *Zostera* needs to be able to photosynthesize and grow submerged under water (Moore and Short, 2006). Light measurements are often reported as "photosynthetically active radiation" ranging from 400-700 nm (E_{PAR}), i.e. the visible spectral range. Light intensity is usually measured as irradiance (E) or radiance (L), referring to photons received or emitted per unit area, respectively (Cohen *et al.*, 2020). The photosynthesis of *Zostera* is located to chloroplasts restricted to the epidermal cells in the leaves (Larkum, Drew and Ralph, 2006; Zimmerman, 2006), and they have a high light demand, ranging from 10-37% of downwelling spectral irradiance ($E_d(\lambda)$; Zimmerman, 2006) . Eutrophication is the main contributor to seagrass decline globally, which in turn increases phytoplankton and epiphytic algae biomass that reduce water clarity and light access (Short and Coles, 2001; Orth *et al.*, 2006; Short *et al.*, 2011; Ralph *et al.*, 2006). Turf algae is a collective designation for filamentous macroalgae, belonging to the class Phaeophyceae (brown algae) and phyla Rhodophyta (red algae) and Chlorophyta (green algae), growing above the canopy of the seagrass (Han and Liu, 2014). One example is the invasive red turf alga *Lophocladia lallemandii* (Montagne) F. Schmitz, 1893 (Deudero *et al.*, 2010; Marba, Arthur and Alcoverro, 2014). Turf algae has been reported to a large extent in seagrass meadows in southern and western Norway (Gundersen *et al.*, 2018). If there is eutrophication in an area, where excess nutrients like nitrogen and phosphorus are present (Green and Short, 2003), turf algae can increase its biomass heavily and attenuate ambient sunlight so that seagrass is unable to photosynthesize sufficiently and therefore withers (Han and Liu, 2014; Burkholder, Tomasko and Touchette, 2007; Marba, Arthur and Alcoverro, 2014). This leads to a

reduction of the world's seagrass meadows. In Norway, eelgrass meadows have a total distribution of 62 km^2, but large variations in abundance is present throughout the coastline, showing no systematic trends (Gundersen *et al.*, 2018).

Seagrass meadows fuels marine biodiversity, ecosystem services and resources (Orth *et al.*, 2006; Short *et al.*, 2011; Klemas, 2016; IPCC, 2022; Nordlund *et al.*, 2016), including support for commercial fish species as an important nursing habitat (Nordlund *et al.*, 2018b; Green and Short, 2003; Hori, Bayne and Kuwae, 2019), protection of coastal erosion (Ondiviela *et al.*, 2014), nutrient cycling (Marbà *et al.*, 2006; Hemminga and Duarte, 2000), sediment sequestration and CO_2-sequestration that incorporates HCO_3^- from seawater in biomass production (Orth *et al.*, 2006; Duarte, 1989; Hemminga and Duarte, 2000; Marbà *et al.*, 2006). These ecosystem functions provide services that benefit humans directly or indirectly (De Groot, Wilson and Boumans, 2002), whilst the loss of seagrass beds is a threat to the global environment and human society (Short *et al.*, 2011).

1.3 Benthic Habitat Mapping

To obtain information of benthic habitats, current methods include grab samples, sonar surveys and underwater imagery (Holte and Buhl-Mortensen, 2020; Sheehan, Stevens and Attrill, 2010; Sture *et al.*, 2018; Buhl-Mortensen *et al.*, 2015). Traditionally, RGB cameras have been used for non-invasive underwater imaging of seafloor ecosystem (Montes-Herrera *et al.*, 2021; Schoening *et al.*, 2012). There are several downsides with RGB imaging, including the propensity of being too large and time consuming data sets for efficient species identification in an area, the need for correction of the inherent optical properties (IOPs) of the seawater that reduce image quality, scale variation, image mosaicking, red channel information loss, elimination of subjective errors and time-consuming manual sampling methods (Montes-Herrera *et al.*, 2021; Schoening *et al.*, 2012; Blanchet *et al.*, 2016; Horning *et al.*, 2020). IOPs are defined as photon absorption and scattering by water molecules and particulate matter, typically consisting of colored dissolved organic matter (cDOM), total suspended matter (TSM) and phytoplankton biomass indicated as chlorophyll *a* (Chl *a*) concentration (Cohen *et al.*, 2020). On the other hand, apparent optical properties (AOPs) depend on IOPs and the ambient radiance distribution affected by sun angle (intensity and spectral composition), surface waves, rain and cloud cover (Sakshaug, Johnsen and Volent, 2009).

In recent years, new technology has been developed, enabling optical remote sensing techniques for benthic ecosystem mapping, i.e., satellites and unmanned aerial vehicles (UAVs) with RGB cameras (Duffy *et al.*, 2018), LiDAR-sensors, multi- and hyperspectral imagers (HI; Velez-Reyes *et al.*, 2006; Veettil *et al.*, 2020; Volent, Johnsen and Sigernes, 2009; Hossain and Hashim, 2019). Traditional methodology for seagrass distribution estimation includes pre-recorded grid patterns or collection of data from transects and sampling points (Short and Coles, 2001). Optical remote sensing techniques are the most applied methods for blue carbon ecosystem mapping, and Landsat time-series are most widely used for monitoring changes on larger scales (Pham *et al.*, 2019). Remote sensing imagery with high spatial resolution can improve seagrass classification accuracy and create high quality maps of species distribution (Pham *et al.*, 2019; Veettil *et al.*, 2020). By submerging the hyperspectral imager under water, the spatial resolution can be amplified from 1-4 m to 0.5 cm per pixel (Volent, Johnsen and Sigernes, 2007; Summers *et al.*, 2022; Klonowski, Fearns and Lynch, 2007), and reduce, for example, the challenges turbid waters have on airborne hyperspectral imagers (Vahtmäe *et al.*, 2006).

1.3.1 Underwater Hyperspectral Imagery

An underwater hyperspectral imager (UHI) is a push-broom sensor which records one pixel row at the time and renders a transect image in the across-track direction of the sensor (Johnsen *et al.*, 2020). Each pixel contains optical information channels (wavelengths) ranging from 380-800 nm, with a maximum of 0.5 nm spectral resolution, and records the upwelling spectral radiance ($L_u(\lambda)$) from an object of interest (OOI) on the seafloor with a maximum of 0.5 cm spatial resolution (Johnsen *et al.*, 2013; Summers *et al.*, 2022). This demands ample amounts of radiance sent back from the object (spectral reflectance) to the sensor in order to obtain a good signal-to-noise (dark current) ratio (Montes-Herrera *et al.*, 2021). The $L_u(\lambda)$ are influenced by back-scattering from the bottom substrate, water column and surface reflectance (Mutanga, Adam and Cho, 2012). An active sensing approach includes an external light source added to the system, in contrast to a passive approach where solar irradiance is the only light source (Montes-Herrera *et al.*, 2021). Figure 1.3 illustrates the deployment of an UHI on a sensor carrying platform, in addition to the main components in the UHI housing. Raw UHI data quality is dependent on ample light intensity, spectral resolution of the sensor, OOIs, vehicle movement and the IOPs of the seawater, whilst influence the absorption and scattering (attenuation) of the light signal as it passes the water column (Johnsen *et al.*, 2020; Johnsen *et al.*, 2013). The water attenuates wavelengths increasingly towards the red part of the electromagnetic spectrum (>550 nm), entirely absorbed at 15m depth in clear oceanic water (Cho, Kirui and Natarajan, 2008; Kirk, 2010; Horning *et al.*, 2020). cDOM absorbs yellow light (575 nm; (Green *et al.*, 2000). Additionally, phytoplankton absorb E_{PAR} before the light reaches the seafloor due to their pigment content (Johnsen *et al.*, 2013; Hurd *et al.*, 2014).

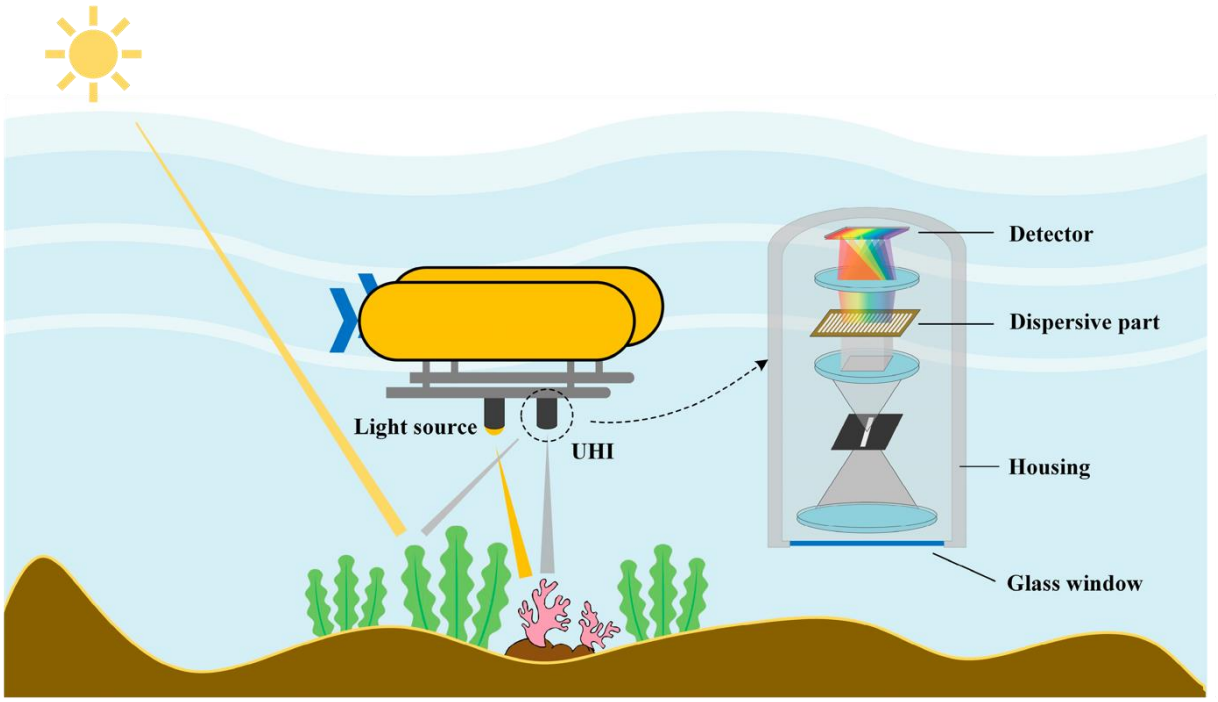

Figure 1.3: An overview of an underwater hyperspectral imager (UHI) deployed on a sensor carrying platform. The reflected optical signal from the object of interest passes a glass window in the UHI housing, then a narrow slit where the signal is spread by a spectral splitter (often a prism or grating) before detection by a detector (Liu *et al.*, 2020). An active sensing approach uses an artificial light source, and a passive sensing approach utilizes only the ambient light from the sun. Modified from Liu *et al.* (2020).

The UHI provides a great magnification of spectral information (e.g. R(λ) of 300 discrete wavelengths per image pixel) compared to traditional RGB cameras, which only use three broad information channels; Red, Green and Blue illustrated in Figure 1.4 (Johnsen *et al.*, 2013; Johnsen *et al.*, 2020). This enables detection of small differences in intensity of reflected wavelengths, which comprise a spectral reflectance curve (optical signature) from the OOIs (Pettersen *et al.*, 2014). The aforementioned differences are a result of characteristic optical properties of the OOI, which in a biological context is related to species-, group- or class-specific composition of pigments, chromophores and optical structures (Chennu *et al.*, 2017). The relative spectral reflectance (R(λ); 0-1, where 1 equals 100% reflection) at a given wavelength can be calculated by equation 1.1 (Johnsen *et al.*, 2013).

$$\mathrm{R}(\lambda) = \frac{L_d(\lambda)}{E_d(\lambda)} \qquad 1.1$$

Relative reflectance is usually the parameter utilized in hyperspectral data analyses for qualitative and quantitative mapping. Hence, UHI can be used as a bio-optical taxonomic tool, where spectral reflectance of an organism is the inverse of pigment absorption spectra (Pettersen *et al.*, 2014; Volent, Johnsen and Sigernes, 2009; Dumke *et al.*, 2018b). This enables the creation of quantitative and qualitative maps of benthic habitats (Johnsen *et al.*, 2013). UHI technology has been demonstrated in creating biogeochemical maps of seafloor properties and sulphide exploration (Johnsen *et al.*, 2013; Sture, Snook and Ludvigsen, 2019), underwater habitat mapping (Foglini *et al.*, 2018; Foglini *et al.*, 2019; Dumke *et al.*, 2018b), mapping of coral health (Letnes *et al.*, 2019), detection of sealice in aquaculture (Pettersen *et al.*, 2019), and marine archeology (Mogstad *et al.*, 2020).

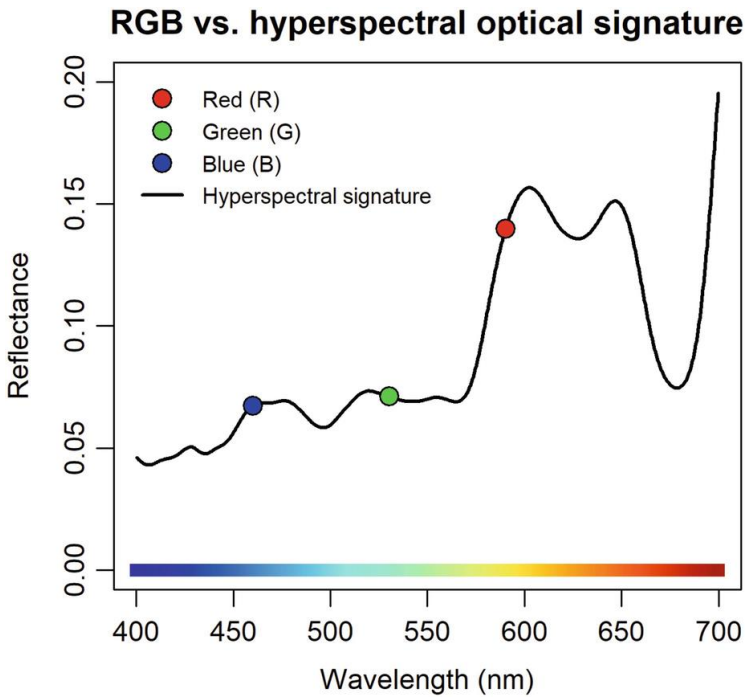

Figure 1.4: The optical signature of a red coralline algae represented using RGB (colored dots) and hyperspectral wavelengths (contiguous black line), which is the output from one digital camera pixel and one underwater hyperspectral imager pixel with 0.5 nm spectral resolution, respectively. Reprinted from Johnsen *et al.* (2020).

The UHI can be carried by numerous platforms, e.g. Diver-operated unit (Chennu *et al.*, 2017), electric rail (Chennu *et al.*, 2013; Cimoli *et al.*, 2017; Johnsen *et al.*, 2013), under-ice sled (Cimoli *et al.*, 2019), fixed stationary platform (Dumke *et al.*, 2019), remotely operated vehicle (ROV; Johnsen *et al.*, 2016), autonomous underwater vehicle (AUV; Sture *et al.*, 2017; Johnsen *et al.*, 2013); Johnsen *et al.,* 2013) and unmanned surface vehicle (USV; Mogstad, Johnsen and Ludvigsen, 2019). An USV is an autonomous sensor carrying platform with a wide range of applications (Sørensen *et al.*, 2020; Specht, Switalski and Specht, 2017; Pieterkosky *et al.*, 2017; Gu *et al.*, 2018), including possibilities for seagrass habitat mapping. USV-based UHI enables mapping of shallow water ecosystems unavailable for ROVs, AUVs and diver operated HI, within an optimal depth range of 1-2m (Mogstad, Johnsen and Ludvigsen, 2019; Chennu *et al.*, 2017; Sørensen *et al.*, 2020). This is a non-intrusive mapping method that makes *in situ* species identification and simultaneous georeferencing possible when the receiver is above sea surface (Mogstad, Johnsen and Ludvigsen, 2019).

1.3.2 Hyperspectral Image Analysis for Seagrass Mapping

Machine learning techniques are useful for hyperspectral image analysis, e.g. Gausian models, support vector machine (SVM) and clustering algorithms (Bioucas-Dias *et al.*, 2013; Gewali, Monteiro and Saber, 2018; Johnsen *et al.*, 2013). This eases the UHI data analysis and makes species detection and creation of distribution maps faster and more objective (Johnsen *et al.*, 2020; Klemas, 2016). Machine learning can automatically learn the relationship between the wanted information and the reflectance curve, whilst being little affected by noise from the spectral and ground truth data (Gewali, Monteiro and Saber, 2018). There exist several kernels for SVM (ways to set the decision boundary that maximize the separation margin between data belonging to different classes), but the Gaussian radial basis function kernel is the most commonly used algorithm for hyperspectral image analysis (Gewali, Monteiro and Saber, 2018; Mountrakis, Im and Ogole, 2011). Other classifiers used for mapping of marine vegetation (seagrass and macroalgae) is unmixing, spectral angle mapper (SAM), principal component analysis (PCA) and ISODATA/CLUSTER classification (Ackleson and Klemas, 1987; Alberotanza *et al.*, 2006; Pasqualini *et al.*, 2005; Pe'eri *et al.*, 2016; Peneva, Griffith and Carter, 2008).

A simple alternative to SVM pixel classification is the utilization of ratios of the reflectance obtained by the hyperspectral imager. For seagrass mapping, spectral characteristics of the leaves (mainly due to chlorophyll *a* and *b*, but also geometric orientation of leaf (Zimmerman, 2006) can be used to create normalized vegetation indices (NDVI; Tucker, 1979) incorporating several wavebands (including infrared wavelengths > 700 nm) using airborne HI (Peñuelas *et al.,* 1993) or pigment specific simple ratios (PSSR) using ratios based on two absorption/reflectance centers (Bargain *et al.,* 2012) from the optical signature belonging to seagrass. For instance, 550/670 nm (Broge & Leblanc, 2000), 555/670 nm (Dierssen *et al.*, 2003), and 547/630 (Pe'eri *et al.*, 2016). Dierssen *et al.* (2003) demonstrated how this classification enabled a non-destructive quantitative measurement of leaf area index (LAI) useful for biomass and photosynthesis estimations, hence the health status of the seagrass meadows (Costa *et al.*, 2021; Klemas, 2016; Wang, 2009).

1.4 Research Objectives

Since seagrass meadows are facing a continued threat due to anthropogenic activities (Tan *et al.*, 2020), and to protect these marine ecosystems, policies that supervise effects from human activities need to be an international priority (Orth *et al.*, 2006; Gumusay *et al.*, 2019; Brown, 2019). Effective management strategies are crucial to reverse seagrass decline, restore the seagrass meadows and strengthen their fundamental position in the ecosystem (Tan *et al.*, 2020; Unsworth *et al.*, 2018), where ecological information from undisturbed ecosystems provides the foundation (Johnsen *et al.*, 2020). Currently, we lack knowledge of global seagrass ecosystem services, and the common acknowledgement of their importance is limited (Nordlund *et al.*, 2018a). More long term and frequent monitoring of seagrass meadows are essential to understand rapid changes of seagrass distribution patterns, drivers of loss, find potential restoration sites and evaluate the restoration effect (Duffy *et al.*, 2019). Remote sensing and enabling technology are ways to achieve this through species identification and high resolution maps of spatial seagrass distribution, which will provide up-to-date information on seagrass status and condition (Grech *et al.*, 2012; Gumusay *et al.*, 2019; Klemas, 2016; Unsworth *et al.*, 2018). This is important for facilitating a substantial upscaling of restoration measures to successfully conserve this valuable ecosystem and the ecological and coastal communities they support (Barrell *et al.*, 2015; Pham *et al.*, 2019; Tan *et al.*, 2020; Gumusay *et al.*, 2019).

The literature shows great promise of UHI as a non-intrusive and cost-efficient method to map benthic ecosystems and estimate biomass (Liu *et al.*, 2020; Mogstad, Johnsen and Ludvigsen, 2019; Summers *et al.*, 2022; Johnsen *et al.*, 2013) but this has not been tested thoroughly and in a broader scale, covering many different ecosystems and organisms (Montes-Herrera *et al.*, 2021). The main goal of this study is to map seasonal variation in a *Zostera* habitat using UHI and USV. Further, the study aims to evaluate and address challenges with USV as instrument carrier for UHI, machine learning and optical techniques for benthic habitat classification and consider the potential of this kind of survey to improve monitoring capabilities of marine ecosystems in shallow coastal waters.

To test this methodology, three hypotheses have been established: (H_1) USV-based UHI mapping is a time efficient and reliable method for mapping of seagrass distribution over a larger area. Following the assumption that the distribution map has an accuracy of ~90% using the SVM-classifier, the method is considered reliable if the resampling precision is high and match the ground truth, and time efficient if the data acquisition and analyses can be done in one day. (H_2) The UHI will not be able to detect all species found during ground truthing. It depends on spatial resolution, environmental factors and size of a given organism of interest. (H_3) The seagrass and macroalgae composition change throughout the year, and it is possible to detect changes in turf algae distribution.

2 Materials and Methods

2.1 Study Area

A perennial seagrass meadow consisting of *Zostera marina* Linnaeus, 1753 (eelgrass) is located in Hopavågen (63°35'N 9°32'E) in Agdenes, Norway (Duarte, Martínez and Barrón, 2002; Lid *et al.*, 2005). Hopavågen is connected to Trondheimsleia through a narrow channel, with water masses influenced by the Norwegian Coastal Current, has a volume of 6.66 x 10^2 m^3 (van Marion, 1996), maximum depth of 32 m and a total area of ~275 000 m^2 (Öztürk, Vadstein and Sakshaug, 2003). The seagrass has a patchy distribution on the southeastern shoreline, varying in depth (Duarte, Martínez and Barrón, 2002; Alvsvåg, 2017), illustrated in Figure 2.1. Growing in and between the eelgrass patches, macroalgae belonging to the class Phaeophyceae (brown algae), Rhodophyta (red algae) and Chlorophyta (green algae) are prominent. Especially the red calcareous algae *Lithothamnion glaciale* Kjellmann, 1883 and *Phymatolithon lenormandii* (Areschoug) W.H. Adey, 1966 are dominating, covering organisms and substrate (Mogstad, Johnsen and Ludvigsen, 2019; Alvsvåg, 2017). The area investigated is a transect line of 37 m, subsetted from the area highlighted in red in Figure 2.1, chosen according to depth criteria (1 m; Johnsen *et al.*, 2020), continuous submersion under water and high density of seagrass. Aerial photos from the Norwegian Mapping Authority (norgeibilder.no) shows the presence of seagrass here already in 1967, but the distribution has changed over the years (see Figure 4.1 in Section 4.5 for more details).

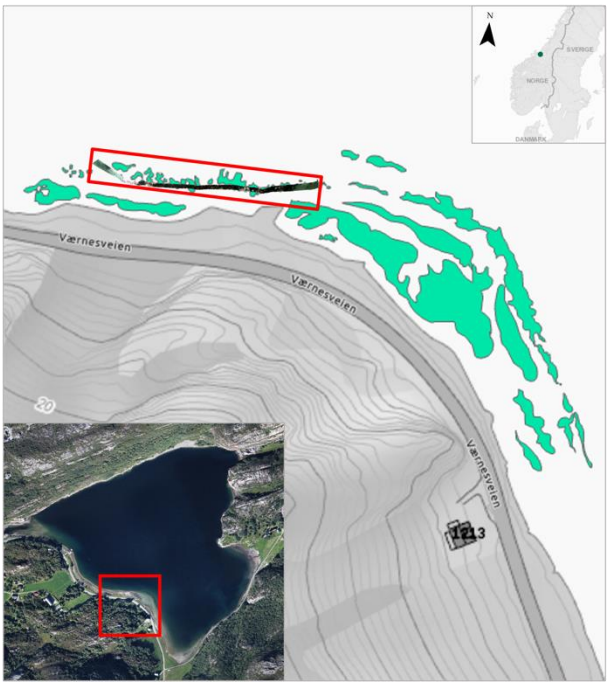

Figure 2.1: The study area at the southeastern coastline in Hopavågen (63°35'N 9°32'E), Agdenes, Norway with the *Zostera* habitat transect line (T2; September) indicated in red. The green polygons represent seagrass distribution in the area in 2015, created using ArcGIS Pro (Esri Inc., Redlands, USA). Illustration: M. Søreng, ©norgeibilder.no.

2.2 Data collection

This study is a continuation of the work and mapping technique presented by (Mogstad, Johnsen and Ludvigsen, 2019) and the underwater hyperspectral imagery acquisition, processing and classification follows (with some alterations) the steps outlined in their pilot study. Ground truthing is also an important part of USV-based UHI mapping of the seagrass habitat. UHI data validation is performed by sampling of environmental data, visual seafloor surveys comprising snorkeling and RGB imagery, sampling of organisms of interest for species identification and *in vivo* spectral reflectance measurements. The Support Vector Machine (SVM) classification accuracy is expected to be ~90% (Mogstad, Johnsen and Ludvigsen, 2019) and forms the basis for correct mapping of spatial and seasonal distribution of marine vegetation in the area of interest. Table 2.1 includes the timeline of data collection and methods used.

Table 2.1: Overview of data collection methods and dates (dd.mm.yy) of sampling. RGB includes pictures and videos from GoPro Hero 4, Hero 7 and Insta360-camera.

	In situ					***In vivo***
Date	UHI	Spectroradiometer	CTD	RGB	Grab	Spectrometer (QE Pro)
05.05.21	x	x				
06.05.21	x (T1)	x		x	x	x
07.05.21			x			
19.06.21				x		
07.09.21						x
08.09.21	x	x		x		
09.09.21	x (T2)	x	x	x		x
10.09.21					x	
08.12.21	x (T3)					
28.02.22	x (T4)					
01.03.22		x		x		
02.03.22		x				

2.2.1 *In situ* Acquisition of Underwater Hyperspectral Imagery

To obtain *in situ* hyperspectral data from the *Zostera* habitat, an underwater hyperspectral imager (UHI4, #4-11; Ecotone AS, Trondheim, Norway) was used. The UHI is a push-broom scanner recording spectral reflectance ($R(\lambda)$) from objects of interests (OOIs) with a maximum spectral resolution of 2.2 nm (spectral range: 380-800 nm, 12-bit radiometric resolution) and across-track spatial resolution of 1936 pixels. Field of view (FOV) in transverse and longitudinal direction are ~60° and ~0.4° respectively.

The UHI was deployed by an autonomous unmanned surface vehicle (USV), the Otter Pro USV #32 from Maritime Robotics AS (Trondheim, Norway), positioning the UHI in the nadir viewing position ~ 30 cm below the water surface as shown in Figure 2.2. The Otter Pro is a 200 x 108 x 81.5 cm electric twin hull USV with a run time of 20 hours. Max speed is 6 knots, and it is equipped with a custom-made geopositioning system from NTNU/Senti Systems (Trondheim, Norway). Appendix 1 contains further details. An acoustic Impact

Subsea ISA500 altimeter (Impact Subsea Ltd., Ellon, UK) was mounted to and synchronized with the UHI and provided seawater temperature and distance between the UHI and seafloor (aft of the UHI in Figure 2.2 b.).

The USV mission control was performed from a laptop (connected to the USV through Ubiquiti AirMax radio) with the software VCS (Vehicle Control Station; Maritime Robotics AS) for executing the preplanned USV mission (Figure 2.3 a.), and remote control of the UHI-build in software Immersion (Ecotone AS, Trondheim, Norway) for recording of UHI data. Waypoints was set to four steel wire frames of 50x50 cm (F1, F2, F3 and F4; Milchakova, 1999) evenly placed out in the area of interest, indicate the transect line subjected to resampling (Figure 2.3 b.). Additionally, an *in situ* spectral light beam attenuation sensor, the Viper #17SXXXXX0 from Trios (m^{-1}; Oldenburg, Germany) was also mounted on the USV for measurements of the spectral light beam attenuation coefficient for IOP information.

Figure 2.2: The Otter Pro prior to deployment at the study area in Hopavågen (a). Close up and positioning of the USV payload; Viper and UHI-4, attached by custom made metal brackets. Photo: M. Søreng.

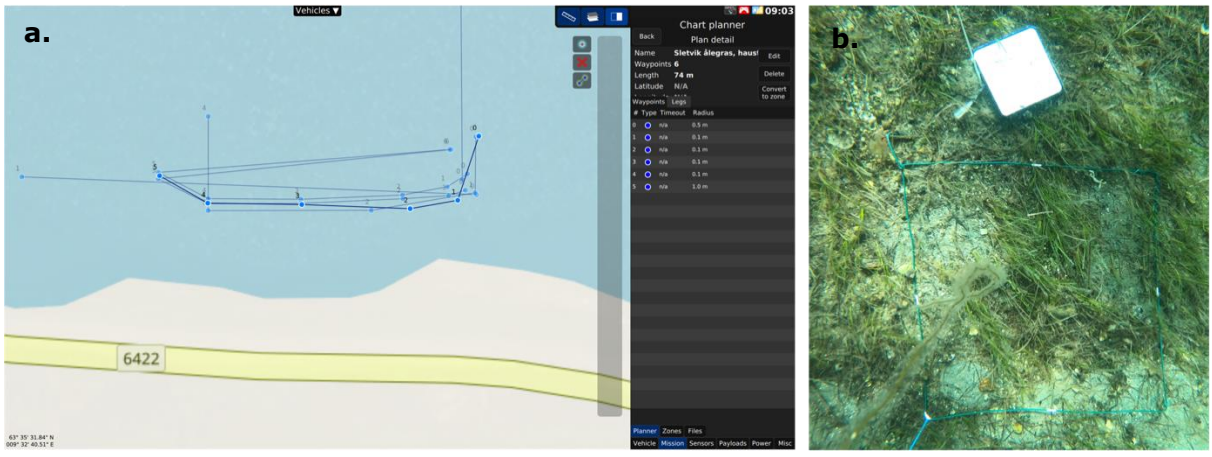

Figure 2.3: Screenshot from the Vehicle Control Station software showing the mission with predetermined waypoints (a). Frame F2 on the seafloor with the white reference plate used for correction of the inherent optical properties of seawater affecting the UHI data (06.05.2021; b). Photo: M. Søreng.

The UHI data acquisition was conducted in late spring (T1; 06.05.21), early fall (T2; 09.09.21), winter (T3; 08.12.21) and early spring (T4; 28.02.22) to obtain the seasonal variation in the *Zostera* habitat throughout the year, and metadata for the UHI recordings is found in Table 2.2. The transects were recorded at 0.5-1 knots with a survey altitude of 1-2 m, following the Norwegian standard *NS-EN 16260:2012: Water quality – Visual seabed surveys using remotely operated and/or towed observation gear for collection of environmental data*. The standard does not include USV and UHI, but this technology provides higher spatial and spectral resolution than the minimum demands for visual seabed mapping outlined by the standard and is assumed to be a valid method. Due to the area of known size, the steel wire frames also worked as spatial reference and ground truth for the UHI data, and were photographed by GoPro HERO7 and HERO4 (GoPro Inc., USA) and Insta360 camera One X2 (Insta360, California, USA). A 15x15 cm Spectralon reflectance standard (SRT-99-050; Labsphere Inc., North Sutton, USA) reflecting 99% of downwelling irradiance from 350-800 nm was placed out in the seagrass meadow next to F2 (Figure 2.3 b.) to correct for the inherent optical properties (IOPs) of the seawater and the intensity of downwelling spectral irradiance.

Table 2.2: Metadata for the UHI recordings from Hopavågen used in the analyses. Weather conditions, recording settings in Immersion, time of day, average altitude above seafloor, length of recording in minutes, sun angle, exposure and speed of Otter above ground used are included. Frame rate is 25 for all recordings.

Date	Transect	Weather	Sun angle	Time of day	Average altitude	Length [min]	Exposure	Otter speed above ground
06.05.2021	T1	Low wind, cloudy	42.63°	12:37:50	1.93 m	00:06:10	45	0.5 ktp
09.09.2021	T2	No wind or waves, cloudy	27.50°	11:14:53	1.72 m	00:06:16	35	0.5 ktp
08.12.2021	T3	Windy, strong gusts and waves, cloudy	3.72°	11:42:37	1.63 m	00:01:19	40	1 ktp
28.02.2021	T4	Cloudy, low wind, some waves and gusts	17.97°	14:26:22	1.75 m	00:03:24	40	0.5 ktp

2.2.2 Collection of Biological and Optical Information

To assess the species detection level of the UHI, two grab samples were collected in May, and one in September 2021 to supplement the work of Alvsvåg (2017), and the species found were identified. Four *Zostera marina* specimens were collected in May and again in September for epigrowth investigation and size documentation. The individuals were pressed and included in the herbarium collection TRH at the NTNU University Museum. Additionally, further examination of morphological characteristics and species abundance was provided by RGB imagery and physical samples retrieved by snorkeling.

Information about the IOPs of seawater at the time of UHI-recordings, was retrieved by a mooring with a μSPEC spectroradiometer LPTBW (In situ marine bio-optics, Perth, Australia) measuring depth and downwelling spectral irradiance (summarized to E_{PAR}; 400-700 nm; Wm^{-2} nm^{-1}), and an ECO Triplet-wB *in situ* fluorometer (WETLabs, Philomath, USA) measuring phytoplankton biomass as chlorophyll a fluorescence (Chl *a*; μg/L), colored dissolved organic matter (cDOM; ppb) and optical backscatter (proxy for total suspended matter (TSM; m^{-1})) was placed next to the area of interest (Figure 2.4). Salinity data was retrieved from a Castaway CTD profile at the center of Hopavågen in May, September and March.

Figure 2.4: The set-up of ECO Triplet sensor and the spectroradiometer at the examined seagrass meadow in Hopavågen. With the first sensor measuring the concentration of phytoplankton (Chl *a*), colored dissolved organic matter (cDOM), total suspended matter (TSM), and the latter measured depth and downwelling spectral irradiance ($E_d(\lambda)$). The sensors ran for 24 hours. Photo: G. Johnsen.

2.2.3 *In vivo* Spectral Reflectance of Collected Species in Hopavågen

A diverse selection of fauna, brown, green and red algae was collected from the southeastern shoreline in May and September 2021, and the *in vivo* spectral reflectance ($R(\lambda)$) of the organisms was measured by a QE Pro spectrometer (Ocean Insight Inc., Orlando, USA), with a HL-2000-HP high power tungsten-halogen light source (Ocean Insight Inc., Orlando, USA), a QR 400-7-VIS-BX reflection probe with optical fibers (Ocean Insight Inc., Orlando, USA) and the Ocean View software (Ocean Insight Inc, Orlando, USA), see Figure 2.5. This was done to verify $R(\lambda)$ for the OOIs *in situ*. To correct for

spectral irradiance from light source(s) the measurements were corrected for by dark current using Ocean View software, and a WS-1 reflectance standard (Ocean Insight Inc, Orlando, USA). The procedure outlined by Mogstad and Johnsen (2017) were applied, and the spectrometer measurements supplemented a reference library made by Aksel A. Mogstad (2021).

The mean spectral reflectance for each taxa of interest was calculated using R (v4.1.2, R Core Team, 2021), Rstudio (v1.1.463, Rstudio Team, 2016) and the packages *"pavo"* (Maia *et al.*, 2019) and *"readxl"* (Wickham and Bryan, 2019), using the reference library with spectral reflectance data (from 400-700 nm; n= 224) of *Zostera marina* (green tissue: n=17; withered tissue: n=8), henceforth referred to as seagrass in the UHI-analysis, and macroalgae (brown algae: n=86; red algae: n=75; green algae: n=38). Bio-optical characteristics as spectral absorption and reflectance relates further to pigment taxonomy (chemotaxonomy) and identification of different pigment types and the species-specific optical signatures (Pettersen *et al.*, 2014; Johnsen *et al.*, 2011; Volent, Johnsen and Sigernes, 2009). Pigment identification were based on literature (Mogstad and Johnsen, 2017; Johnsen, Leu and Gradinger, 2020). This was used as a ground truth for *in situ* spectral reflectance data from the USV-based UHI and for the Band Ratio classification (Dekker, Brando and Anstee, 2005; Fyfe, 2003; Summers *et al.*, 2022).

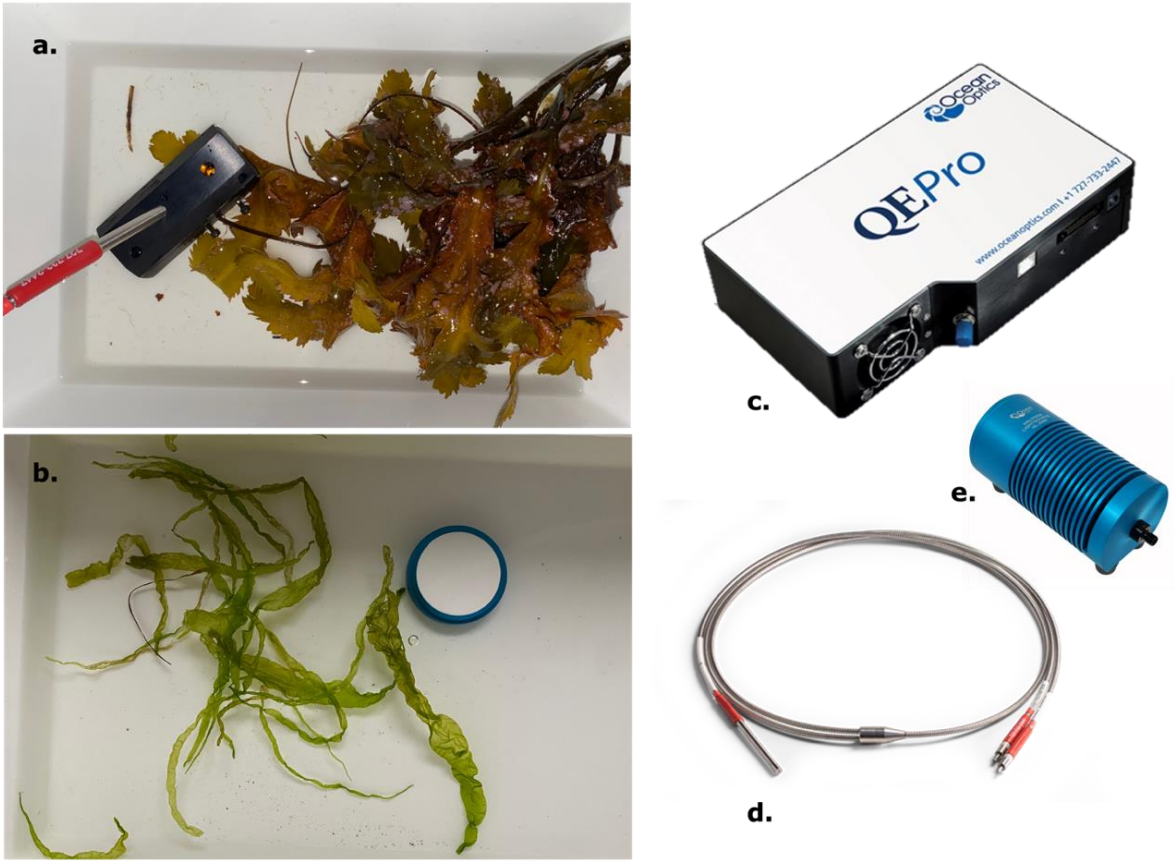

Figure 2.5: Algae specimens collected 09.09.21 from the eelgrass meadow in Hopavågen. Reflection probe with the RPH-1 probe holder (Ocean Insight Inc, Orlando, USA) measuring *Fucus serratus* (a), *Ulva intestinalis* and the WS-1 reflectance standard (b), together with the QE Pro spectrometer (c), a QR 400-7-VIS-BX reflection probe with optical fibers (d) and the HL-2000-HP high power tungsten-halogen light source from Ocean Insight Inc. I. Photo: M. Søreng, Ocean Insight (2022), *Ocean Optics Launches QE Pro Spectrometer* (2014), *Ocean-Optics-HL-2000* (2022).

2.3 UHI Data Processing

The processing of the UHI data collected in Hopavågen included georeferencing, radiometric processing and radiance conversion. By using the *Geo-correct* function in Immersion, the navigational data (latitude, longitude, pitch, roll and yaw of sensor) and altitude integrated in the HDF5 (Hierarchical Data Format) files extracted from the internal solid-state drive of the UHI, the pixels were georeferenced and put in a geospatial context. In the same processing step, raw digital counts were converted to upwelling spectral radiance ($L_u(\lambda)$; W m^2 sr^{-1} nm^{-1}) and integral noise from the sensor was removed. This resulted in a spectral resolution of 2.2 nm and spatial resolution of 1 cm. Some altimeter measurements needed correction, and this was done prior to the georeferencing by finding the mean depth before and after the outlier.

Furthermore, radiance processing was performed in ENVI (Environment for Visualizing Images, v.5.6.2; Harris Geospatial Solutions Inc., Broomfield, USA, 2021). First, the UHI data was mosaiced to one continuous raster with the *Seamless Mosaic* tool. Then a region of interest (ROI) from the reference plate was used to correct for the IOPs of the seawater by performing a flat field reflectance (FFR) correction of the data. This was achieved by the *Flat Field Correction* tool, which divide all spectra in the data set by a mean spectrum from the reference plate ROI, obtaining spectral pseudo-reflectance (post-processed reflectance from OOI). Smoothing of noisy data was performed using THOR Spectral Smoothing, which use the Savitsky-Goaly smoothing filter that removes random noise efficiently (Li, Chen and He, 2020). See Table 2.3 for the adjustable parameter used, comprising Filter Width (determines number of pixels adjacent to the data point, larger number gives smoother result), Order of Derivative (defines which derivative of the signal is smoothed, with default 0) and Degree of Smoothing Polynomial (with options 2-4, lower values produce smoother signal and introduce filter bias, and higher values reduce bias but can introduce more noise).

Table 2.3: Smoothing parameters used in THOR Spectral Smoothing tool in ENVI for noise reduction of the flat field reflectance data from T2, T3 and T4, together with key SVM parameters from found in the SVM tuning of the smoothed UHI rasters.

Smoothing parameters	**T2**	**T3**	**T4**
Filter Width	5	5	8
Order of Derivative	0	0	0
Degree of Smoothing polynomial	2	2	2
SVM tuning			
Gamma in Kernel Function	1	0.0001	0.01
Penalty Parameter	100	1 000 000	100 000

2.4 Classification of UHI Data

There are several ways to perform supervised classification of UHI data. In the experiments reported on here, two types of feature vectors were used, Spectra (490-690 nm) and Band Ratios. ENVI and the built in *Support Vector Machine* (SVM) *Classification* is used for identification of macroalgae and seagrass in the habitat. The radial bias function (RBF) kernel was chosen for the SVM, considered to be fitting for data sets with high complexity and to be a robust classifier (Melgani and Bruzzone, 2004; Wu *et al.*, 2008; Kavzoglu and Colkesen, 2009). Classification based on band ratios were implemented further in the *Decision Tree* (DT) *Classification* in ENVI, conducted as an alternative to the SVM classification.

2.4.1 Support Vector Machine Classification

The pixel classes: seagrass, red algae, brown algae, invertebrates and sediments were manually created with the *Region of Interest* function in ENVI. Each class contained 100 pixels evenly selected from the transect to get a representative training data set of spectral reflectance from the OOIs. The R(λ) data from these pixels were exported as xml-files to find the optimal settings for the SVM algorithm. The SVM tuning was done in Rstudio, using the packages *"openxlsx"* (Schauberger and Walker, 2021)*, "e1070"* (Mayer *et al.*, 2021) and *"caret"* (Kuhn, 2021)*,* and a cross-validation sampling method. The resulting *Gamma in the Kernel function* parameter (γ) sets how much one training pixel should influence the classification. A small value might lead to overfitting, while a large value might lead to over-smoothing (Mountrakis, Im and Ogole, 2011). The *Penalty parameter* (C) is the cost of misclassification, with a higher value resulting in low bias but high variance. The parameters used in the *Support Vector Machine Classifier* is found in Table 2.3.

2.4.2 Band Ratio Classification of Seagrass

The *Band Ratio* tool in ENVI was used to create a seagrass distribution map of the area of interest. Based on maximum and minimum reflectance values, and specific pigment characters for seagrass (chlorophyll *a* and *b*), a band ratio (BR) classification was executed using wavebands 549 nm and 663 nm. The algorithm is calculating the reflectance ratio between these two wavebands for every pixel, and the pixels are assigned a color on the grayscale ranging from black (lowest ratio) to white (highest ratio), according to how well the ratio match a pre-determined threshold. A threshold value of 1.28 was used with the assumption of seagrass having the highest ratio. This was repeated for transect T2, T3 and T4, and worked as a quick method to estimate how much seagrass and chlorophyll was present.

2.4.3 Decision Tree using Band Ratio

Based on the reflectance curves and group specific characters for seagrass, red algae, brown algae and invertebrates from the reference library, four band ratio classifications lead to a Seagrass Index: 549/663, Algae Index: 602/677, Red algae Index: 630/563, Brown algae Index: 645/666 and Invertebrate Index: 699/501. ROIs from the SVM training data set was used to extract pixel data from the BR classified images, which were used as input in an R-script to find DT threshold (Yes/No) using the package *"cutpointr"* (Thiele and Hirschfeld, 2021). The result is the optimum threshold for separation of the OOI compared to the other OOIs based on the band ratio data.

A DT with five nodes was created with the *New decision tree* function in ENVI, see Figure 2.6. For each node (1-5) in the decision tree, the following expressions were used; Data:

B550 GT 0, Sea_I: *B550/B665 GT 1.287*, Alg_I: *B602/B678 GT 1.177*, Inv_I: *B700/B500 GT 2.371 AND B678 GT B602* and Red_I: *B631/B564 GT 1.183*. The pixel is assigned to a class by "Yes" or "No" based on if the pixel value is above or below the threshold, respectively. Due to the spectral resolution of 2.2 nm, the closest fit to the index wavebands were chosen. Color of each node corresponds to the classification result in Figure 3.5.

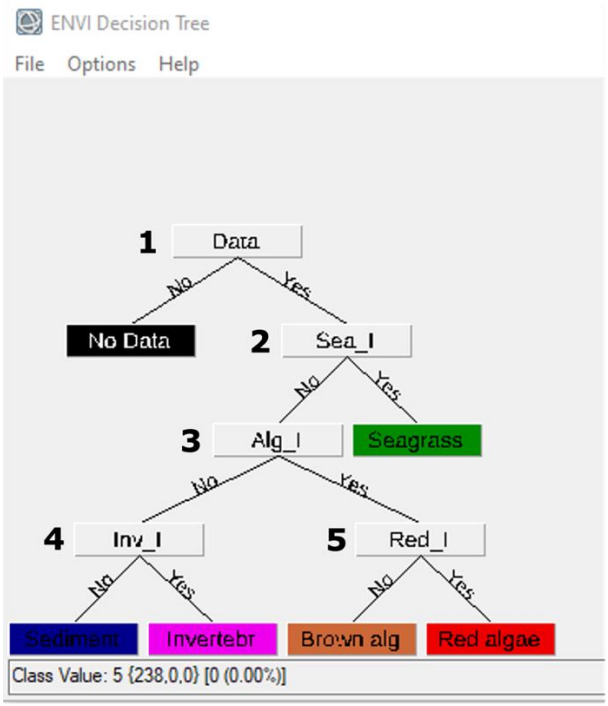

Figure 2.6: The decision tree applied in the DT classification of the UHI data. Node 1 (Data) separates data from no data, Node 2 (Sea_I) separates seagrass from other pixels, Node 3 (Alg_I) separates red and brown algae from invertebrates or sediment, Node 4 (Inv_I) separates invertebrates from sediment, and lastly, Node 5 (Red_I) separated red algae from brown algae. Screenshot from ENVI.

2.5 Estimation of Seasonal Coverage

The distribution change of marine vegetation was assessed by comparing the SVM-classified data from September, December, and February. The SVM-results were spatially compared by selecting a 4.5 m long area between two known geographic locations in each transect line (Figure 3.1), by creating an ROI using a brush size of 25 pixels and choose pixels from the corner of F2 to the tip of a recognizable stone on the seafloor in two parallel lines. These subsets were treated as equal areas, with a total pixel number of 22 500 (T2), 21 250 (T3) and 22 500 (T4). Since each pixel is 1 cm^2 and assigned to one spectral class, this was used to estimate areal coverage (%) of each OOI in the transect line. This gives a proxy for biomass. A screenshot of the T4 subset and respective pixel number for each class is given in Figure 2.7. The results from each season were compared and visually represented as a bar plot made in R using *"ggplot2"* (Wickham, 2016).

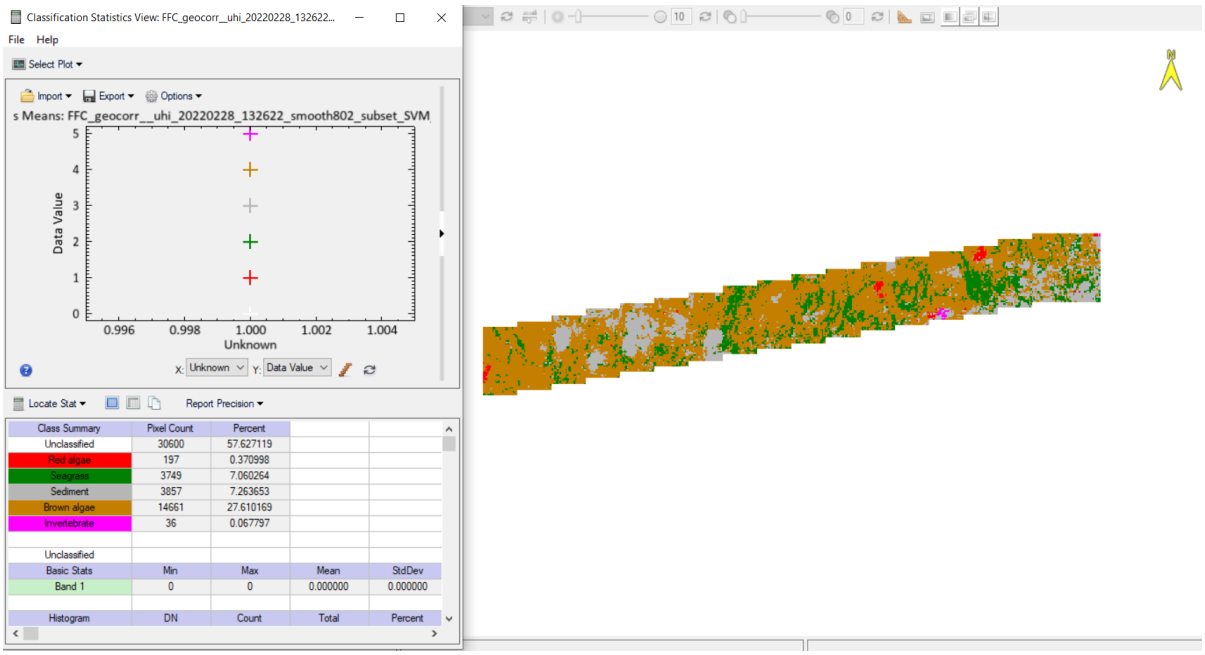

Figure 2.7: SVM classified subset from February (T4) in the Classification Statistics View in ENVI, with pixel number assigned to each spectral class (total of 22 500 pixels). This is further used to calculate pixel percentage from early spring. The Unclassified class is omitted. Screenshot from ENVI.

2.5.1 Accuracy Assessment

2.5.1.1 Algorithm accuracy

The SVM classification accuracy of FFR data is here assumed to be ~90%, according to (Mogstad, Johnsen and Ludvigsen, 2019) with similar USV-UHI based mapping procedure in Hopavågen. Here, accuracy is defined as the ability to correctly assign a pixel to its respective class, and precision is the ability is to achieve the same classification of the pixel each time. Visual ROI class annotation was performed by hand picking pixels from each class based on examination of the RGB images and *in vivo* R(λ) curves from the reference library (ground truthing/verification). An accuracy test based on comparison of a predicted pixel category against a known pixel category, as done by Chennu *et al.,* (2017), involves validation based on hand-picked pixels not used in the training data. Since this resulted in a 95.7% accuracy of their SVM classification of UHI data, here, the SVM performance is believed to be similar when the training data is based on ground truthed pixels. The RGB photomosaic was visually compared the BR and SVM result, looking for and evaluating mismatches. Finally, the DT classification accuracy was assessed by using the SVM result as a ground truth image in the function *Confusion Matrix by Ground truth Image* in ENVI.

2.5.1.2 Coverage estimation accuracy

To evaluate the precision of the areal coverage estimation from the SVM pixel classification, an analogue method with a printed RGB image of frame F2 was performed. The RGB image was the ground truth compared to the SVM classified image, using data from T2. The paper was weighed prior to cutting out identified OOI, such as brown algae, seagrass, sediment, withered seagrass and invertebrates (red algae was not found). Each paper fraction (area of OOI) was weighed, and percent was calculated, further conveyed as percent coverage of each group of interest. The SVM classified image of F2 consisted of 2351 pixels, and percent pixels in each class were calculated. Lastly, the percent error of the SVM estimation was calculated by subtracting the ground truth value from the SVM value and dividing by the ground truth value.

3 Results

3.1 *In situ* UHI data

3.1.1 Transect Lines

The three post-processed RGB photomosaic representations (Red: 641 nm, Green: 532 nm, Blue: 459 nm) of the transect lines from September (T2), December (T3) and February (T4), with corresponding subsets, are shown in Figure 3.1. The transects are variable in terms of recorded seafloor area and georeferencing precision (see Appendix 1). This is evident in the different deviation from the attitude line set by the waypoints in the Otter mission, together with shape distortion of the square reference plate. The conditions for high quality UHI data acquisition were nearly optimal in September with no wind/waves, providing a slow and steady speed above ground for the USV. The total length of the transect line is 37 m, making a total sampled area of 55.9 m^2, 57.4 m^2 and 64.8 m^2 for T2, T3 and T4, respectively. These areas were subsetted to 4.5 x 0.5 m (area in the pink rectangle), enlarged to the right in Figure 3.1. The subsets represent the same area on the seafloor, with pixel numbers T2: 22 500, T3: 21 250 and T4: 22 500, enabling a comparable percent coverage of the groups of interest in Section 3.3, and visual inspection of the seasonal variation. There are prominent turf algae in T2, which disappears in T3, together with a clear reduction of green seagrass from T2 to T4.

3.1.2 *In situ* Spectral Reflectance

Mean *in situ* spectral reflectance R(λ) curves from 490-690 nm (wavelengths outside the selected range is considered too noisy to be included in the analysis) for seagrass, red algae, brown algae, invertebrates and sediment based on 100 hand selected pixels of identified OOIs belonging to each group of interest (validated by RGB imagery and *in vivo* reflectance) are found in Figure 3.2. The standard deviation is visualized in grey, and is largest for red algae and invertebrates all seasons, but nearly non-existent for seagrass and brown algae in December and February. The light conditions in December and February were low, compared to May (see Section 3.5.5), influencing the signal-to-noise ratio and R(λ). The reflectance from the February data set was overall lower than from the other data sets, with almost overlapping seagrass and brown algae curves around 5% reflectance. The maximum reflectance peak with corresponding wavelength for each curve in each transect can be found in Table A.2 in Appendix 2. Red algae had highest reflectance each season, with a maximum of 0.256% at wavelength 603 nm in September. The values for Invertebrates reflectance determined by the limits set in the R code, at 681 nm (T2, T4) and 685 nm (T3) where the curve continues the steep incline. Otherwise, the maximum reflectance for each group of interest is consistently found at the same wavelengths, except for the invertebrate and sediment maximum in December.

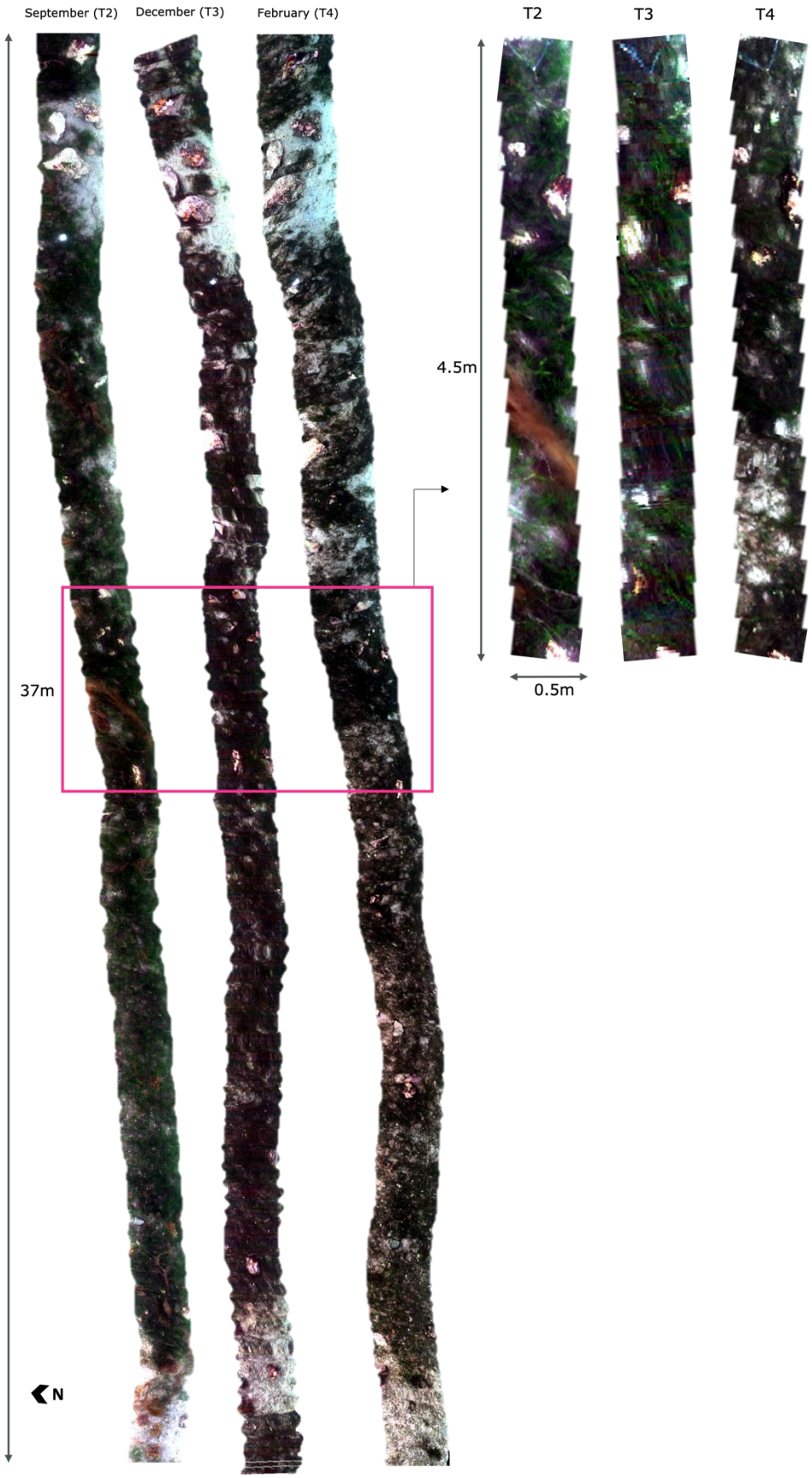

Figure 3.1: USV-UHI based RGB photomosaic representations (R: 641 nm, G: 532 nm, B: 459 nm) of total transect lines from September (T2), December (T3) and February (T4) in Hopavågen is shown to the left, and subset areas within the transects to the right, marked by a pink rectangle. The subsets are assumed to cover the same 4.5 x 0.5 m area on the seafloor.

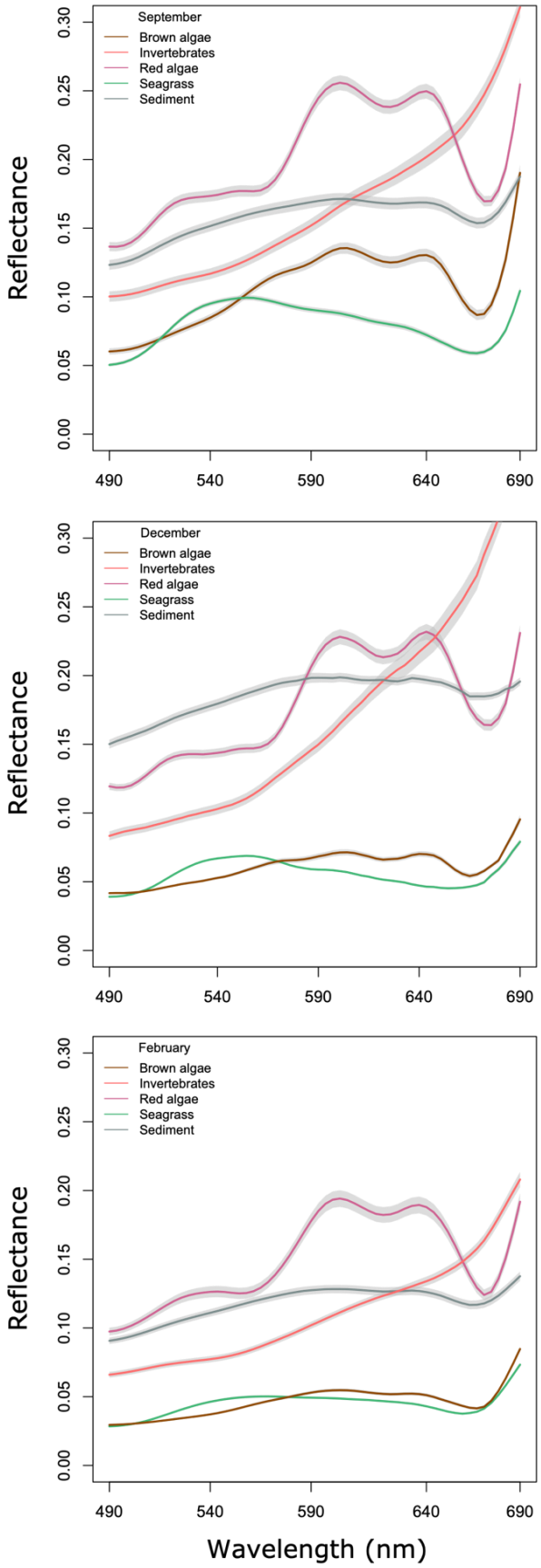

Figure 3.2: Mean spectral reflectance from USV-UHI data calculated from 100 hand-picked pixels belonging to brown algae, red algae, seagrass, invertebrates and sediment from each transect, with line color of correspondingly brown, red, green, coral and grey. The waveband interval is 490-690 nm on the x-axis, and relative reflectance on the y-axis (percent if multiplied by 100).

3.2 Classification of UHI data

The results from the SVM classifier in ENVI is shown in Figure 3.3 and Figure 3.5 (T2 only), and a change in marine vegetation is evident. Training data pixels used in the algorithm was chosen from the total transect line, thereupon the classification result was subsetted. Figure 3.3 includes a table with pixel number assigned to each spectral class (seagrass, brown algae, red algae, invertebrate and sediment) from the SVM subsets. Subset T2 contains most pixels classified as seagrass (78.15%) and T4 the least (16.66%). Brown algae had an increase from T2 to T3, followed by a slight decrease in T4. The decline in seagrass and brown algae together with an increase in classified sediment (from 3.1 to 17.14%) implies a significant reduction in biomass. The invertebrates and red algae spectral class stayed low in pixel number for each data set, which is reasonable since invertebrates in the subsets were largely constituent of sessile *Meritridium senile* on a rock (top right) in the subsets. However, the T3 result only identified 10 invertebrate pixels, but the same individuals were observed in the area.

The resulting image from the BR classification for each transect shows seagrass cover on the seafloor in the transect lines (Figure 3.4). The same band ratio (549/663 nm corresponding to reflectance maximum and minimum) is used on all UHI data sets, and the images show distinct differences in seagrass cover between the seasons. Each pixel is assigned a shade on the grayscale ranging from black to white. This depends on how close the reflectance difference at the two wavebands matches the threshold value of 1.28. Rocks are black, brown algae are grey and seagrass is white (covering 27.84 m^2 of the total T2 transect). At the beginning of T4, there is probably green algae film on the seafloor due to the homogenous white shade without prominent structure matching the pigment absorption of seagrass.

Figure 3.5 compares different UHI data analyses from September in terms of a RGB photomosaic representation of the data set, SVM classified image and DT classified image in the left panel. The SVM image shows a more homogeneous seagrass cover than the DT, which have classified more brown algae, sediment and invertebrate pixels scattered over the seagrass delimited area. (363 633 seagrass pixels and 83 399 brown algae pixels (SVM) compared to 188 713 and 214 224 (DT)). Notably, the SVM seems to classify the prominent turf algae in the middle of the transect line and match the RGB photomosaic well, while the DT classify the turf algae with less smooth and clear-cut edges. When compared to the BR classification (furthest to the right), a mix of the classification results from the SVM and DT would likely be a better representation of the actual coverage of spectral classes. The confusion matrix panel illustrates the estimated classification error of DT compared to SVM as ground truth, and this will be further explained in section 3.4.2.

3.3 Seasonal Coverage of Marine Vegetation

Based on the pixel number found by the SVM classification for each group of interest, the percent areal coverage in the transect subsets were calculated and represented in the stacked bar plot in Figure 3.3. There is a reduction in seagrass from 78.2% in T2, to 24.4% in T3 and 16.7% in T4. This coincides with visible biomass in the RGB images in Figure 3.6. The brown algae are increasing from 17.6% in T2, to 72.8% and 65.2% in T4. The amount of exposed sediments had an increase from 3.1% in September to 17.1 % in February coinciding with the above-stated biomass decline exposing the substrate underneath. As has been noted, red algae did not change considerably, in agreement with slow growth of calcareous red algae. Furthermore, seeing a negligible percent of invertebrate coverage in the subsets, this group was omitted from the bar plot.

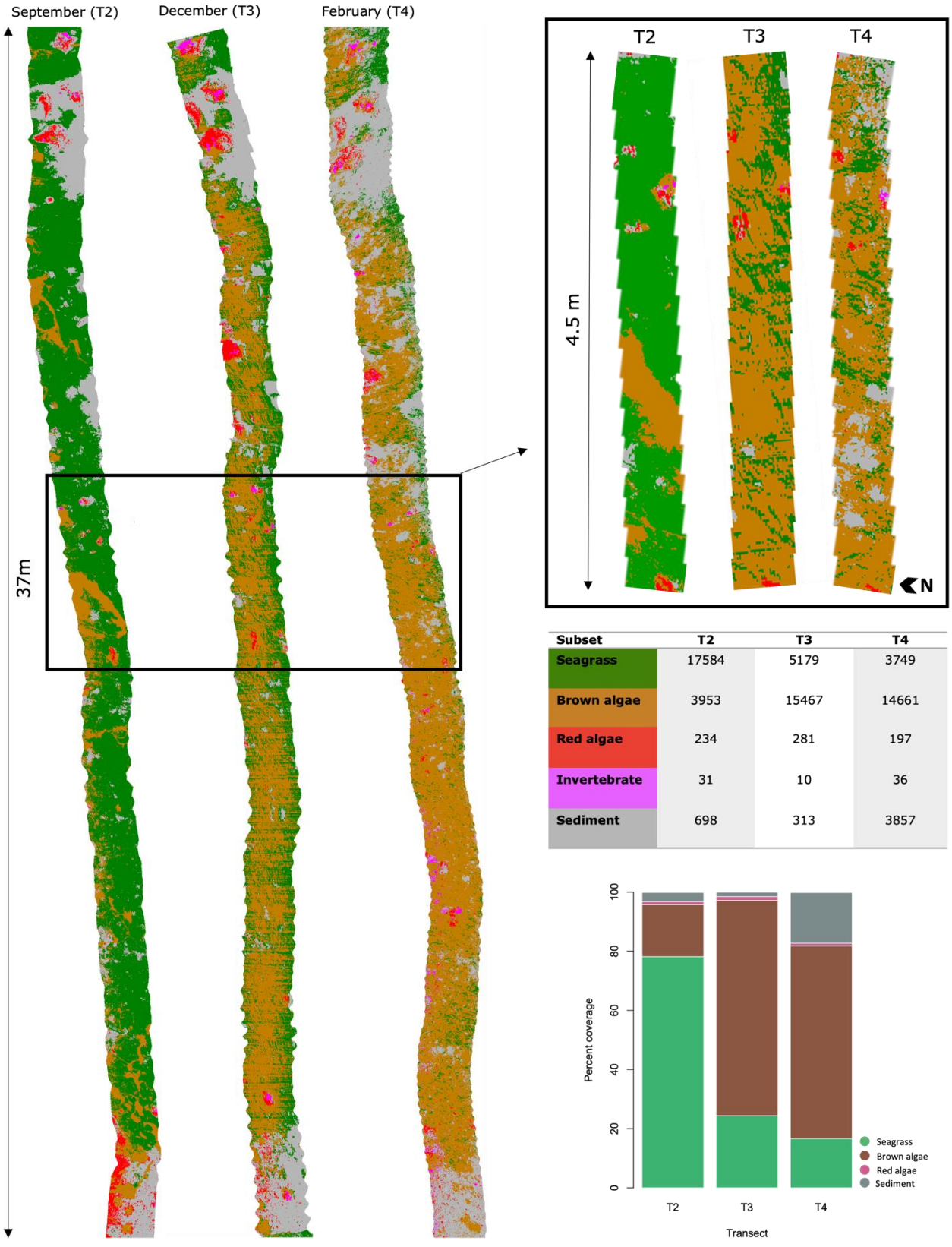

Subset	T2	T3	T4
Seagrass	17584	5179	3749
Brown algae	3953	15467	14661
Red algae	234	281	197
Invertebrate	31	10	36
Sediment	698	313	3857

Figure 3.3: Total USV-UHI transect lines from September (T2), December (T3) and February (T4) in Hopavågen classified by Support Vector Machine (SVM). The transect subsets are shown to the right, above a table with number of spectrally classified pixels (each pixel cover 1 cm^2 of the seafloor) assigned to each group of interest: seagrass, brown algae, red algae, invertebrate and sediment. The stacked bar plot shows the percent distribution of pixels in each transect subset (T2, T3 and T4) which is an estimation of percent areal coverage of each group. Data is retrieved from ENVI.

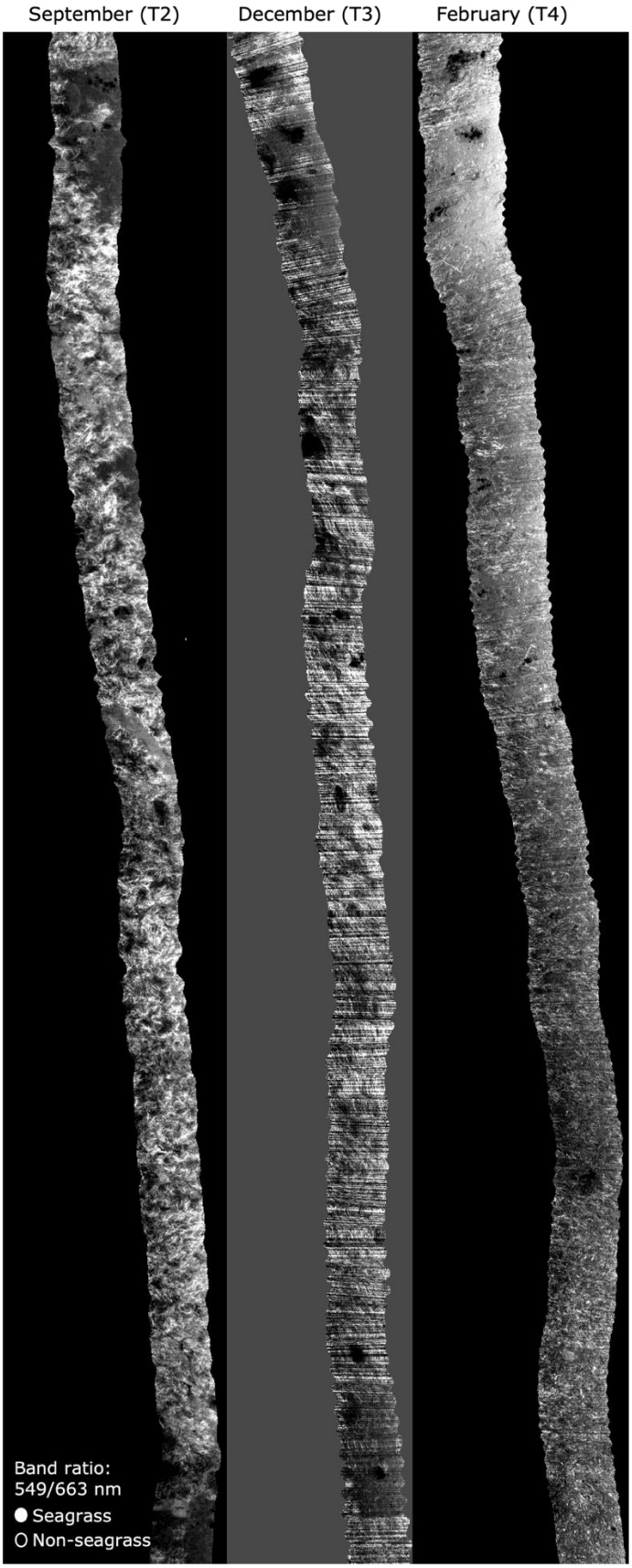

Figure 3.4: USV-UHI based photomosaics of seagrass distribution in Hopavågen. The maps are created in ENVI using the band ratio 549/663 nm on transects from September, December and February. The pixels are assigned to the black-white color gradient according to how well they match the band ratio threshold of 1.2, where the whitest pixels are the closest match and indicate seagrass.

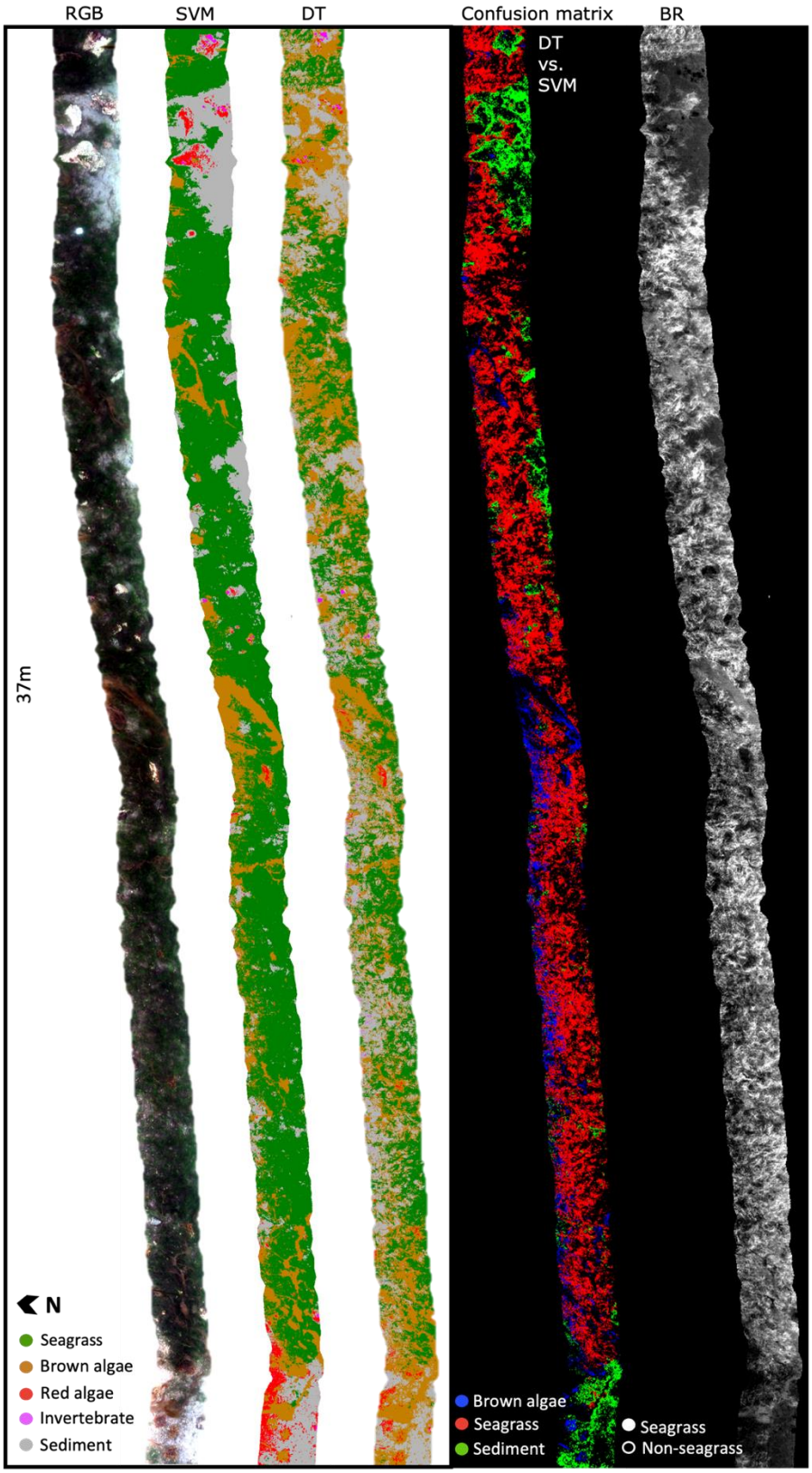

Figure 3.5: Comparison of USV-UHI based photomosaic, Support Vector Machine (SVM) and Decision Tree (DT) classification of data from September, 2021, Hopavågen. From the left: RGB photomosaic (R: 641 nm, G: 532 nm, B: 459 nm), SVM and DT classified distribution maps with five classes; seagrass, brown algae, red algae, invertebrates, and sediment. The Confusion matrix output from ENVI compares DT to the SVM results, with seagrass pixels classification error (red), brown alga error (blue) and sediment error (green), and lastly, the BR classification result (549/663 nm).

3.4 Assessment of Classification Accuracy

3.4.1 Comparison of SVM image to Ground truth RGB image

The classification and coverage estimation accuracy are given as percent error for each spectral class in Table 3.1. Figure 3.6 illustrate the SVM result of F2, and the RGB image is found in Figure 3.7 e. The calculated classification errors were 21.9% for seagrass, -77.9% for brown algae and -33.3% for sediment. This indicates a large misclassification of brown algae and sediment, where the negative sign represents underestimation of percent coverage in the frame. Further, the SVM algorithm did not identify any invertebrates or withered seagrass (not included as a spectral class), but they were identified in the ground truth. If the withered seagrass would have been included as seagrass in the ground truth, the overestimation of pixels by the SVM algorithm would be reduced, and the accuracy for seagrass classification would have been slightly improved.

Table 3.1: Percent error for each designated spectral class used in the SVM classification. The areal coverage (%) of each class identified in the ground truth image is estimated using the paper weight of each fraction divided by total weight of the RGB image of the 50 x 50 cm frame F2. Data from September (T2) is compared.

F2 from T2	Seagrass	Brown algae	Red algae	Invertebrate	Sediment	Withered seagrass
RGB (%)	70.9	4.97	-	0.224	18.9	5.19
SVM (%)	86.4	1.1	-	-	12.6	-
% Error	**21.9**	**- 77.9**	**0**	**-100**	**- 33.3**	**- 100**

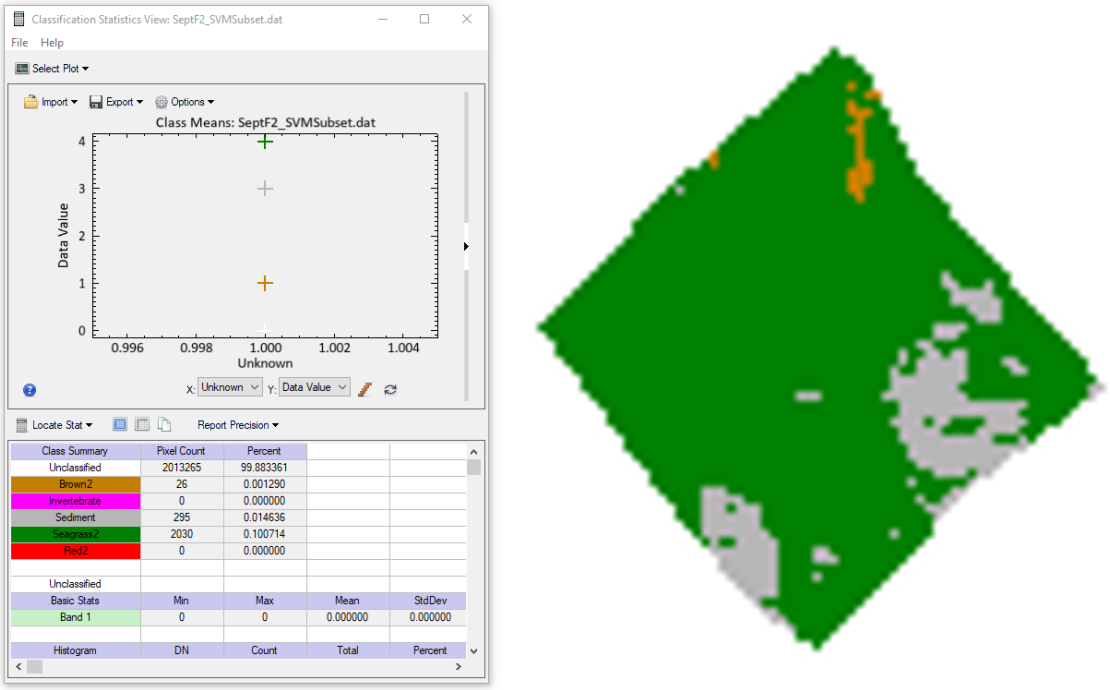

Figure 3.6: Screenshot from the Classification Statistics View in ENVI with pixel number in each class in frame F2 from September (T2; total of 2351 pixels), used further to calculate pixel percentage delimited by the frame. The Unclassified class contains pixels with no data and is omitted. The colors in the left panel corresponds to the pixel colors to the right.

3.4.2 Confusion Matrix

The output from the confusion matrix calculated in ENVI, comparing the DT classifier to the SVM classifier used on the UHI data set T2, is found in Table 3.2. The Overall Classification Accuracy is 53%, and the Kappa Coefficient is 0.3079, indicating no difference between the two classifiers and an eventual random chance. The producer accuracy (PA; total number of correctly classified pixels in a class by the DT, divided by the total pixel number belonging to the class identified by the ground truth (SVM)) is highest for invertebrates (75.94%) and lowest for red algae (11.71%). Thus, the DT and SVM were most in agreement concerning invertebrate classification, but least for red algae. The seagrass class PA was only 49.97%. However, the user accuracy (UA; total number of correctly classified seagrass pixels, divided by the total number of pixels assigned as seagrass by the DT) in the seagrass case was 96.09%, indicating that almost all pixels classified as seagrass by the DT was coinciding with the SVM. Then again, ~50% of the seagrass pixels found by the SVM were assigned to other classes by the DT. UA identifies false positives, and this is evident for brown algae with the lowest UA of 26.56%, and 157 241 pixels were wrongly assigned to this class (assuming the SVM is correct).

Table 3.2: Confusion matrix of Decision Tree (DT) classification compared to Support Vector Machine (SVM) classification of photomosaics of the UHI data set from T2 (Ground Truth).

Predicted Spectral Class	**Ground Truth (Pixels)**						**Producer Accuracy (%)**	**User Accuracy (%)**
	Seagrass	**Brown algae**	**Red algae**	**Invertebrate**	**Sediment**	**Total**		
Seagrass	181337	5823	9	0	1544	188713	49.87	96.09
Brown algae	110511	56983	9552	0	37268	214224	68.22	26.56
Red algae	0	3034	1839	0	59	4932	11.71	37.29
Invertebrate	235	527	10	830	311	1913	75.94	43.39
Sediment	71550	17122	4300	263	55430	148665	58.59	37.29
Total	363633	83399	15710	1093	94612	558447		
Overall Classification Accuracy: 53.06%, Kappa Coefficient: 0.3079*								

**For comparison: smoothed DT vs. unsmoothed SVM: Overall Classification Accuracy: 64.40%, Kappa Coefficient: 0.4703*

3.4.3 RGB images of Seafloor

A compilation of RGB camera images taken of frame F1, F2 and F3 from May (06.05.2021; GoPro Hero 7; Fig. 3.7 a-c), September (09.09.2021; GoPro Hero 4; Fig. 3.7 d-f) and March (01.03.2022; snapshots from Insta360 video; Fig. 3.7 g-i) visualize the seasonal distribution change of the OOIs, with variations in biomass and IOPs of the seawater. The *Zostera* was still growing in May, reaching its maximum length during the summer and the coverage in September was high. This contrasts with March, where the majority of *Zostera* had withered and the green leaves were short and more dispersed on the seafloor. Brown algae were also observed. The *Metridium senile* Linnaeus, 1761 on the rock in F3 where persistent, additionally, many *Ophiocomina nigra* Abildgaard, 1789 specimens inhabited the habitat in fall and early spring.

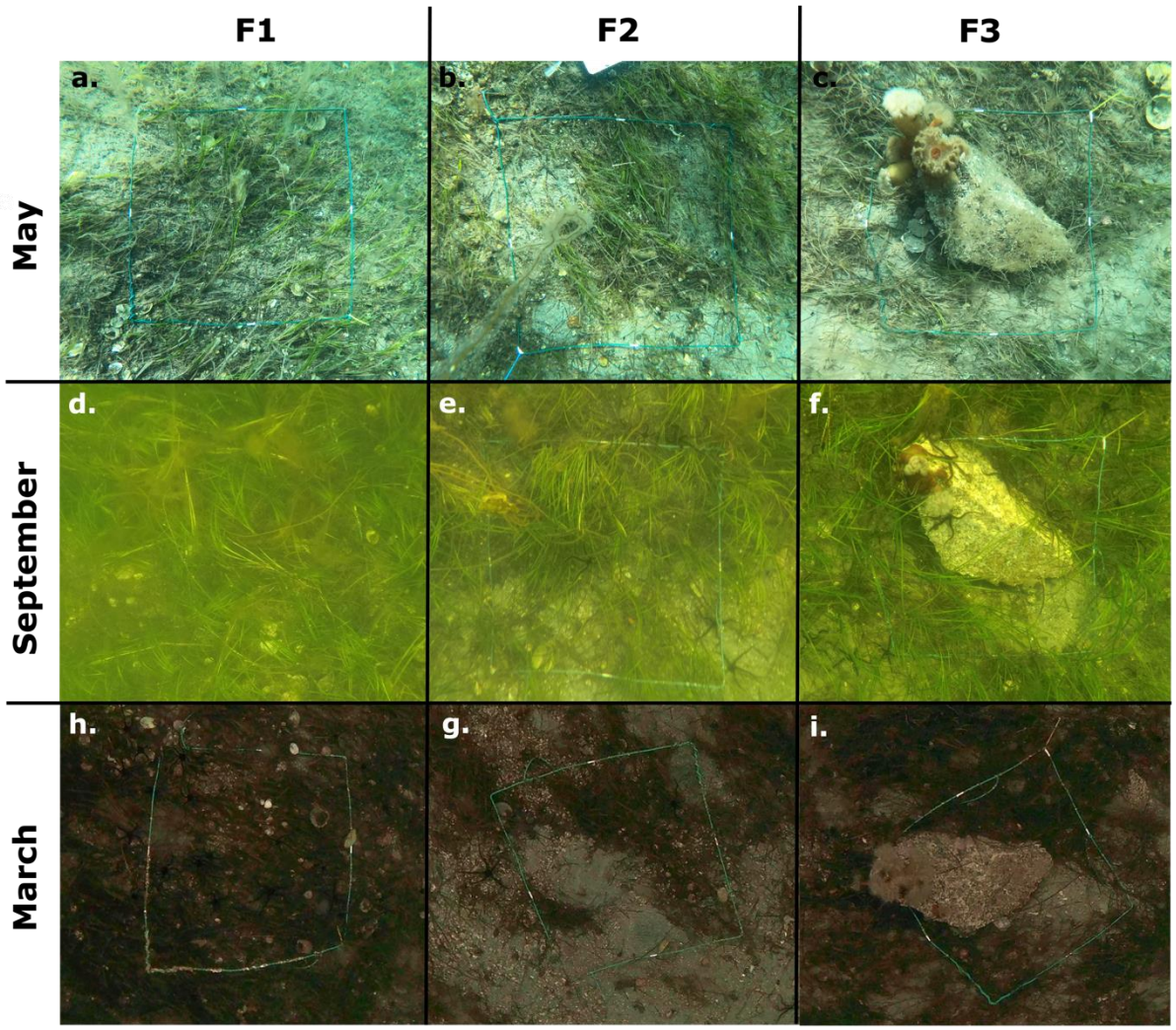

Figure 3.7: Revisited 50 x 50 cm areas on the seafloor for biomass comparison and ground truth. The first row from May (a-c; 06.05.2021), second row from September (d-f; 09.09.2021) and third row from March (g-I; 01.03.2022). Frame F1 is the first column, then F2 and F3 to the right. Photo: M. Thu, M. Bjerkvoll, G. Johnsen

3.4.4 Effects of Smoothing on *In situ* UHI data

Altogether, the differences caused by smoothing of spectral reflectance data augment uncertainties towards the classification accuracy. In the UHI data post-processing, different smoothing parameters were tested for each transect to find the best settings to reduce noise in the *in situ* R(λ) data and the effect on SVM classification accuracy. As shown in Figure 3.8, there is an overestimation of brown algae in the unsmoothed transect compared to the photomosaic and the transect processed with Filter Width setting 5. The latter are the final settings used in the UHI-analysis (see Table 2.3). The unsmoothed classified image was run with SVM settings; Gamma in Kernel Function: 1, Penalty Parameter: 1000. The seagrass class was also consisting of more pixels in the smoothed data compared to unsmoothed. Lastly, when the unsmoothed SVM was compared to DT, the overall accuracy was higher (64.40%), and had a Kappa coefficient of 0.4703.

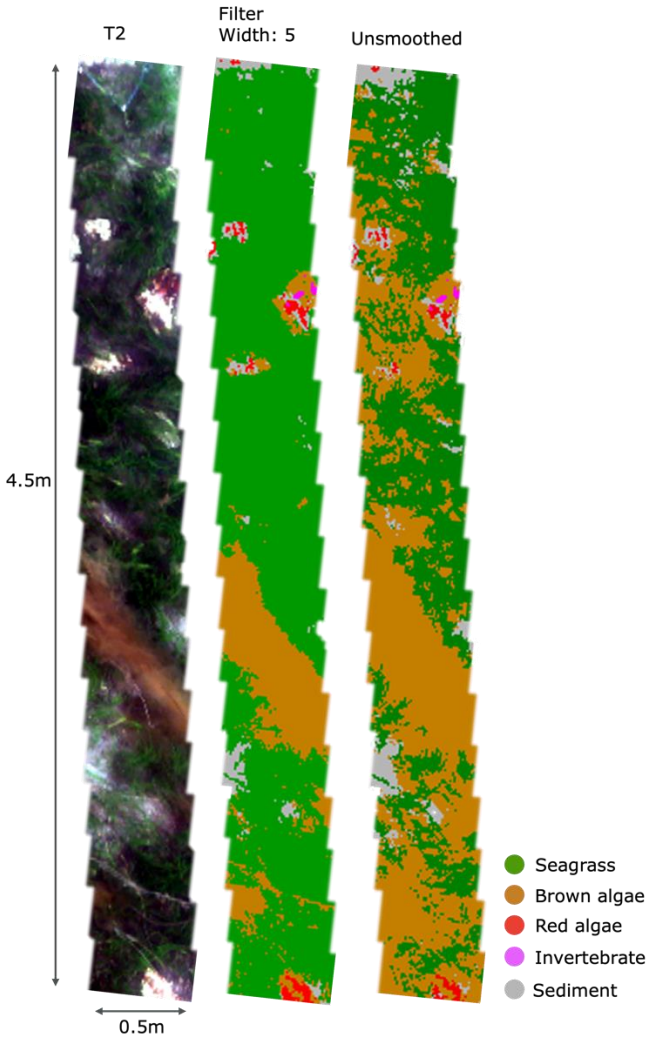

Figure 3.8: Transect subset from September (T2) with an RGB representation of the USV-UHI photomosaic in Hopavågen to the left, followed by the SVM classified subset smoothed with *Thor Spectral Smoothing* in ENVI and Filter width 5. The unsmoothed SVM subset is to the right.

3.5 Ecological Information and UHI Data Validation

3.5.1 Biodiversity in the *Zostera* habitat

The *Zostera* habitat consists of *Zostera marina* (Figure 3.9 and 3.11 a) and several macroalgae species, including the green algae *Codium fragile* (Suringar) Hariot, 1889 and *Ulva* sp., the brown algae *Fucus serratus* Linnaeus, 1753*, Chorda filum* (Linnaeus) Stackhouse, 1797 *and* turf algae. Red algae were dominated by the calcareous *Lithothamnion glaciale* (Figure 3.11 b) and *Phymatolithon lenormandii*. The latter is a dominating epigrowth species growing on the *Zostera* leaves and the substrate. The sea urchins *Echinus esculentus* Linnaeus, 1758 and *Strongylocentrotus droebachiensis* O. F. Müller, 1776*,* the brittle star *Ophiocomina nigra* and the plumose anemone *Metridium senile* are dominating invertebrates found in the area. Additionally, *Littorina littorea* Linnaeus, 1758*, Spirobranchus triqueter* Linnaeus, 1758*, Pagurus bernhardus* Linnaeus, 1758 and *Carsinus maenas* Linnaeus, 1758 are common. A selection of species found in the grab samples and by snorkeling can be found in Figure 3.10. Appendix 3 contains a list of all collected and identified species from the meadow.

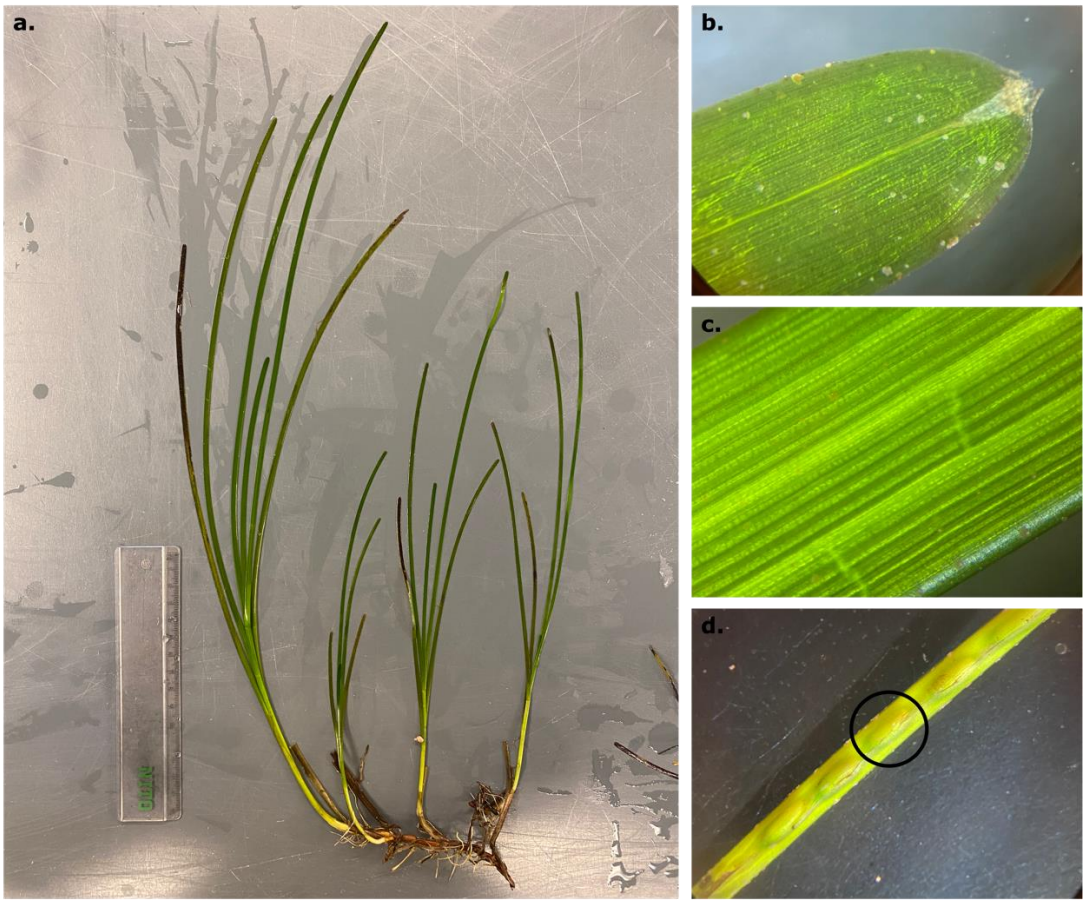

Figure 3.9: *Zostera marina* collected 09.09.2021 with a grab, showing horizontal growth pattern with shoots emerging from the root system (a). Close up of leaf tip with emargination (b), three well-defined veins in the leaf plate (c) and seed capsule with immature seeds (d). Photo: M. Søreng

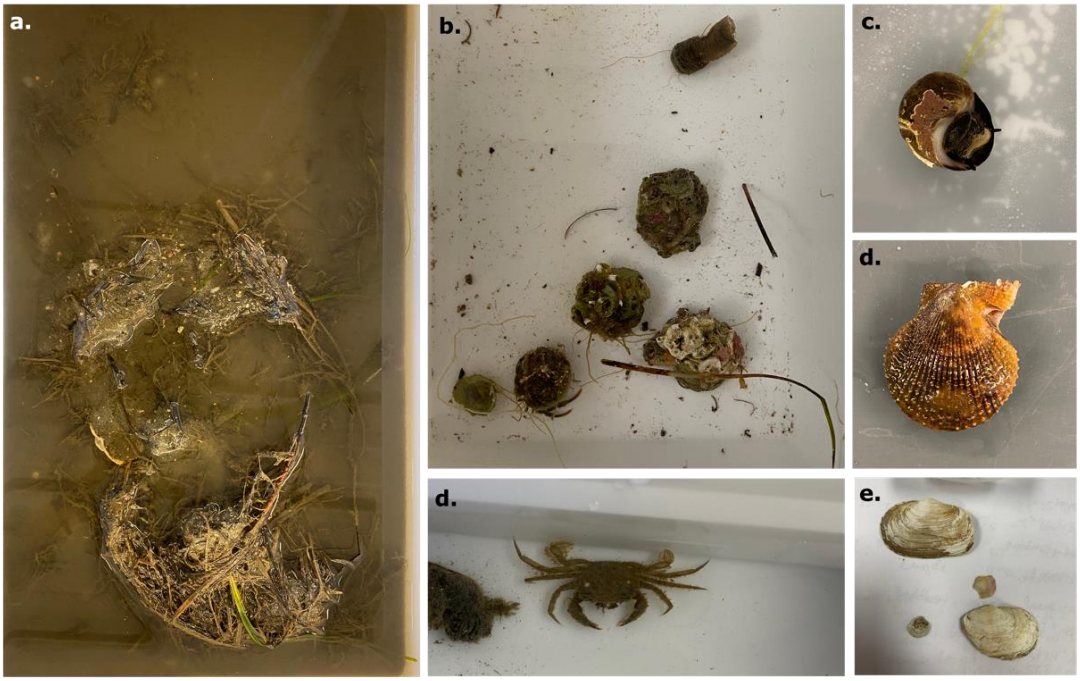

Figure 3.10: Selection of fauna found in the *Zostera* habitat 06.05.2021. Unsorted grab sample with sediment, organic matter and fauna (a), organisms picked from frame F1 at the start of the transect line (b), *Littorina littorea* with *Phymatolithon lenormandii* (c), *Mimachlamys varia* (d), *Liocarcinus* sp.(d), dead Mollusca found in the grab sample (e). Photo: M. Søreng

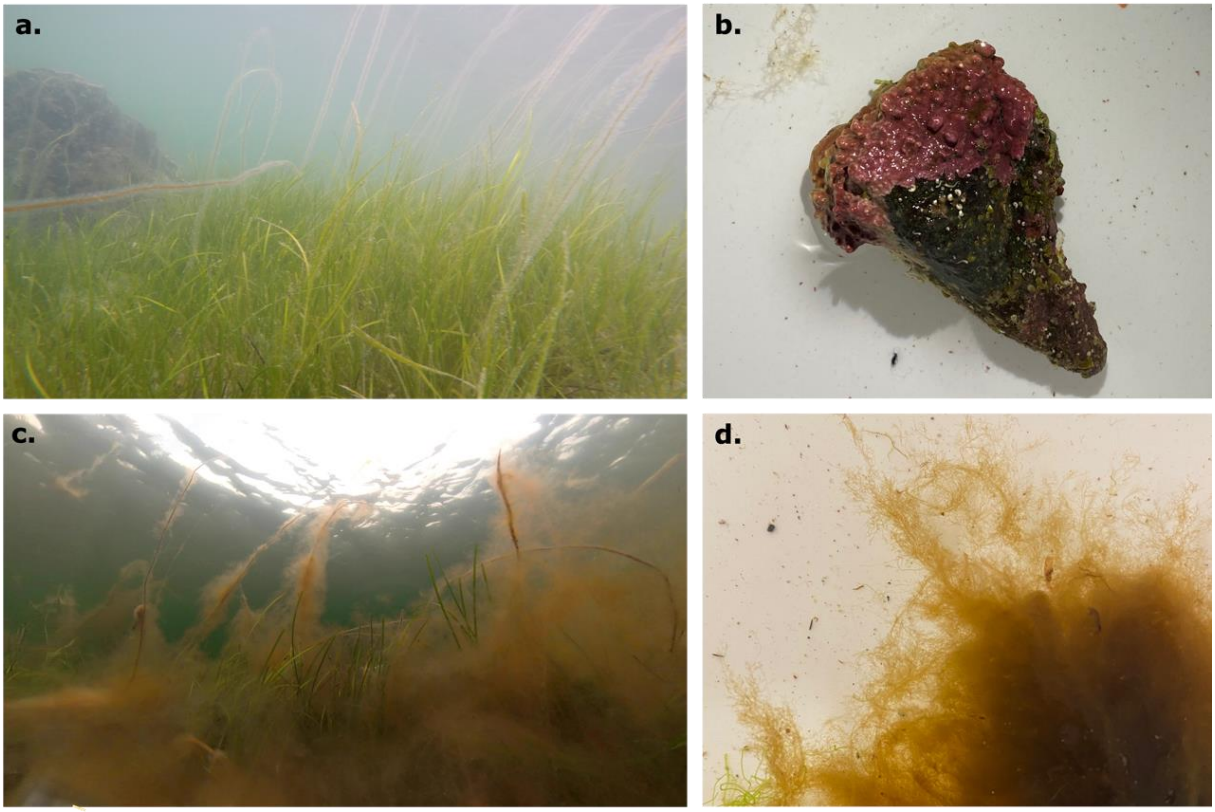

Figure 3.11: The *Zostera* habitat with dominating red and brown algae collected 09.09.2021. To the left: *In situ* close-up *Zostera marina* with *Chorda filum* from May (a) and September (c) with turf algae coverage (Phaeophyceae). To the right: *Lithothamnion glaciale* growing on a rock typically found in the habitat (b) and a close-up of the turf algae (d). Photo: M. Søreng

3.5.2 Epigrowth and Withered Seagrass

During collection of biological material, red calcareous algae was found growing on the *Z. marina* leaves in September (Figure 3.12 a). Old and withered leaves attached to a living specimen (Figure 3.12 b.) also had epigrowth, which will have an impact on the spectral reflectance of the OOIs. Green algae film is also covering organisms and substrate as seen on the *Spirobranchus triqueter* in Figure 3.12 c.

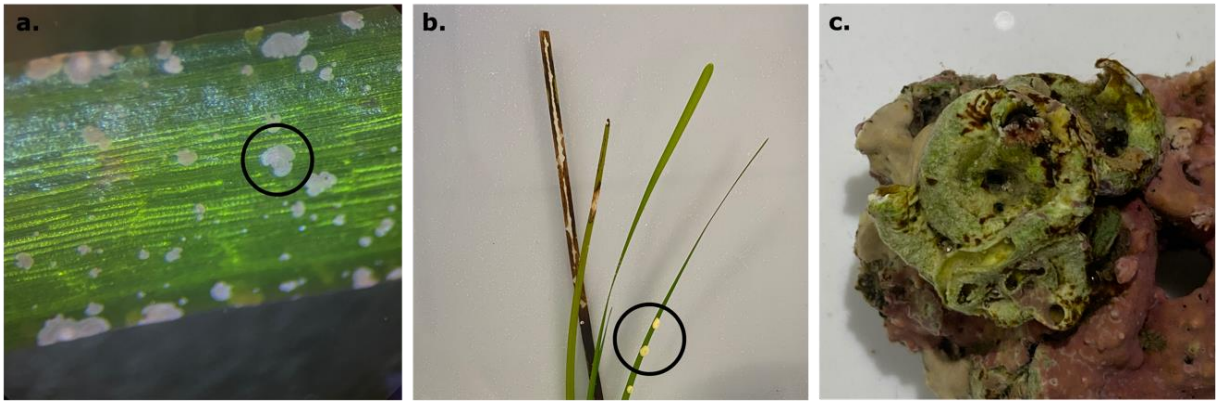

Figure 3.12: *Zostera marina* specimen with red calcareous algae using the leaf as a substrate (a) and a specimen with withered leaf and *Lacuna* sp. eggs (b). A rock with red calcareous algae and *Spirobranchus triqueter* covered in green algae film is shown in panel c. Photo: M. Søreng

3.5.3 *In vivo* Spectral Reflectance

Spectral reflectance data from the reference library collected by the QE Pro spectrometer is used in the graphs in Figure 3.13 and 3.14. The left panel in Figure 3.13 visualizes the mean spectral reflectance for seagrass, brown, red and green algae, with their standard deviation. The within group variance in reflectance is especially large around the reflectance peaks. Green algae and seagrass show similarities in reflectance maxima and minima, but green algae have a slightly higher reflectance. Further, seagrass pigments absorb almost all wavelengths from 400-485 nm before a strong reflection of green wavelengths causing an absorption escalation from ~550-665 nm. Red algae have two characteristic R(λ) peaks at 600 and 650 nm, but also four noticeable dips at 440, 500, 565 and 680 nm. The right panel contains the R(λ) curves for withered seagrass and brown algae for comparison purposes. The reflectance peaks for withered seagrass are positioned at similar wavelengths as the peaks for brown algae, at ~600 and ~645 nm, and a reflectance dip at ~675. This, together with the two dips matching the red algae curve, indicate red algae epigrowth (see Figure 3.12 a). Additionally, a large variation in the measured spectra is present, believed to correspond to different stages of senescence and epiphytes. The maximum R(λ) for withered seagrass is 8.67% at 599 nm, and 5.75% at 597 nm for brown algae, see Table A.2.

The most prominent group specific pigments are identified in Figure 3.14 based on available literature. Pigments characterized in the marine vegetation are chlorophyll *a*, *b* and *c,* carotenoids comprising lutein, zeaxanthin, antheraxanthin, neoxanthin, β,β-carotene, violaxanthin and fucoxanthin, and finally phycobiliproteins dominated by phycoerythrin. From 400-600 nm, all pigment groups are absorbing wavelengths, but from 600-700 nm, there is only absorption from chlorophylls. The seagrass and green algae reflectance curves have two equally positioned reflectance shoulders from approximately 590-630 nm, which can be linked with absorption by epigrowth. The *in vivo* absorption peak range for Chl *a* is from 663-680 nm, together with a pigment "absorption window" with unutilized wavelength ranging from 540-560 nm apparent in the seagrass curve.

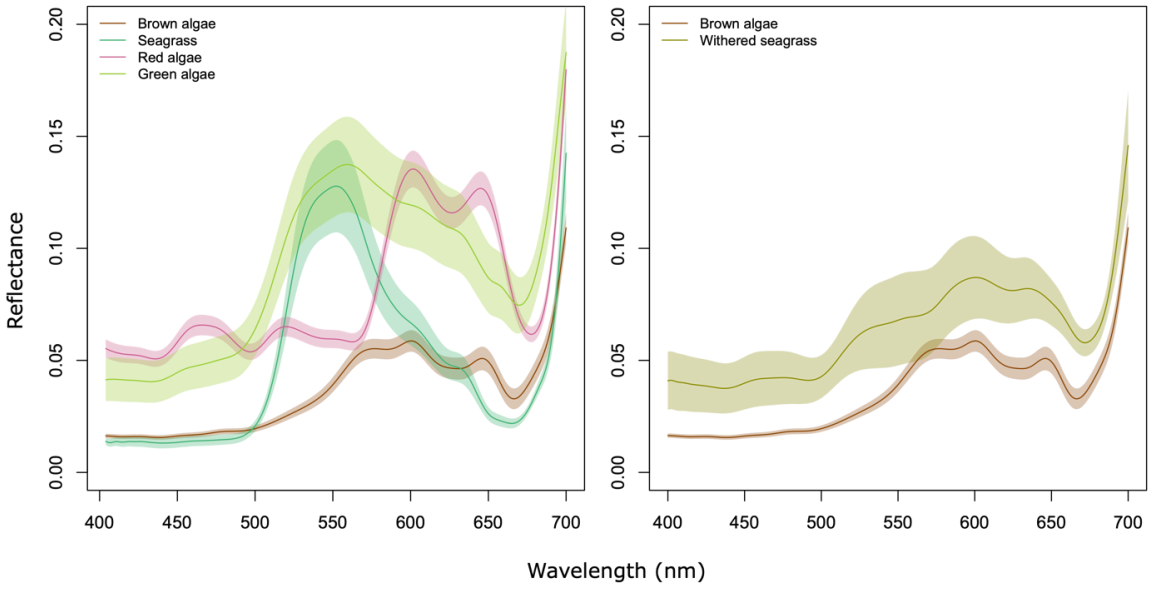

Figure 3.13: Left panel: Mean *in vivo* spectral reflectance for each group of interest with standard error; seagrass, brown algae, red algae and green algae illustrated with their respective color. The wavelength interval on the x-axis is 400-700 nm, with the mean relative reflectance on the y-axis corresponding to percent if multiplied by 100. Right panel: Comparison of mean spectral reflectance of withered seagrass and brown algae, with reflectance peaks at similar wavelengths.

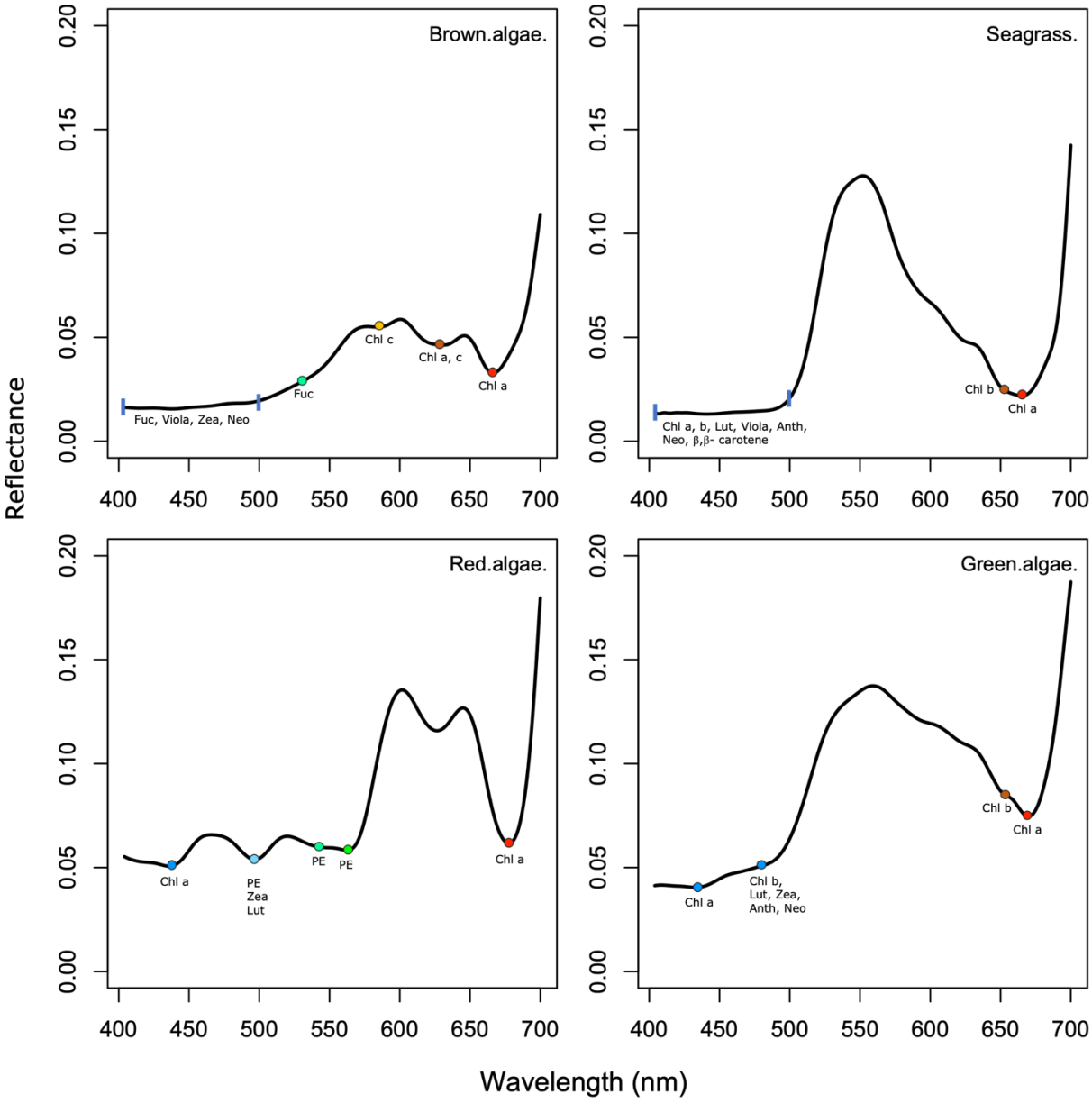

Figure 3.14: The four panels to the left contains the mean *in vivo* spectral reflectance for brown algae, seagrass, red algae and green algae, with reference library data measured by the QE Pro spectrometer. Characteristic pigment absorption maxima, corresponding to reflectance dips, are identified and marked on the curves. The absorption from 400-600 nm is dominated by chlorophylls (Chl *a*, *b*, *c*), phycobiliproteins mainly consisting of phycoerythrin (PE), and the carotenoids lutein (Lut), zeaxanthin (Zea), fucoxanthin (Fuc), neoxanthin (Neo), violaxanthin (Viola), β,β-carotene and antheraxanthin (Anth). Absorption from 600-700 nm comes from chlorophylls only. The colors refer to the hue of the wavelengths absorbed (Johnsen, Leu and Gradinger, 2020; Johnsen *et al.*, 2011; Mogstad and Johnsen, 2017; Fyfe, 2003; Hurd *et al.*, 2014; Alvsvåg, 2017).

3.5.4 Key Environmental Variables

Seawater temperature values retrieved from the altimeter data from the UHI-recordings are included in Table 3.3, together with the measurement from the spectroradiometer and ECO Triplet sensor; salinity, total suspended matter (TSM; m^{-1}), colored dissolved organic matter (cDOM; ppb), and Chlorophyll *a* fluorescens (μg/L). The data from May and September is an average of two measurements at 1.5m below sea surface from the profile measurement in the middle of Hopavågen. The March data comes from the mooring placed on the seafloor next to the seagrass meadow. No environmental variables were measured during the data collection in December, except the seawater temperature of 4.8 °C. The seawater contained more Chl *a* and cDOM in September (1.732 μg/L and 2.843 ppb) compared to March, and had the highest temperature (13.4 °C) measured. The high particulate matter coincides with the yellow hue seen in the frame images in Figure 3.6 d-f, but interestingly the TSM and cDOM is higher in May with water appearing clearer.

Table 3.3: Data from a recording profile at the center of Hopavågen, the measurements are from 1.5 m below sea surface. The data from 1st of March is from the mooring at southeastern shoreline in Hopavågen. Parameters are total suspended matter (TSM), chlorophyll a concentration (Chl *a*), colored dissolved organic matter (cDOM) and salinity. Seawater temperature is measured by the altimeter on the USV.

Date	Seawater temperature [°C]	Salinity [S]	TSM [m^{-1}]	Chl *a* [μg/L]	cDOM [ppb]
07.05.2021	7.8	32.10	0.00135	1.324	4.317
09.09.2021	13.4	29.554	0.000915	1.732	2.843
08.12.2021	4.8	-	-	-	-
01.03.2022	4.5	-	0.000725	0.456	0.867

3.5.5 Downwelling Spectral Irradiance

The spectroradiometer used to measure downwelling spectral irradiance next to the seagrass meadow logged every 2nd minute over 24 hours. Here, a time interval from 10:00 to 15:00 is chosen to include the time of day the UHI data was recorded. The sun angle was approximately 42.6°, 27.5° and 18.7° at the time of E_d measuring (mid-day) in May, September and March, respectively. The spectroradiometer data was averaged to E_{PAR} (W/m^2) and the measurements from May, September and March is given in blue, green and red lines, see Figure 3.15.

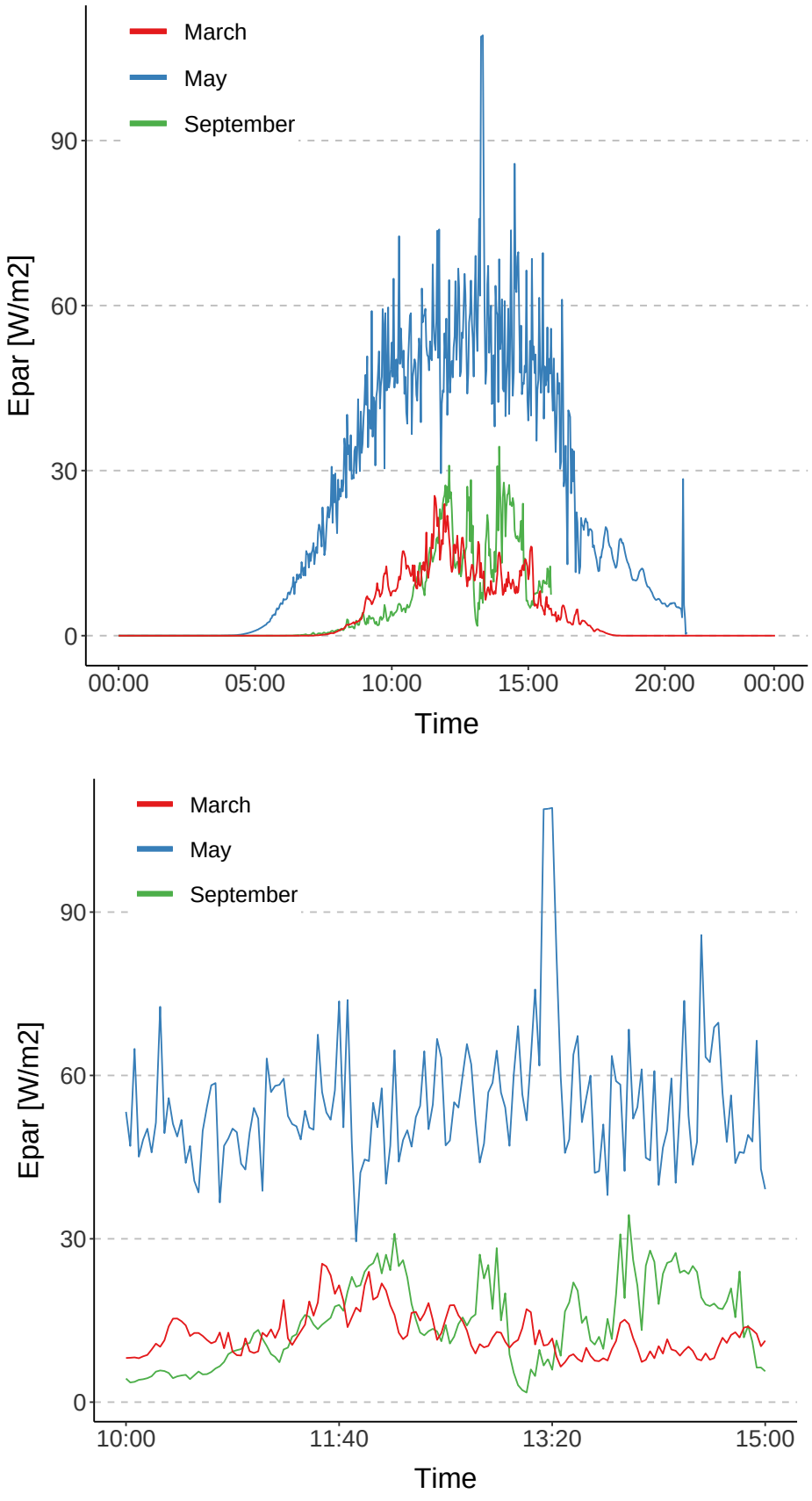

Figure 3.15: Average downwelling spectral irradiance, E_{PAR} (W/m^2), during 24 hours in the top panel, and between 10:00 and 15:00 at mid-day in the lower panel, with colored lines showing measurements with the spectrophotometer from 6th of May (blue), 9th of September (green) and 2nd of March (red).

4 Discussion

In this study, UHI is used as a bio-optical taxonomic tool for species identification and percent coverage estimation in a *Zostera* habitat, as an application of the methodology introduced by Pettersen *et al.* (2014) and Johnsen *et al.* (2013). The UHI detects characteristic pigment signatures further related to pigment groups in marine vegetation (seagrass and macroalgae), given that reflectance spectra are the inverse absorption spectra from different OOIs (Volent, Johnsen and Sigernes, 2009; Thorhaug, Richardson and Berlyn, 2007), Other work have demonstrated this bio-optical method for e.g. micro- and macroalgae (Volent, Johnsen and Sigernes, 2009), *Zostera noltei* (Bargain *et al.*, 2013), coralline algae (Mogstad and Johnsen, 2017), sponges (Pettersen *et al.*, 2014) and cold-water corals (Elde *et al.*, 2012).

To my knowledge, no previous mapping surveys have utilized USV-based UHI to map seagrass (Montes-Herrera *et al.*, 2021; Liu *et al.*, 2020). Here, different temporal UHI data sets are analyzed, which require stricter requirements of georeferencing and navigation to ease the areal comparison. Alvsvåg (2017) used an USV (Jetyak) to map the seagrass meadow in Hopavågen using RGB cameras, but image-analysis is time-consuming work (Schoening *et al.*, 2012). With applying UHI, the amount of information collected regarding time use and workload have been amplified many times, aided by machine learning (Klemas, 2016). This study is also a contribution to the biological survey done by Teacă, Ungureanu and Mureșan (2017) and Duarte, Marťínez and Barrón (2002), which investigated this seagrass meadow, and further an *in situ* application of the laboratory work from Thorhaug, Richardson and Berlyn (2007) that found distinct spectral reflectance spectra between seagrass species and macroalgae. The reflectance maximum of the algae and seagrass examined in this study coincides with the absorption minimum found in literature (Chennu *et al.*, 2013; Fyfe, 2003; Volent, Johnsen and Sigernes, 2009), but little work is found on withered seagrass, implying an interesting finding worth further investigation.

The main goal of mapping seasonal variation in a *Zostera* habitat using USV and UHI is achieved, and the hypotheses conclusions is briefly summarized below. These findings are further discussed.

- Hypothesis 1: USV-based UHI mapping is a time efficient and reliable method for mapping of seagrass distribution over a larger area is confirmed, with some prevailing limitations.
- Hypothesis 2: the UHI will not be able to detect all species found during ground truthing, and the hypothesis is confirmed. It depends on spatial resolution, environmental factors and size of a given organism of interest.
- Hypothesis 3: states that seagrass and macroalgae composition change throughout the year, and it is possible to detect changes in turf algae distribution. This is only partly confirmed since the method was not able to detect changes in turf algae distribution, only brown algae as a group.

4.1 Mapping of Seasonal Variation in *Zostera* habitat

There is seasonal variation in distribution of marine vegetation in the *Zostera* habitat at the southeastern shore in Hopavågen. The seagrass showed greatest extent in September with 78.2% coverage in the subsetted area of 2.25 m^2 and was reduced to 16.7% in February, coinciding with previous work on seasonal variation (Costa, 1988; Duarte, 1989). Withered seagrass is probably included in the brown algae classification, as of similarities in their optical signature (Figure 3.13). Brown algae showed an increase from 17.6% coverage in September to 72.8% in December, and a small reduction again to 65.2% in February. This indicates that brown algae grow substantially during fall and winter compared to seagrass. The SVM classification compared to the ground truth RGB image resulted in a 21.9% error for seagrass, - 77.9% for brown algae and -33.3% for sediment. No invertebrates or withered seagrass was found by the SVM, and no red algae was detected in the ground truth image in frame F2. Physical samples show on the other hand calcareous red algae growing on the substrate, but too small to be detected by the UHI and RGB camera.

4.2 Comparison of Different Classifiers

To compare BR, SVM and DT algorithms for UHI data classification, the September UHI data set was used, and a confusion matrix compared pixel classification for DT and SVM. Both are common classifiers used for hyperspectral analysis (Mountrakis, Im and Ogole, 2011; Gewali, Monteiro and Saber, 2018), and confusion matrices have formerly been demonstrated as accuracy assessments (Mogstad, Johnsen and Ludvigsen, 2019; Foglini *et al.*, 2019; Bioucas-Dias *et al.*, 2013), thus used here. The BR classification highlights seagrass distribution based on characteristic reflectance properties from Chl *a* and *b* at wavelengths 549 and 663 nm (similar to Broge and Leblanc (2001), giving an estimate coinciding with the RGB photomosaic and field observations. The DT classification assigns less pixels as seagrass (33.79%) compared to SVM (65.12%), giving a producer accuracy of 49.87% and user accuracy of 96.09% for seagrass classification indicating that the DT assigned seagrass pixels with high confidence, but missed almost half of the pixels identified as seagrass by the SVM. The BR classifier found 49.85% seagrass pixels (determined by an ROI with threshold 1.2), which is an intermediate result. The highest producer accuracy from the confusion matrix was evident for invertebrates (75.94%) mainly comprising *Metridium senile* and *Echinus esculentus*, which is reasonable when the optical signature for invertebrates is quite distinct from the others and noise are less of a distorting factor (Mogstad, Johnsen and Ludvigsen, 2019; Elde *et al.*, 2012). The lowest producer accuracy was evident for red algae (11.71%), probably due to difficulties by separating red and brown algae in the DT classification. The confusion matrix results in an overall accuracy of 53%, and Kappa Coefficient of 0.307, implying that the classifiers are not in agreement, with most divergence in red algae identification. The classification error of seagrass, brown algae and sediment is highlighted by the colors red, blue and green, respectively in Figure 3.5.

4.3 Biological Assessment

4.3.1 Environmental Variables

Most influential on the quality of the UHI data are the environmental variables related to seawater IOPs, hence the concentration of TSM, cDOM and phytoplankton Chl *a*, as stated by Johnsen *et al.* (2013), reducing the upwelling irradiance to be detected by the sensor

due to attenuation in the water column. The highest particulate content in the seawater was measured in May (TSM: 0.00135 m^{-1}, Chl *a*: 1.324 μg/L, cDOM: 4.317 ppb), presumably due to algae post bloom (Thu, 2022) and a heavy rainfall that increased runoff from land. The TSM concentration was 0.000951 m^{-1} in September and 0.000725 m^{-1} in March, Chl *a* was 1.732 and 0.456 μg/L and cDOM 2.843 and 0.867 ppb, respectively. In contrast, the ground truth RGB images (Figure 3.7 d-f.) show a yellow hue of the seawater, indicating a higher cDOM content in September than May. It is unknown why the particulate content of the water is measured to be higher in May when this appears clearer. One explanation can be the formation of a pycnocline aggregating a higher cDOM concentration in the upper layer of the water column (similar to mechanisms observed for marine snow (Diercks *et al.*, 2019) where the camera was positioned. When the CTD sampling point was at 1.5m depth at the center of Hopavågen, this could have been below the pycnocline, albeit this should be investigated further.

Light conditions vary with seasons (Rayl, Young and Brownson, 2013), and the highest downwelling spectral irradiance (E_{PAR}; ~60 W/m^2 at 1 m depth) was measured in May, with sun angle 42.63°. The E_{PAR} curves in Figure 3.15 fluctuates, indicating changes in cloud cover and irradiance (Ahmad *et al.*, 2003), thus effecting the strength of the signal detected by the UHI and R(λ) (Johnsen *et al.*, 2013). Low downwelling spectral irradiance in December and February leads to low signal-to-noise ratio in the *in situ* spectral reflectance, especially for dark (optically dense) seagrass and brown algae, which seems to almost overlap. Contrasting to the *in vivo* spectral reflectance curves for the two, that are quite distinct. Such differences are also found by (Pu *et al.*, 2012). The *in vivo* R(λ) of seagrass is at its maximum at 550 nm and minimum at 665 nm, with small reflectance peaks at 600 and 630 nm, most likely due to epigrowth of coralline algae commonly found on seagrasses (Borowitzka, Lavery and van Keulen, 2006). The R(λ) for brown algae obtained a maximum at 597 nm and three dips with the minimum R(λ) at 666 nm, with overall reflectance intensity lower than seagrass. However, similarities in brown algae and withered seagrass spectral reflectance curves (higher reflectance intensity for withered seagrass, Figure 3.13) are observed, both with maximum reflectance at ~600 nm. The seagrass has lost its characteristic Chl *b* dip at 650 nm (Johnsen, Leu and Gradinger, 2020).

4.3.2 Biodiversity

Prominent species in the investigated area are *Zostera marina, Phymatolithon lenormandii* and *Lithothamnion glaciale* (red coralline algae), turf algae, *Fucus serratus* and *Chorda filum* (brown algae), *Echinus esculentus* and *Strongylocentrotus droebachiensis* (sea urchins)*, Ophiocomina nigra* (black brittle star), *Metridium senile* (plumose anemone). More extensive species list is found in Appendix 3. The abundant turf algae found in September is either *Ectocarpus* sp. or *Pylaiella* sp., but further taxonomic identification was not possible without seeing the cell structure using dissection microscope. Smaller species of Molluscs and Crustaceans, as well as other macrofauna, were detected by ground truthing (coinciding with Gullström, Baden and Lindegarth (2011), Hori, Bayne and Kuwae (2019) and Alvsvåg (2017), but the size range was below the detection limit of the UHI of 1 cm. Green algae film was also present.

The *Zostera* specimens collected had little epigrowth overall, but *Phymatolithon lenormandii* was found on the leaves during all field missions. *Lacuna* sp. eggs were also found attached to some of the leaves in May. The eelgrass grew taller from May to September (~ 20 cm, see Appendix 4), but a markedly dieback was observed in February, coinciding with a perennial lifecycle (Hori, Bayne and Kuwae, 2019). A quick leaf turnover

rate can function as a way to avoid the epigrowth challenges (Borowitzka, Lavery and van Keulen, 2006), believed to influence the degree of senescence observed in the habitat. Depending on environmental factors influencing the development of characteristic traits, correct identification of the *Z. marina* ecotype is difficult (Lid *et al.*, 2005).

4.4 Method Evaluation

4.4.1 Time Efficiency

USV-based UHI mapping is a time efficient method for standardized seagrass mapping and minimal observer bias in terms of using classification algorithms and preplanned mission (Sørensen *et al.*, 2020). The method requires less work and post-processing than traditional RGB camera based mapping (Montes-Herrera *et al.*, 2021; Johnsen *et al.*, 2020), and it is possible to cover large areas – here ~60 m^2 was recorded in ~2 min. This shows a lower cost-reward ratio in terms of time use and amount of data collected, compared to e.g. underwater RGB imagery (Klemas, 2016; Alvsvåg, 2017), also supported by Barell *et al.* (2015). By deploying the USV from the shoreline, without the need for boats or lifting equipment, it is a time efficient and low effort mapping technique that can access the area of interest quickly. The field mission conducted in December only required 4 people and 2 hours, thus enabling a higher revisit frequency compared to e.g. ROV-missions that requires a ship and many people involved (Klemas, 2016; Johnsen *et al.*, 2016).

However, the UHI data analysis, including the SVM classification in ENVI and learning of the software, is time consuming, and improvements by more efficient classification methods and algorithms are preferable (Klemas, 2016; Macreadie *et al.*, 2019). Thus, the Band Ratio and Decision Tree classifiers were used in an attempt to create a general procedure for marine vegetation identification and areal coverage for different temporal UHI data sets. Instead of using hand-picked pixels of known class as training data set for the SVM algorithm (~4h), intrinsic pigment characteristics and R(λ) can be implemented, and potentially eliminate the need for extensive ground truthing (Dumke *et al.*, 2018b).

4.4.2 Mapping Accuracy using USV-based UHI

4.4.2.1 Classification using machine learning

Seemingly, the DT classification is not accurate and consistent enough when used on noisy data sets (especially when applied to T3 and T4), thereupon discarded as areal coverage estimation method. The BR classification worked well for seagrass mapping, coinciding with the seagrass coverage identified by RGB photomosaic of the UHI data set and RGB camera images, but less for the other groups of interest. Seagrasses contain pigments with absorption maxima (Chl *a*; 440 and 679 nm, Chl *b*; 470 and 650 nm) producing the distinct reflectance maximum and minimum observed (Thorhaug, Richardson and Berlyn, 2007; Roy *et al.*, 2011). Especially the Chl *a* absorption center at ~675 nm (Figure 3.14) can be utilized for detection and quantification of photosynthesizing biomass without influence by other pigments (Bargain *et al.,* 2012). Here, the wavebands 549 and 663 nm was chosen for the BR classification to represent the *in vivo* R(λ) peak from 540-560 nm and dip from 650-680 nm with an R(λ) ratio of 5. The other groups have a different pigment and phycobiliprotein composition, not producing the same distinct band ratio as seagrass (Peñuelas *et al.*, 1993; Dekker, Brando and Anstee, 2005; Thorhaug, Richardson and Berlyn, 2007), see Figure 3.14. This, together with environmental conditions and similarities of the wavelengths at R(λ) maximum and minimum between withered seagrass,

brown algae and red algae, are likely a major reason for wrong classification using DT. By performing a confusion matrix of the SVM classified image as ground truth, and the DT as input data, the two classifiers showed only 53% agreement regarding pixel classification. Interestingly, seagrass scores best in the confusion matrix, which is also indicated by the BR result. Since SVM is a well-accepted method for hyperspectral data analysis and assumed to be accurate and repeatable for multi-category classification (Mountrakis, Im and Ogole, 2011; Gewali, Monteiro and Saber, 2018), this was chosen as the classifier in the areal coverage estimations. With this in mind, a single category BR classification using 549/663 nm shows promise of being a quick and easy way of seagrass mapping.

4.4.2.2 Areal coverage

The accuracy of the species distribution maps using SVM was assumed to be close to ~90% (Mogstad, Johnsen and Ludvigsen, 2019), but the areal coverage estimation accuracy of this study is lower and introduce uncertainty regarding correct classification of the OOIs. The seagrass estimation is best (% error: 21.9), and the brown algae estimation is worst (% error: -77.9). Firstly, this accuracy assessment should preferably be replicated several times to produce mean values giving a more confident result, but the main utility of this was to make the difference between an expert opinion and the classifier perceptible. An alternative would have been to assign each pixel in the subset manually, which is extremely time consuming (Johnsen *et al.*, 2020; Mogstad, Johnsen and Ludvigsen, 2019). Secondly, the SVM classification do not include a withered seagrass class since the large standard deviation (Figure 3.13) indicate much variability in the optical signatures, believed to be due to stages of senescence and epigrowth (Thorhaug, Richardson and Berlyn, 2007; Fyfe, 2003), and it was anticipated to result in misclassification. The ground truth estimation included withered seagrass to underline the presence of this biomass in the area of interest. Since very little brown algae is classified by the SVM in this assessment, the algorithm probably assigns most of the withered seagrass to the seagrass class, instead of the underestimated sediment class with % error of -33.3%. This is positive for the SVM classification of seagrass. However, since the BR classifier use reflectance characteristic in the photosynthesizing tissue (Thorhaug, Richardson and Berlyn, 2007; Broge and Leblanc, 2001), this is evaluated as the best method utilized here for exclusively map distribution of healthy and photosynthesizing seagrass biomass, in agreement with Bargain *et al.,* 2012 and their work on *Z. noltei*. Other band ratios can be used for specific macroalgae groups with different pigment absorption (Hurd *et al.*, 2014).

4.4.2.3 Noise

The fundamentals for mapping accuracy and species detection are good quality UHI data with a high signal-to-noise ratio (Johnsen *et al.,* 2016). Noise-levels here were influenced by environmental and technological factors, including AOPs (especially sun angle, cloud cover and wave actions), IOPs (attenuation due to suspended particulate matter), UHI sensor properties (spectral and spatial resolution), physical disturbances (wind, waves) and georeferencing precision (positioning system of the Otter). This has also been outlined by (Johnsen *et al.*, 2013; Berge, Johnsen and Cohen, 2020). The September data shows higher concentrations of TSM, Chl *a* and cDOM compared to February, but interestingly, it still has better data quality likely due to higher downwelling spectral irradiance ($E_d(\lambda)$). The *in situ* spectral reflectance in September are more coinciding with the reference spectra and have a higher signal-to-noise ratio. This indicate that the UHI data processing can account for much of the noise introduced by the IOPs of the seawater and reduce the signal scattering, supported by (Mogstad, Johnsen and Ludvigsen, 2019). Noise in the UHI data is believed to mainly be introduced by low light conditions during winter and early spring

(Figure 3.15) being at the signal detection limit for the UHI, which reduces signal strength and obscures the spectral reflectance detection. This, in addition to the mixing of spectral reflectance from several OOIs (spectral mixing) delimited by each 1 cm^2 pixel (Bioucas-Dias *et al.*, 2013; Qi and Wu, 1996) is introducing noise. The *Z. marina* leaves were only 2-4 mm wide, so the surrounding or underlying matter reflected other parts of the light spectrum. Lastly, the Otter cruising speed and wave action distort the optical signatures obtained in the data set. Consequently, flat field correction and different smoothing parameters were used to compensate for the especially low signal-to-noise ratio in December and February, the water attenuation coefficient and smooth the curves (Veettil *et al.,* 2020). This has also previously been done in ENVI by (Li, Chen and He, 2020), showing an effectively removal of random noise.

To summarize, the hypothesis (H_1) USV-based UHI mapping is a time efficient and reliable method for mapping of seagrass distribution over a larger area is confirmed. The method is reliable in terms of the ability to revisit the same area and record data all seasons, but it depends on high precision georeferencing, well-functioning technology, good light conditions and minimal wave and wind action to acquire good quality data. The seagrass estimation using band ratio classifier is evaluated as the most consistent, time efficient and robust method for seagrass distribution mapping, for the aforementioned reasons.

4.4.3 Seasonal Distribution Change

4.4.3.1 Change detection

Mapping of habitat biodiversity is restricted by spatial resolution, movement of organisms (e.g. seagrass leaf orientation, mobile fish and sea urchins) and different species with similar optical characteristics that are not distinguishable (e.g. *Fucus serratus* and *Fucus vesiculosus*). This will be further discussed in section 4.5. Infauna (e.g. species in the sediment found by grab samples) is not possible to detect, and epigrowth will camouflage the optical signature belonging to the species they cover. For instance, coralline algae absorb more irradiant light than e.g. filamentous algae epiphytes (Borowitzka, Lavery and van Keulen, 2006). As a result, the UHI will not be able to detect all species found by ground truthing, and hypothesis 2 is confirmed. This is the reason for choosing five groups of interest over specific species in the supervised classification and creation of species distribution maps. Invertebrate and sediment were included in the classification to avoid them being misclassified as marine vegetation, which would affect the coverage estimation.

Even though the SVM classification is not 100% accurate, it is an acceptable error for comparison purposes when concerning large submerged areas where there is presently no other methods with higher degree of information detail and accuracy level (Montes-Herrera *et al.*, 2021; Johnsen *et al.*, 2013; Liu *et al.*, 2020; Veettil *et al.*, 2020). If the same error is present in every transect analysis, and the same area is analyzed, the results will be comparable, and the change detected will be true. By mapping the seagrass habitat at three seasons and estimating the areal coverage for seagrass and macroalgae, the composition change has been shown. Similar results are found by (Dekker, Brando and Anstee, 2005) and (Pe'eri *et al.*, 2016). Going from most coverage and biomass of *Zostera* in September to lowest in February, with a simultaneous increase of brown algae. Red algae stayed more or less the same.

4.4.3.2 Seasonal impacts

Seasonal variation in the distribution maps, further explained in a biological context, include pigment concentration change throughout the year. For example with increasing concentrations towards summer, followed by a decrease for *Z. marina* (Alvsvåg, 2017) and *Z. noltei* (Bargain *et al.,* 2013) with highest pigment content in July. Two studies on brown algae (Selvaraj, Case and White, 2021; Blain and Shears, 2019) found higher pigment concentrations during winter as a low irradiance acclimation strategy. Necessary growth factors compiling nutrient availability, competition, sufficient light conditions and temperature affects the physiological state of the OOIs, their pigment concentration, biomass density and R(λ) across seasons (Plus *et al.*, 2001; Milchakova, 1999; Short and Coles, 2001; Vahtmäe *et al.*, 2006; Fyfe, 2003). Given these points, the *in situ* R(λ) obtained by the UHI is changing with season, and forthwith the distribution change estimation.

The dominating turf algae (Phaeophyceae) were to a large degree correctly identified as brown algae by the SVM algorithm. However, it is not possible to spectrally separate other brown algae and turf algae by this method due to similar pigmentation. When taking a closer look at the habitat with RGB camera, smaller turf algae are growing on the seagrass leaves and other substrate, not being detected by the SVM due to small size and low density. Thereupon, the underlying substrate absorbs light and pollute the optical signature in the pixel (Minghelli *et al.*, 2021). For these reasons, hypothesis 3 is only partly confirmed. More work is needed to find a method to separate turf algae from other species.

4.5 Assumtions and Limitations

4.5.1 Corrections of raw UHI data

The underlaying assumptions of this survey, concerning UHI data processing are flat seafloor, constant depth and downwelling spectral irradiance for all pixels. The geocorrection processing step take this into account and assign the pixels to the correct location in space, i.e. georeferencing the data (Mogstad *et al.*, 2020; Wang *et al.*, 2015). But high precision geolocalization is necessary to do this accurately. As seen in Figure A.1 in Appendix 1, left corner of F2 had an offset ranging from 50-86 cm, due to low georeferencing precision for the USV (coincides with the results from Bjerkvoll (2022). This, together with varying area covered in each total transect line, makes it difficult to directly compare the data sets in terms of spatial distribution of the OOIs. This is the reason for subsetting the transect lines and make sure they cover the same seafloor area. Moreover, there is an assumption of constant IOPs in the transect and the same concentration of KEV-variables at the center of Hopavågen 1.5 m below the surface and 1.5 m below the surface in the *Zostera* habitat, pertinent for the radiometric correction of UHI data.

4.5.2 Species Detection and Coverage

Further, I assume the SVM classifier has high accuracy and is the best classifier used in this thesis for seagrass and macroalgae distribution (Mogstad, Johnsen and Ludvigsen, 2019; Dumke *et al.*, 2018a; Foglini *et al.*, 2019). Spectral Angle Mapping (SAM) based on the spectral reference library for random sampling of pixels of known class (as demonstrated by Bjerkvoll (2022) could have been implemented in acquisition of training data for the SVM (Mogstad, Johnsen and Ludvigsen, 2019; Summers *et al.*, 2022; Foglini *et al.*, 2019), but due to the low light conditions and low signal-to-noise ratio, hand picking pixels were considered the best option to reduce misclassification. Moreover, the hand

selected pixels for the SVM training data set are expected to be correctly assigned to its spectral class, as of a small number of mislabeled pixels will drastically reduce the accuracy (Mountrakis, Im and Ogole, 2011). A thorough biological assessment would be ideal, but due to the small abundance of seagrass in the area, sampling disturbance and time constrains, this was done by two grab samples, observations from RGB cameras and snorkeling, and previous biodiversity work from Hopavågen (Teacă, Ungureanu and Mureșan, 2017; Alvsvåg, 2017). For the seagrass classification, I assume there is no other green algae in the transect. This is not coinciding with the ground truthing, showing a few specimens in the habitat, but the SVM classifier was anticipated to not be able to separate them based on the *in vivo* R(λ) spectra. The spectra show similarities in the 400-530 nm and 580-680 nm ranges as of Chl *a* is the prominent pigment in both groups (Thorhaug, Richardson and Berlyn, 2007; Johnsen, Leu and Gradinger, 2020).

Lastly, to estimate the areal coverage, percent classified pixels in the subsets is used as a proxy with the assumption that pixels translate to biomass. This does not take into account overlapping leaves and algae, positioning of the specimens in the habitat (i.e. seagrass leaf orientation) or the depth dimension. Seagrass leaves standing up straight will only be detected in one pixel, contrasting leaves laying more horizontally detected in several pixels (further explained by Bjerkvoll (2022)). Also, the spatial resolution provided results in spectral mixing, implying a source for misclassification. Keeping this in mind, the pixels will give an objective estimation of areal coverage of biomass for each group. Albeit without quantifying the actual carbon stock or the natural variation throughout a *Zostera* habitat, which would need further calculations, e.g. using R(λ) magnitude as a proxy for seagrass density and find the leaf area index (LAI) subsequently converted to standing biomass (Dierssen *et al.*, 2003).

4.5.3 Survey Altitude

There are several limitations to this method, and the most protruding limitation, as mentioned previously, is too low species-specific mapping accuracy based on UHI data that detect pigment signatures of living specimens. Varying environmental conditions and bio-optical properties are a substantial reason for this, together with technological limitations regarding UHI data acquisition soon to be discussed. Seagrass mapping require minimum 1 m dept, but seagrass can grow from 0-90 m (Duarte, 1991). When the UHI is attached to the USV, submerged ~30 cm below the surface, it cannot adjust the altitude. Thus, USV-based UHI mapping is in general not recommended at deep seagrass locations (>2 m depth) or shallow locations (< 1m). Albeit the depth range may be expanded to 1-5 m if the environmental conditions are optimal (low IOPs and high $E_d(\lambda)$; Vahtmäe *et al.* (2006). Tides influence the recording distance from seafloor to the sensor, further affecting the optical signals retrieved from the OOIs. Even though this is largely accounted for by the simultaneous altimeter measurements and georeferencing, the area covered when the habitat is resampled, given the USV drives the same route each time, will change with the tides. Increasing the distance from the seafloor gives a wider FOV, and an area recorded will differ (Chennu *et al.,* 2017). This is a challenge for accurate comparison of areal coverage and species distribution change, although this is a less prominent problem for resampling in Hopavågen due to a narrow tidal window from 0.3-0.7 m (van Marion, 1996).

4.5.4 Effects of Wind and Waves

The spatial resolution obtained by the UHI depends on the performance of the USV and sensor control, USV size, and physical disturbance (Sørensen *et al.*, 2020). Waves and wind affect the UHI-recording by making the USV wobble (affecting pitch, roll and yaw combined with differences in speed) and alter the crab angle to compensate for the forces pushing it sideways. The crab angle is a specified angle between the sought USV heading and the tangential direction of the preplanned path (Li, Jin and Wang, 2022). This disturbs the sampling by compressing the UHI data in length-direction and distort the USV position (in the yaw-axis) so that the push-broom scan is unaligned with the heading, which makes the resulting UHI photomosaic undulate and intensify the motion blur (Mogstad, Johnsen and Ludvigsen, 2019; Johnsen *et al.*, 2013; Johnsen *et al.*, 2016). When the data is georeferenced, the algorithms will stretch the data, and often duplicate or average adjacent pixels in order to fill in the gaps (Mogstad *et al.*, 2020). This influences the mapping accuracy and the SVM can identify pixels incorrectly, further influencing the areal coverage estimation. Under these circumstances, a gyro attachment of the UHI to the USV (e.g. a gimbal with motors; Johnsen *et al.* (2013)) would have been beneficial, together with better station keeping abilities of the USV. Wind and waves will also push the Otter off track, making it hard to resample the same area (here indicated by the frames) every time. Consequently, the current navigation and georeferencing system of the Otter is inadequate to compensate for these weather conditions. Base station for Real Time Kinetic Global Navigation Satellite System (RTK-GNSS) was available, and should be implemented next USV-survey, but unfortunately, several problems during field missions sabotaged this navigational set-up. There were also some data calculations regarding the Kalman filter in the positioning system lacking in order to get a proper geocorrection of the May transect, which is the reason for no UHI data analysis from May.

4.5.5 Epiphytes

Epigrowth is also a challenge for accurate mapping, inasmuch as *in situ* spectral reflectance are affected. E.g. the *Zostera* leaves and other substrates were covered by calcareous red algae throughout the transect, which influence the spectral reflectance in each pixel. Furthermore, green algae bio-film was observed covering organisms and substrate, seen as a Chl *a* $R(\lambda)$ dip at ~670 nm in the pixel spectrum (Summers *et al.*, 2022; Dumke *et al.*, 2018b). For instance, the top part of T4 in the band ratio map (Figure 3.4) probably shows green algae film covering the sediment due to the homogenous white hue in the image. Epigrowth can also affect the photosynthesis and pigment absorption of $E_d(\lambda)$ of OOIs (Borowitzka, Lavery and van Keulen, 2006). Interestingly, leaf fouling have little effect on *Z. capricorni* reflectance, but is evident by an increase in the 575-630 nm region (Fyfe, 2003).

4.6 This Study in Context of Literature

Current reviews by Montes-Herrera *et al.* (2021) and Liu *et al.* (2020), highlighted the need for further demonstration of UHI as a mapping technique, and this is the objective for this study by mapping a *Zostera* habitat. Previous work has shown successful mapping of seagrass by hyperspectral imagers deployed on satellites and UAVs (Pe'eri *et al.*, 2016; Veettil *et al.*, 2020; Duffy *et al.*, 2019), and Klemas (2016) emphasize that the technology development aids high accuracy of the mapping and surveying of submerged aquatic vegetation. The main limitations of these techniques are the need for proper correction of distortion of the optical path through the atmosphere, air-water interface and the water column, surface reflectance and low spatial resolution (Chennu *et al.*, 2017; Duffy *et al.*,

2018; Castillo-López *et al.*, 2017; Dierssen *et al.*, 2010; Klonowski, Fearns and Lynch, 2007). UHI carried by AUVs and ROVs have also been demonstrated, with the drawbacks of lower spatial resolution (Sture *et al.,* 2017) and difficulties with controlling ROV movements (pitch, roll and yaw), access to sufficient ambient light, georeferencing and keeping a constant altitude (Johnsen *et al.,* 2016). In this study, USV-based UHI is shown to be a better technique in terms of bio-optical taxonomy and distribution mapping of OOIs with 1 cm spatial resolution and less challenges regarding light attenuation, compared to satellite and airborne HI with pixel size range of 1-30 m (Duffy *et al.*, 2018; Mutanga, Adam and Cho, 2012). By adding an altimeter to the UHI, enabling simultaneous altitude and upwelling irradiance recordings, the accuracy of the georeferencing have been improved, and thus the mapping accuracy, as recommended by the pilot study conducted by (Mogstad, Johnsen and Ludvigsen, 2019). In contrast to the pilot study, this work expanded the method application to include temporal variation in a given area of interest (exemplified by the *Zostera* habitat).

4.6.1 Potential for Conservation

The results indicate that USV-based UHI mapping have great potential as a tool for conservation and monitoring purposes, by amplifying the ecological information available for researchers and decision makers. Despite inaccuracies of the SVM classification highlighted here, this is still considered a species identification tool with advantages over traditional RGB imagery due to time efficient data analysis and identification using machine learning, and the ability of the UHI to record in remote areas without sufficient ambient light, e.g. deep sea fauna (Dumke *et al.*, 2018a; Dumke *et al.*, 2018b). Another major advantage is the ability to map without disturbing the ecosystem, which is necessary in many of the common seagrass research methods outlined by Short and Coles (2001). USV-based UHI enables an *in situ* snapshot of the natural species distribution (Liu *et al.*, 2020), and the area of interest can easily be revisited, which is useful for seagrass conservation and biomass estimation (Costa *et al.*, 2021). Duffy and coworkers (2018) demonstrated mapping of intertidal seagrass meadows using optical imagery with 4 mm spatial resolution from a lightweight drone, but one main shortcoming with this method is low spectral resolution (only RGB), forthwith the lack of detailed optical information which enables rapid and comprehensive species detection. Pe'eri et. al (2016) conducted a hyperspectral study where they mapped two spectral classes (seagrass and macroalgae) using ENVI, DT and a band ratio of 547/630 nm, with promising results. Here I took this one step further and mapped 6 spectral classes with a more in depth macroalgae ground truthing, giving a higher level of species detection by applying USV-based UHI imagery with higher spatial resolution (pixel size of 0.01 m^2 compared to 2.5 m^2). With more work, this mapping technique could also possibly aid a confident separation of turf algae and withered seagrass from the other brown algae species.

4.6.2 Pigment Absorption

Further, several studies have identified different absorption maxima for chlorophyll *a* in different seagrass species (675 or 673 nm; (Bargain *et al.*, 2012), 680 nm; (Han and Liu, 2014; Pu *et al.*, 2012), 670 nm; (Broge and Leblanc, 2001), showing a disagreement with my results of absorption maximum at 665 nm in a broad R(λ) dip. Explanations could be species-specific proteins shifting the absorption maxima for Chl *a*, different light regimes during measurements (concerning both IOPs and AOPs) and corrections during data processing (Johnsen *et al.* 2013). Here, the *in vivo* R(λ) of red, green and brown algae have an Chl *a* absorption centra spanning from 665-680 nm, and if the group specific spectral characteristics are sensitive to disturbances during UHI data acquisition (Johnsen

et al., 2016), this will infer identification challenges regarding differences in optical signatures from the *in situ* and *in vivo* measurements (Pu *et al.,* 2012). For instance, if PSSRs and NDVI indices are used in mapping, which is dependent on a consistent absorption maxima for different OOIs (Bargain *et al.*, 2012; Barillé *et al.*, 2010; Peñuelas *et al.*, 1993; Dierssen *et al.*, 2003), ground truthing should be performed until a universal and robust method is established.

4.6.3 Seasonal Change

The seagrass extent in an area can change over time, both be reduced and increased (Barillé *et al.*, 2010; Baden *et al.*, 2003). The eelgrass meadow in Hopavågen (63°35'N 9°32'E), shows seasonal variation in biomass, which is common for temperate seagrass communities, with maximum biomass between July and August (Duarte, 1989). In bays, the eelgrass beds present during the summer may be absent or strongly reduced in winter and spring (Costa, 1988), coinciding with my findings of little seagrass coverage (16.7%) in early spring compared to 72.8%, late summer in September. Considering the low light condition at these latitudes, one should have thought the eelgrass would have an annual lifecycle instead of a perennial life cycle. As discussed by (Duarte, Marťınez and Barrón, 2002), the eelgrass in Hopavågen has probably stored excess carbohydrates during the summer months, facilitating the continued growth and meet the metabolic demands during the winter months with almost complete darkness. New growth replaces older seagrass leaves, which dies/withers and becomes a resource for microbial communities (Klemas, 2016), which has been observed in this habitat. Moreover, the seasonal variation in brown algae species distribution found during winter is supported by Selvaraj, Case and White (2021) and Blain and Shears (2019) that stated that brown algae can acclimatize to light conditions by changing their pigment composition in order to photosynthesize during the winter.

On a larger time scale, the eelgrass distribution in Hopavågen has changed significantly from 1967 to 2015, as seen in the compilation of orthophotos and rasters with seagrass extent at 4 different years in Figure 4.1. The reason for the observed decline in Hopavågen is unknown, with physiological limitations suggested not to affect long term persistence (Duarte, Marťınez and Barrón, 2002). However, the reduction is coinciding with reports from other parts of the world, as of a global decline of 110 km^2 per year between 1980-2006 (Waycott *et al.*, 2009; Duarte, 2017), despite a reversal in European seagrass trends the recent years (de Los Santos *et al.*, 2019). USV-based UHI have the advantage of mapping shallow coastal areas at ~1 m depth, which is otherwise unavailable for other sensor-carrying platforms like ROV, AUV and diver operated units (Sørensen *et al.*, 2020; Chennu *et al.*, 2017). Since the method demonstrated in this study is considered a time efficient and accurate mapping technique, by aforementioned reasons, it enables a higher temporal, spatial and spectral resolution of the UHI data sets than usually seen by airborne hyperspectral imagery (Sørensen *et al.*, 2020; Veettil *et al.*, 2020; Volent, Johnsen and Sigernes, 2007). This will aid the monitoring of seagrass meadows and has potential to detect small scale changes in e.g. sediment-water interface interactions, biogeochemical properties and phototrophic activity (Brandt *et al.*, 2016; Bicknell *et al.*, 2016; Johnsen *et al.*, 2013) which can be important for inspecting seagrass health status and future research that look into drivers of seagrass distribution change.

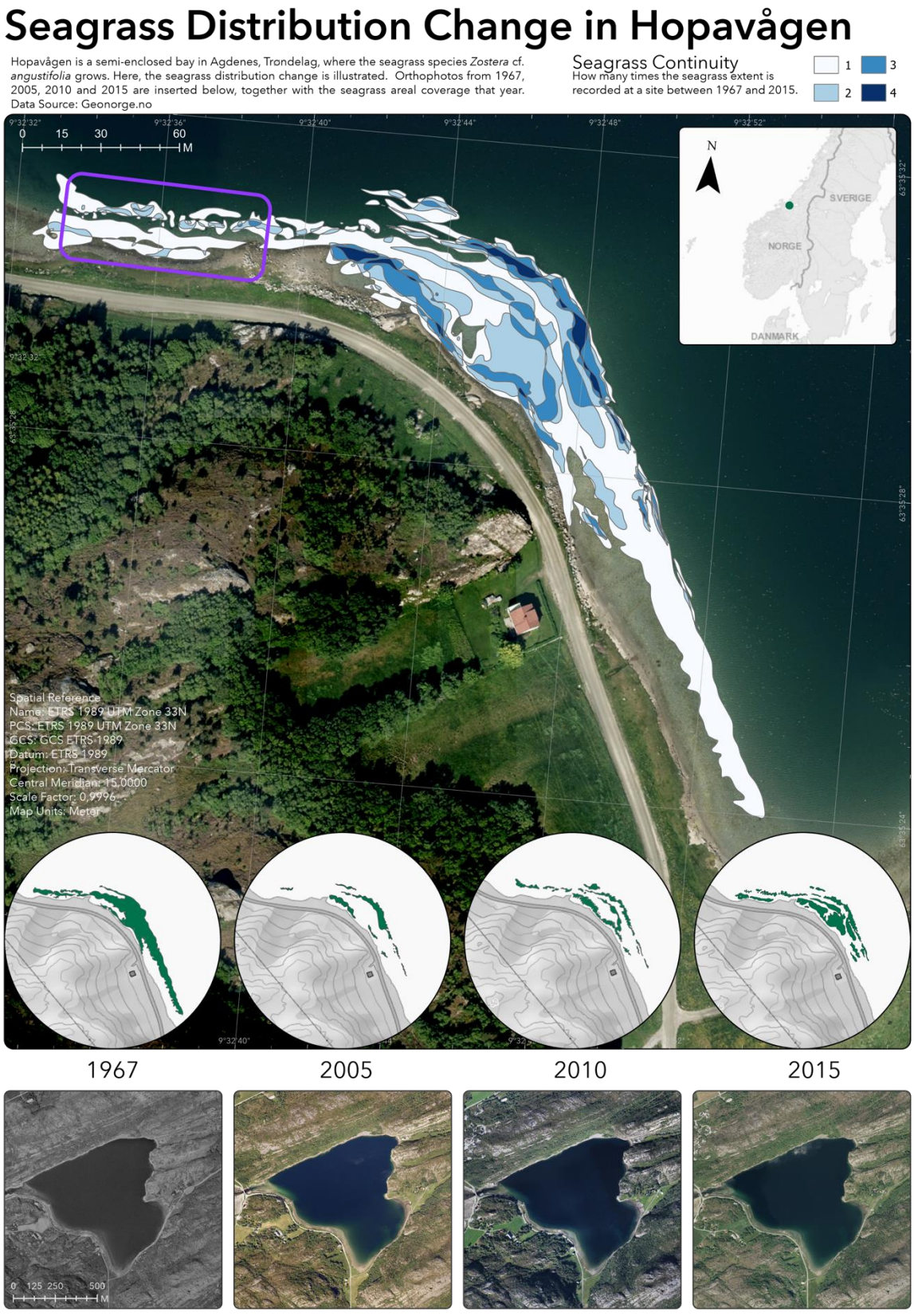

Figure 4.1: Seagrass distribution change from 1967 to 2015 in Hopavågen (63°35'N 9°32'E), Norway, based on four orthophotos from the Norwegian Mapping Authority retrieved from geonorge.no and the respective areal coverage in that year (round panels). The color code represents how many times the seagrass is recorded at the specific location (lightest color: 1 time, darkest color: 4 times). Area examined 2021/2022 is indicated in purple. The map is created in ArcGIS Pro (Esri Inc., Redlands, USA) by M. Søreng (2021), ©norgeibilder.no.

4.7 The Way Forward

The way forward would be to increase quality of the data set by improving the quality of the UHI data acquisition and analysis. This can be achieved by developing the technological aspects of the method, improving resampling abilities and UHI data processing. More specifically: better geopositioning system, better compensation for motion blur, and better classifiers. The incorporation of RTK-GNSS and the Viper-measurements would also be valuable add on´s to the UHI data processing (Mogstad, Johnsen and Ludvigsen, 2019), abolishing the need for a reference plate for radiance conversion, if E(λ) measurements are also included. It is also possible to use an artificial light source, providing constant $E_d(\lambda)$ to enhance a higher and constant signal-to-noise ratio, demonstrated by several studies (Montes-Herrera *et al.*, 2021; Dumke *et al.*, 2018b; Summers *et al.*, 2022). Larger rocks in the area of interest was a challenge for the USV mission planning, and obstacle recognition (Wang *et al.*, 2012) would be helpful to avoid potential collisions and equipment damage.

Improved precision of blue carbon ecosystem mapping and change detection of 10% or less is important for effective monitoring (Macreadie *et al.*, 2019; Duarte, Marťınez and Barrón, 2002). Maps are limited by the number of spectral classes they depict (Barell *et al.*, 2015), forthwith the need for more robust and accurate classification methods, e.g. random forest classification or a multi-classifier approach (Blanchet *et al.,* 2016). As shown in this study, the classification of pixels from the same data set vary according to smoothing settings in the UHI data processing step, classifier and settings used. Here the researcher needs to make a decision and execute the same data processing on each data set in order to get a comparable result between seasons. ENVI is a great software with many applications of use, but only a handful is necessary for UHI data classification and mapping. A program designed for macroalgae and seagrass classification which include cross-validation of training data set, deep-learning and several classifiers would speed up the identification process and make the results more reliable and comparable every time. This is an ambiguous task since many factors have potential to introduce variability in optical signatures (Gewali *et al.,* 2018), moreover an accessible database of reference spectra should be implemented.

Turf algae are especially interesting to separate and quantify with high precision due to a prominent threat to seagrass meadows in Norway and other places (Gundersen *et al.*, 2018; Marba, Arthur and Alcoverro, 2014). Bringing in texture as a new factor in the classification could be useful, as proposed by Veettil *et al.* (2020). Seagrass and green algae species have similar pigment composition and shape of their *in vivo* R(λ) curves, but they differ in reflectance intensity (Thorhaug, Richardson and Berlyn, 2007; Fyfe, 2003). Optical techniques in combination with acoustic data have potential to increase the level of biological information (Shao *et al.*, 2021; Liu *et al.*, 2020) by including e.g. height of seagrass canopy (for biomass and carbon stock estimations), detection of turf algae cover and species identification of marine vegetation. This was out of scope for this thesis but would be a useful next step in the development of a user-friendly and efficient mapping process for conservational purposes. More research is needed to identify the underlying reasons for distribution change of a seagrass population (Macreadie *et al.*, 2019), and mapping with higher temporal resolution should be accomplished in order to detect rapid changes of growth and withering. The possibilities for using USV-based UHI to aid this work and assess the health status and biomass of seagrasses should be a topic of further research.

5 Conclusion

Here, the UHI-USV based seasonal mapping of a *Zostera* habitat have been demonstrated, showing great potential in reproducibility, efficiency, and capacity of being a reliable identification tool for organisms of interest. Eelgrass was shown to have highest areal coverage in September followed by a dieback in December and February. Withered seagrass leaves were probably classified as brown algae, due to similar optical signatures difficult to separate by the SVM-classifier in a noisy data set. This is also supported by the increase in brown algae cover in December and February. There are several shortcomings with this mapping technique regarding signal-to-noise ratio, depth limitations, georeferencing and classification. A high precision classification algorithm would increase the reliability of the methodology outlined here even further, by correctly identifying OOIs at a 1 cm^2 resolution. Turf algae was not possible to separate from other brown algae. For temporal comparison, a standard for post-processing of UHI data should be established, taking into account the variability in environmental conditions related to light availability, IOPs and wind effecting the UHI data acquisition. However, the single category band ratio classification was a quick and easy way of estimating the areal coverage of seagrass with the least influence of external factors, by taking advantage of the distinct spectral characteristics of the inherent photosynthesizing pigments in the seagrass tissue. The take –home message is that by improving georeferencing and correction for variable environmental conditions, the USV-based UHI mapping of seagrass habitats with multi-category classification would be a valuable high resolution (spatial, spectral and temporal) tool for seagrass monitoring and conservation.

References

Ackerman, J. D. (2006) Sexual Reproduction of Seagrasses: Pollination in the Marine Context, in Larkum, A. W. D., Orth, R. J. and Duarte, C. M. (ed.) *Seagrasses: Biology, Ecology and Conservation.* Dordrecht: Springer Netherlands, pp. 89-109. doi: 10.1007/978-1-4020-2983-7_4.

Ackleson, S. G. and Klemas, V. (1987) Remote sensing of submerged aquatic vegetation in lower Chesapeake Bay: A comparison of Landsat MSS to TM imagery, *Remote Sensing of Environment*, 22(2). doi: 10.1016/0034-4257(87)90060-5.

Ahmad, Z. *et al.* (2003) Seasonal variation of UV radiation in the ocean under clear and cloudy conditions, *Conference on Ultraviolet Ground- and Space-based Measurements, Models and Effects III*, *San Diego, Ca*, *Aug 04-06*. pp. 63-73.

Alberotanza, L. *et al.* (2006) Classification of submersed aquatic vegetation of the Venice lagoon using MIVIS airborne data, *Annals of Geophysics*, 49(1). doi: 10.4401/ag-3147.

Alvsvåg, D. M. (2017) *Mapping of seagrass habitat in Hopavågen, Sør-Trøndelag, with the use of an Autonomous Surface Vehicle combined with optical techniques*. Master thesis, Norwegian University of Science and Technology.

Baden, S. *et al.* (2003) Vanishing Seagrass (Zostera marina, L.) in Swedish Coastal Waters, *Ambio*, 32, pp. 374-377. doi: 10.1579/0044-7447-32.5.374.

Bargain, A. *et al.* (2012) Spectral response of the seagrass Zostera noltii with different sediment backgrounds, *Aquatic Botany*, 98(1), pp. 45-56. doi: 10.1016/j.aquabot.2011.12.009.

Bargain, A. *et al.* (2013) Seasonal spectral variation of Zostera noltii and its influence on pigment-based Vegetation Indices, *Journal of Experimental Marine Biology and Ecology*, 446, pp. 86-94. doi: 10.1016/j.jembe.2013.04.012.

Barillé, L. *et al.* (2010) Increase in seagrass distribution at Bourgneuf Bay (France) detected by spatial remote sensing, *Aquatic Botany*, 92(3), pp. 185-194. doi: 10.1016/j.aquabot.2009.11.006.

Barrell, J. *et al.* (2015) Evaluating the complementarity of acoustic and satellite remote sensing for seagrass landscape mapping, *International journal of remote sensing*, 36(16), pp. 4069-4094. doi: 10.1080/01431161.2015.1076208.

Berge, J., Johnsen, G. and Cohen, J. H. (2020) *POLAR NIGHT Marine Ecology : Life and Light in the Dead of Night*. Springer International Publishing : Imprint: Springer. doi: 10.1007/978-3-030-33208-2.

Bicknell, A. W. J. *et al.* (2016) Camera technology for monitoring marine biodiversity and human impact, *Frontiers in ecology and the environment*, 14(8), pp. 424-432. doi: 10.1002/fee.1322.

Bioucas-Dias, J. M. *et al.* (2013) Hyperspectral Remote Sensing Data Analysis and Future Challenges, *IEEE geoscience and remote sensing magazine*, 1(2), pp. 6-36. doi: 10.1109/MGRS.2013.2244672.

Bjerkvoll, M. (2022) *Areal and Underwater Hyperspectral Imagery for Shallow Benthic Nature Type Mapping*. Master thesis, Norwegian University of Science and Technology.

Blain, C. O. and Shears, N. T. (2019) Seasonal and spatial variation in photosynthetic response of the kelp Ecklonia radiata across a turbidity gradient, *Photosynth Res*, 140(1), pp. 21-38. doi: 10.1007/s11120-019-00636-7.

Blanchet, J.-N. *et al.* (2016) Automated annotation of corals in natural scene images using multiple texture representations. PeerJ Preprints. doi: 10.7287/peerj.preprints.2026v2.

Borowitzka, M. A., Lavery, P. S. and van Keulen, M. (2006) Epiphytes of Seagrasses, in Larkum, A. W. D., Orth, R. J. and Duarte, C. M. (ed.) *Seagrasses: Biology, Ecology and Conservation.* Springer Netherlands, pp. 441-461. doi: 10.1007/978-1-4020-2983-7_19.

Brandt, A. *et al.* (2016) Cutting the umbilical: New technological perspectives in benthic deep-sea research, *Journal of Marine Science and Engineering*, 4(2), pp. 36. doi: 10.3390/jmse4020036.

Broge, N. H. and Leblanc, E. (2001) Comparing prediction power and stability of broadband and hyperspectral vegetation indices for estimation of green leaf area index and canopy chlorophyll density, *Remote Sensing of Environment*, 76(2), pp. 156-172. doi: 10.1016/S0034-4257(00)00197-8.

Brown, R. (2019) First Global Planning Meeting for the United Nations Decade of Ocean Science for Sustainable Development (2021–2030), *PICES press*, 27(2), pp. 24-25. Available at: https://www.proquest.com/scholarly-journals/first-global-planning-meeting-united-nations/docview/2281056230/se-2?accountid=12870 (Accessed: 15.05.2022).

Buhl-Mortensen, L. *et al.* (2015) *The Norwegian sea floor: new knowledge from MAREANO for ecosystem-based management*. S.l.: Mareano.

Burkholder, J. M., Tomasko, D. A. and Touchette, B. W. (2007) Seagrasses and eutrophication, *Journal of Experimental Marine Biology and Ecology*, 350(1-2), pp. 46-72. doi: 10.1016/j.jembe.2007.06.024.

Castillo-López, E. *et al.* (2017) The importance of atmospheric correction for airborne hyperspectral remote sensing of shallow waters: application to depth estimation, *Atmospheric Measurement Techniques*, 10(10), pp. 3919-3929. doi: 10.5194/amt-10-3919-2017.

Chennu, A. *et al.* (2013) Hyperspectral imaging of the microscale distribution and dynamics of microphytobenthos in intertidal sediments, *Limnology and Oceanography: Methods*, 11(10), pp. 511-528. doi: 10.4319/lom.2013.11.511.

Chennu, A. *et al.* (2017) A diver-operated hyperspectral imaging and topographic surveying system for automated mapping of benthic habitats, *Scientific reports*, 7(1), pp. 1-12. doi: 10.1038/s41598-017-07337-y.

Cho, H. J., Kirui, P. and Natarajan, H. (2008) Test of multi-spectral vegetation index for floating and canopy-forming submerged vegetation, *International journal of environmental research and public health*, 5(5), pp. 477-483. doi: 10.3390/ijerph5050477.

Cimoli, E. *et al.* (2017) Towards improved estimates of sea-ice algal biomass: Experimental assessment of hyperspectral imaging cameras for under-ice studies, *Annals of glaciology*, 58(75), pp. 68-77. doi: 10.1017/aog.2017.6.

Cimoli, E. *et al.* (2019) An under-ice hyperspectral and RGB imaging system to capture fine-scale biophysical properties of sea ice, *Remote Sensing*, 11(23), pp. 2860. doi: 10.3390/rs11232860.

Cohen, J. H. *et al.* (2020) Light in the Polar Night, in Berge, J., Johnsen, G. and Cohen, J. H. (ed.) *POLAR NIGHT Marine Ecology: Life and Light in the Dead of Night.* Springer International Publishing, pp. 37-66. doi: 10.1007/978-3-030-33208-2_3.

Costa, J. E. (1988) *Eelgrass in Buzzards Bay: Distribution, production and historical changes in abundance*. Washington, DC: U.S. Environmental Protection Agency.
Costa, V. *et al.* (2021) Use of hyperspectral reflectance to non-destructively estimate seagrass Zostera noltei biomass, *Ecological Indicators*, 121, pp. 107018. doi: 10.1016/j.ecolind.2020.107018.
Coyer, J. A. *et al.* (2013) Phylogeny and temporal divergence of the seagrass family Zosteraceae using one nuclear and three chloroplast loci, *Systematics and Biodiversity*, 11(3), pp. 271-284. doi: 10.1080/14772000.2013.821187.
D'Avack, E. A. S. *et al.* (2019) Zostera (Zostera) marina beds on lower shore or infralittoral clean or muddy sand, in Tyler-Walters, H. and Hiscock, K. (ed.) *Marine Life Information Network: Biology and Sensitivity Key Information Reviews.* Available at: https://www.marlin.ac.uk/habitat/detail/257 (Accessed: 16.05.2022).
De Groot, R. S., Wilson, M. A. and Boumans, R. M. (2002) A typology for the classification, description and valuation of ecosystem functions, goods and services, *Ecological economics*, 41(3), pp. 393-408. doi: 10.1016/S0921-8009(02)00089-7.
de Los Santos, C. B. *et al.* (2019) Recent trend reversal for declining European seagrass meadows, *Nature communications*, 10(1), pp. 1-8. doi: 10.1038/s41467-019-11340-4.
Dekker, A. G., Brando, V. E. and Anstee, J. M. (2005) Retrospective seagrass change detection in a shallow coastal tidal Australian lake, *Remote Sensing of Environment*, 97(4), pp. 415-433. doi: 10.1016/j.rse.2005.02.017.
Deudero, S. *et al.* (2010) Interaction between the invasive macroalga Lophocladia lallemandii and the bryozoan Reteporella grimaldii at seagrass meadows: density and physiological responses, *Biological Invasions*, 12(1), pp. 41-52. doi: 10.1007/s10530-009-9428-1.
Diercks, A. *et al.* (2019) Vertical marine snow distribution in the stratified, hypersaline, and anoxic Orca Basin (Gulf of Mexico), *Elementa-Science of the Anthropocene*, 7. doi: 10.1525/elementa.348.
Dierssen, H. M. *et al.* (2003) Ocean color remote sensing of seagrass and bathymetry in the Bahamas Banks by high-resolution airborne imagery, *Limnology and Oceanography*, 48(1part2), pp. 444-455. doi: 10.4319/lo.2003.48.1_part_2.0444.
Dierssen, H. M. *et al.* (2010) Benthic ecology from space: optics and net primary production in seagrass and benthic algae across the Great Bahama Bank, *Marine Ecology Progress Series*, 411, pp. 1-15. doi: 10.3354/meps08665.
Duarte, C. M. (1989) Temporal biomass variability and production/biomass relationships of seagrass communities, *Marine ecology progress series. Oldendorf*, 51(3), pp. 269-276. doi: 10.3354/meps051269.
Duarte, C. M. (1991) Seagrass depth limits, *Aquatic Botany*, 40(4), pp. 363-377. doi: 10.1016/0304-3770(91)90081-f.
Duarte, C. M., Marťınez, R. and Barrón, C. (2002) Biomass, production and rhizome growth near the northern limit of seagrass (Zostera marina) distribution, *Aquatic Botany*, 72(2), pp. 183-189. doi: 10.1016/S0304-3770(01)00225-X.
Duarte, C. M. (2017) Reviews and syntheses: Hidden forests, the role of vegetated coastal habitats in the ocean carbon budget, *Biogeosciences*, 14(2), pp. 301-310. doi: 10.5194/bg-14-301-2017.
Duffy, J. E. *et al.* (2019) Toward a coordinated global observing system for seagrasses and marine macroalgae, *Frontiers in Marine Science*, 6. doi: 10.3389/fmars.2019.00317.

Duffy, J. P. *et al.* (2018) Spatial assessment of intertidal seagrass meadows using optical imaging systems and a lightweight drone, *Estuarine, Coastal and Shelf Science*, 200, pp. 169-180. doi: 10.1016/j.ecss.2017.11.001.

Dumke, I. *et al.* (2018a) First hyperspectral imaging survey of the deep seafloor: High-resolution mapping of manganese nodules, *Remote Sensing of Environment*, 209, pp. 19-30. doi: 10.1016/j.rse.2018.02.024.

Dumke, I. *et al.* (2018b) Underwater hyperspectral imaging as an in situ taxonomic tool for deep-sea megafauna, *Scientific reports*, 8(1), pp. 1-11. doi: 10.1038/s41598-018-31261-4.

Dumke, I. *et al.* (2019) Underwater Hyperspectral Imaging Using a Stationary Platform in the Trans-Atlantic Geotraverse Hydrothermal Field, *IEEE Transactions on Geoscience and Remote Sensing*, 57(5), pp. 2947-2962. doi: 10.1109/TGRS.2018.2878923.

Elde, A. C. *et al.* (2012) Pigmentation and spectral absorbance signatures in deep-water corals from the Trondheimsfjord, Norway, *Marine drugs*, 10(6), pp. 1400-1411. doi: 10.3390/md10061400.

Erftemeijer, P. L. A. and Robin Lewis III, R. R. (2006) Environmental impacts of dredging on seagrasses: a review, *Marine pollution bulletin*, 52(12), pp. 1553-1572. doi: 10.1016/j.marpolbul.2006.09.006.

Foglini, F. *et al.* (2018) Underwater Hyperspectral Imaging for seafloor and benthic habitat mapping, *2018 IEEE International Workshop on Metrology for the Sea; Learning to Measure Sea Health Parameters (MetroSea)*, *Bari*, *8-10 Oct. 2018*. pp. 201-205.

Foglini, F. *et al.* (2019) Application of Hyperspectral Imaging to Underwater Habitat Mapping, Southern Adriatic Sea, *Sensors*, 19(10), pp. 2261. doi: 10.3390/s19102261.

Fyfe, S. K. (2003) Spatial and Temporal Variation in Spectral Reflectance: Are Seagrass Species Spectrally Distinct?, *Limnology and Oceanography*, 48(1), pp. 464-479. doi: 10.4319/lo.2003.48.1_part_2.0464.

Gewali, U. B., Monteiro, S. T. and Saber, E. S. (2018) Machine learning based hyperspectral image analysis: A survey, *ArXiv*, abs/1802.08701.

Grech, A. *et al.* (2012) A comparison of threats, vulnerabilities and management approaches in global seagrass bioregions, *Environmental Research Letters*, 7(2), pp. 024006-024008. doi: 10.1088/1748-9326/7/2/024006.

Green, E. *et al.* (2000) *Remote Sensing Handbook for Tropical Coastal Management*. United Nations Educational, Scientific and Cultural Organization (UNESCO).

Green, E. P. and Short, F. T. (2003) *World atlas of seagrasses*. Berkley, USA: University of California Press.

Gu, H. T. *et al.* (2018) Automated Recovery of the UUV based on the Towed system by the USV, *OCEANS - MTS/IEEE Kobe Techno-Oceans Conference (OTO)*, *Kobe, JAPAN*, *May 28-31*.

Guiry, M. D. and Guiry, G. M. (2022) *AlgaeBase*. World-wide electronic publication, National University of Ireland, Galway (taxonomic information republished from AlgaeBase with permission of M.D. Guiry). *Zostera marina* Linnaeus, 1753. Available at: World Register of Marine Species at: https://www.marinespecies.org/aphia.php?p=taxdetails&id=495077 (Accessed: 29.04.2022).

Gullström, M., Baden, S. and Lindegarth, M. (2011) Spatial patterns and environmental correlates in leaf-associated epifaunal assemblages of temperate seagrass

(Zostera marina) meadows, *Marine Biology*, 159(2), pp. 413-425. doi: 10.1007/s00227-011-1819-z.
Gumusay, M. U. *et al.* (2019) A review of seagrass detection, mapping and monitoring applications using acoustic systems, *European Journal of Remote Sensing*, 52(1), pp. 1-29. doi: 10.1080/22797254.2018.1544838.
Gundersen, H. *et al.* (2018) Marin undervannseng, Marint gruntvann, *Norsk rødliste for naturtyper. Artsdatabanken, Trondheim*. Available at: https://artsdatabanken.no/RLN2018/18 (Accessed: 12.05.2022).
Han, Q. and Liu, D. (2014) Macroalgae blooms and their effects on seagrass ecosystems, *Journal of Ocean University of China*, 13(5), pp. 791-798. doi: 10.1007/s11802-014-2471-2.
Hemminga, M. A. and Duarte, C. M. (2000) *Seagrass ecology*. Cambridge: Cambridge University Press.
Holte, B. and Buhl-Mortensen, L. (2020) Does grab size influence sampled macrofauna composition? A test conducted on deep-sea communities in the northeast Atlantic, *Marine Environmental Research*, 154, pp. 104867-104867. doi: 10.1016/j.marenvres.2019.104867.
Hori, M., Bayne, C. J. and Kuwae, T. (2019) Blue Carbon: Characteristics of the Ocean's Sequestration and Storage Ability of Carbon Dioxide, in Kuwae, T. and Hori, M. (ed.) *Blue Carbon in Shallow Coastal Ecosystems.* Singapore: Springer Singapore, pp. 1-31. doi: 10.1007/978-981-13-1295-3_1.
Horning, N. *et al.* (2020) *Remote sensing for ecology and conservation: a handbook of techniques*. Oxford University Press. Available at: https://search.ebscohost.com/login.aspx?direct=true&db=nlebk&AN=330631&site=ehost-live&scope=site.
Horton, T. *et al.* (2021) Recommendations for the Standardisation of Open Taxonomic Nomenclature for Image-Based Identifications, *Frontiers in Marine Science*, 8. doi: 10.3389/fmars.2021.620702.
Hossain, M. S. and Hashim, M. (2019) Potential of Earth Observation (EO) technologies for seagrass ecosystem service assessments, *International Journal of Applied Earth Observation and Geoinformation*, 77, pp. 15-29. doi: 10.1016/j.jag.2018.12.009.
Hurd, C. L. *et al.* (2014) *Seaweed ecology and physiology*. Cambridge University Press doi: 10.1017/CBO9781139192637.
IPCC (2022) *Climate Change 2022: Impacts, Adaptation and Vulnerability*. (Contribution of Working Group II to the Sixth Assessment Report of the Intergovernmental Panel of Climate Change). In Press. Available at: https://www.ipcc.ch/report/ar6/wg2/ (Accessed: 10.05.2022).
Jayathilake, D. R. and Costello, M. J. (2018) A modelled global distribution of the seagrass biome, *Biological Conservation*, 226, pp. 120-126. doi: 10.1016/j.biocon.2018.07.009.
Johnsen, G. *et al.* (2011) In vivo bio-optical properties of phytoplankton pigments, in Llewellyn, C. A.*, et al.* (ed.) *Phytoplankton pigments: Characterization, chemotaxonomy and applications in oceanography.* pp. 496-537. doi: 10.1017/CBO9780511732263.019.
Johnsen, G. *et al.* (2013) Underwater hyperspectral imagery to create biogeochemical maps of seafloor properties, in Watson, J. and Zielinski, O. (ed.) *Subsea Optics and Imaging.* Woodhead Publishing, pp. 508-540. doi: 10.1533/9780857093523.3.508.

Johnsen, G. *et al.* (2016) The use of underwater hyperspectral imaging deployed on remotely operated vehicles - methods and applications, *IFAC-PapersOnLine*, 49(23), pp. 476-481. doi: 10.1016/j.ifacol.2016.10.451.

Johnsen, G., Leu, E. and Gradinger, R. (2020) Marine Micro- and Macroalgae in the Polar Night, in Berge, J., Johnsen, G. and Cohen, J. H. (ed.) *POLAR NIGHT Marine Ecology: Life and Light in the Dead of Night.* Springer International Publishing, pp. 67-112. doi: 10.1007/978-3-030-33208-2_4.

Johnsen, G. *et al.* (2020) Operative Habitat Mapping and Monitoring in the Polar Night, in Berge, J., Johnsen, G. and Cohen, J. H. (ed.) *POLAR NIGHT Marine Ecology: Life and Light in the Dead of Night.* Springer International Publishing, pp. 277-305. doi: 10.1007/978-3-030-33208-2_10.

Kavzoglu, T. and Colkesen, I. (2009) A kernel functions analysis for support vector machines for land cover classification, *International Journal of Applied Earth Observation and Geoinformation*, 11(5), pp. 352-359. doi: 10.1016/j.jag.2009.06.002.

Kirk, J. T. O. (2010) *Light and photosynthesis in aquatic ecosystems, third edition*. Cambridge University Press online books. doi: 10.1017/CBO9781139168212.

Klemas, V. V. (2016) Remote Sensing of Submerged Aquatic Vegetation, in Finkl, C. and Makowski, C. (ed.) *Seafloor Mapping along Continental Shelves.* Springer International Publishing, pp. 125-140. doi: 10.1007/978-3-319-25121-9_5.

Klonowski, W., Fearns, P. and Lynch, M. (2007) Retrieving key benthic cover types and bathymetry from hyperspectral imagery, *Journal of Applied Remote Sensing*, 1(1), pp. 011505. doi: 10.1117/1.2816113.

Kuhn, M. (2021) caret: Classification and Regression Training (R package version 6.0-90 edn.). Available at: https://CRAN.R-project.org/package=caret.

Kummu, M. *et al.* (2016) Over the hills and further away from coast: global geospatial patterns of human and environment over the 20th-21st centuries, *Environmental Research Letters*, 11(3). doi: 10.1088/1748-9326/11/3/034010.

Kuo, J. and den Hartog, C. (2006) Seagrass Morphology, Anatomy, and Ultrastructure *Seagrasses: Biology, Ecology and Conservation.* Dordrecht: Springer Netherlands, pp. 51-87. doi: 10.1007/978-1-4020-2983-7_3.

Larkum, A. W. D., Drew, E. A. and Ralph, P. J. (2006) Photosynthesis and Metabolism in Seagrasses at the Cellular Level, in Larkum, A. W. D., Orth, R. J. and Duarte, C. M. (ed.) *Seagrasses: Biology, Ecology and Conservation.* Dordrecht: Springer Netherlands, pp. 323-345. doi: 10.1007/978-1-4020-2983-7_14

Letnes, P. A. *et al.* (2019) Underwater hyperspectral classification of deep sea corals exposed to 2-methylnaphthalene, *PLoS One*, 14(2), pp. e0209960. doi: 10.1371/journal.pone.0209960.

Li, X., Chen, K. and He, Y. (2020) In situ and non-destructive detection of the lipid concentration of Scenedesmus obliquus using hyperspectral imaging technique, *Algal Research*, 45, pp. 101680. doi: 10.1016/j.algal.2019.101680.

Li, X. F., Jin, Z. Y. and Wang, L. H. (2022) A Systematic Pipelaying Control Method Based on the Sliding Matrix for Dynamically Positioned Surface Vessels, *Journal of Sensors*, 2022. doi: 10.1155/2022/9702532.

Lid, J. *et al.* (2005) *Norsk flora*. 7. edn. Oslo: Samlaget.

Liu, B. *et al.* (2020) Underwater Hyperspectral Imaging Technology and Its Applications for Detecting and Mapping the Seafloor: A Review, *Sensors*, 20(17), pp. 1-21. doi: 10.3390/s20174962.

Macreadie, P. I. *et al.* (2019) The future of Blue Carbon science, *Nature communications*, 10(1), pp. 3998. doi: 10.1038/s41467-019-11693-w.

Maia, R. *et al.* (2019) pavo 2: new tools for the spectral and spatial analysis of colour in R (1097-1107 edn., vol. 10(7)): Methods in Ecology and Evolution. doi: 10.1111/2041-210x.13174.

Marba, N., Arthur, R. and Alcoverro, T. (2014) Getting turfed: The population and habitat impacts of Lophocladia lallemandii invasions on endemic Posidonia oceanica meadows, *Aquatic Botany*, 116, pp. 76-82. doi: 10.1016/j.aquabot.2014.01.006.

Marbà, N. *et al.* (2006) Seagrass Beds and Coastal Biogeochemistry, in Larkum, A. W. D., Orth, R. J. and Duarte, C. M. (ed.) *Seagrasses: Biology, Ecology and Conservation.* Dordrecht: Springer Netherlands, pp. 135-157. doi: 10.1007/978-1-4020-2983-7_6.

Mayer, D. *et al.* (2021) e1071: Misc Functions of the Department of Statistics (R package version 1.7-9 edn.). TU Wien: Probability Theory Group (Formerly: E1071). Available at: https://CRAN.R-project.org/package=e1071.

McKenzie, L. J. *et al.* (2020) The global distribution of seagrass meadows, *Environmental Research Letters*, 15(7), pp. 074041. doi: 10.1088/1748-9326/ab7d06.

Melgani, F. and Bruzzone, L. (2004) Classification of hyperspectral remote sensing images with support vector machines, *IEEE Transactions on Geoscience and Remote Sensing*, 42(8), pp. 1778-1790. doi: 10.1109/TGRS.2004.831865.

Milchakova, N. A. (1999) On the status of seagrass communities in the Black Sea, *Aquatic Botany*, 65(1), pp. 21-31. doi: 10.1016/S0304-3770(99)00028-5.

Minghelli, A. *et al.* (2021) Benefit of the Potential Future Hyperspectral Satellite Sensor (BIODIVERSITY) for Improving the Determination of Water Column and Seabed Features in Coastal Zones, *IEEE Journal of Selected Topics in Applied Earth Observations and Remote Sensing*, 14, pp. 1222-1232. doi: 10.1109/jstars.2020.3031729.

Mogstad, A. A. and Johnsen, G. (2017) Spectral characteristics of coralline algae: a multi-instrumental approach, with emphasis on underwater hyperspectral imaging, *Applied Optics*, 56(36), pp. 9957-9975. doi: 10.1364/AO.56.009957.

Mogstad, A. A., Johnsen, G. and Ludvigsen, M. (2019) Shallow-Water Habitat Mapping using Underwater Hyperspectral Imaging from an Unmanned Surface Vehicle: A Pilot Study, *Remote Sensing*, 11(6), pp. 685. doi: 10.3390/rs11060685.

Mogstad, A. A. *et al.* (2020) Mapping the Historical Shipwreck Figaro in the High Arctic Using Underwater Sensor-Carrying Robots, *Remote Sensing*, 12(6), pp. 997. doi: 10.3390/rs12060997.

Mogstad, A. A. *et al.* (2021) *Underwater hyperspectral imaging as a tool for benthic habitat mapping*, Norwegian University of Science and Technology, Faculty of Natural Sciences, Department of Biology.

Montes-Herrera, J. C. *et al.* (2021) Underwater hyperspectral imaging (UHI): A review of systems and applications for proximal seafloor ecosystem studies, *Remote sensing,* 13(17), pp. 3451. doi: 10.3390/rs13173451.

Moore, K. A. and Short, F. T. (2006) Zostera: Biology, Ecology, and Management, in Larkum, A. W. D., Orth, R. J. and Duarte, C. M. (ed.) *Seagrasses: Biology, Ecology and Conservation.* Dordrecht: Springer Netherlands, pp. 361-386. doi: 10.1007/978-1-4020-2983-7_16.

Mountrakis, G., Im, J. and Ogole, C. (2011) Support vector machines in remote sensing: A review, *ISPRS journal of photogrammetry and remote sensing*, 66(3), pp. 247-259. doi: 10.1016/j.isprsjprs.2010.11.001.

Mutanga, O., Adam, E. and Cho, M. A. (2012) High density biomass estimation for wetland vegetation using WorldView-2 imagery and random forest regression

algorithm, *International Journal of Applied Earth Observation and Geoinformation*, 18, pp. 399-406. doi: 10.1016/j.jag.2012.03.012.
Nordlund, L. M. *et al.* (2016) Seagrass ecosystem services and their variability across genera and geographical regions, *PLoS One*, 11(10), pp. e0163091. doi: 10.1371/journal.pone.0163091.
Nordlund, L. M. *et al.* (2018a) Seagrass ecosystem services – What's next?, *Marine pollution bulletin*, 134, pp. 145-151. doi: 10.1016/j.marpolbul.2017.09.014.
Nordlund, L. M. *et al.* (2018b) Global significance of seagrass fishery activity, *Fish and Fisheries*, 19(3), pp. 399-412. doi: 10.1111/faf.12259.
Ocean Insight (2022) *qr400-7-vis-bx*. [Digital image]. Available at: https://www.oceaninsight.com/products/fibers-and-probes/probes/reflectionbackscatter-probes/qr400-7-vis-bx/?qty=1 (Accessed: 10.05.2022).
Ocean Optics Launches QE Pro Spectrometer (2014) [Digital image]. Available at: https://www.labbulletin.com/articles/new-high-sensitivity-qe-pro-spectrometer-from-ocean-optics (Accessed: 15.05.2022).
Ocean-Optics-HL-2000 (2022) [Digital image]. Available at: https://spectraservices.com/product/ocean-optics-hl2000-hp.html (Accessed: 05.05.2022).
Olsen, J. L. *et al.* (2013) Eelgrass Zostera marina populations in northern Norwegian fjords are genetically isolated and diverse, *Marine Ecology Progress Series*, 486, pp. 121-132. doi: 10.3354/meps10373.
Ondiviela, B. *et al.* (2014) The role of seagrasses in coastal protection in a changing climate, *Coastal engineering* 87, pp. 158-168. doi: 10.1016/j.coastaleng.2013.11.005.
Orth, R. J. *et al.* (2006) A global crisis for seagrass ecosystems, *BioScience*, 56(12), pp. 987-996. doi: 10.1641/0006-3568(2006)56[987:AGCFSE]2.0.CO;2.
Pasqualini, V. *et al.* (2005) Use of SPOT 5 for mapping seagrasses: An application to Posidonia oceanica, *Remote Sensing of Environment*, 94(1), pp. 39-45. doi: 10.1016/j.rse.2004.09.010.
Pe'eri, S. *et al.* (2016) Eelgrass and macroalgal mapping to develop nutrient criteria in new hampshire's estuaries using hyperspectral imagery, *Journal of coastal research*, (76 (10076)), pp. 209-218. doi: 10.2112/SI76-018.
Peneva, E., Griffith, J. A. and Carter, G. A. (2008) Seagrass mapping in the northern Gulf of Mexico using airborne hyperspectral imagery: a comparison of classification methods, *Journal of coastal research*, 24(4), pp. 850-856. doi: 10.2112/06-0764.1.
Peñuelas, J. *et al.* (1993) Assessing community type, plant biomass, pigment composition, and photosynthetic efficiency of aquatic vegetation from spectral reflectance, *Remote Sensing of Environment*, 46(2), pp. 110-118. doi: 10.1016/0034-4257(93)90088-F.
Pettersen, R. *et al.* (2014) Development of hyperspectral imaging as a bio-optical taxonomic tool for pigmented marine organisms, *Organisms Diversity & Evolution*, 14(2), pp. 237-246. doi: 10.1007/s13127-013-0163-1.
Pettersen, R. *et al.* (2019) Detection and classification of Lepeophterius salmonis (Krøyer, 1837) using underwater hyperspectral imaging, *Aquacultural Engineering*, 87, pp. 102025. doi: 10.1016/j.aquaeng.2019.102025.
Pham, T. D. *et al.* (2019) A review of remote sensing approaches for monitoring blue carbon ecosystems: Mangroves, seagrassesand salt marshes during 2010–2018, *Sensors*, 19(8), pp. 1933. doi: 10.3390/s19081933.

Pieterkosky, S. *et al.* (2017) BIV Meets ASV: Bio-inspired Fish Drones and Autonomous Surface Vehicles for Coral Reef Monitoring, *Conference on OCEANS*, *Anchorage, AK*, *Sep 18-21*.

Plus, M. *et al.* (2001) Factors influencing primary production of seagrass beds (Zostera noltii Hornem.) in the Thau lagoon (French Mediterranean coast), *Journal of Experimental Marine Biology and Ecology*, 259(1), pp. 63-84. doi: 10.1016/S0022-0981(01)00223-4.

Pu, R. *et al.* (2012) Discrimination of seagrass species and cover classes with in situ hyperspectral data, *Journal of coastal research*, 28(6), pp. 1330-1344. doi: 10.2112/JCOASTRES-D-11-00229.1.

Qi, Y. and Wu, J. (1996) Effects of changing spatial resolution on the results of landscape pattern analysis using spatial autocorrelation indices, *Landscape ecology*, 11(1), pp. 39-49. doi: 10.1007/BF02087112.

R Core Team (2021) R: A language and environment for statistical computing. Vienna, Austria: R Foundation for Statistical Computing. Available at: https://www.R-project.org/.

Ralph, P. J. *et al.* (2006) Human Impacts on Seagrasses: Eutrophication, Sedimentation, and Contamination, in Larkum, A. W. D., Orth, R. J. and Duarte, C. M. (ed.) *Seagrasses: Biology, Ecology and Conservation.* Dordrecht: Springer Netherlands, pp. 567-593. doi: 10.1007/978-1-4020-2983-7_24

Rayl, J., Young, G. S. and Brownson, J. R. S. (2013) Irradiance co-spectrum analysis: Tools for decision support and technological planning, *Solar Energy*, 95, pp. 364-375. doi: 10.1016/j.solener.2013.02.029.

Roy, S. *et al.* (2011) *Phytoplankton pigments: characterization, chemotaxonomy and applications in oceanography*. Cambridge University Press.

RStudio Team (2016). RStudio: Integrated Development for R. RStudio, Inc., Boston, MA Available at: http://www.rstudio.com/

Rueness, J. (1998) *Alger i farger : en felthåndbok om kystens makroalger*. Oslo: Almater forl.

Sakshaug, E., Johnsen, G. and Volent, Z. (2009) Light, in Sakshaug, E., Johnsen, G. and Kovacs, K. (ed.) *Ecosystem Barents Sea.* Trondheim: Tapir Academic Press, pp. 117-138.

Schauberger, P. and Walker, A. (2021) openxlsx: Read, Write and Edit xlsx Files (R package version 4.2.5 edn.). Available at: https://CRAN.R-project.org/package=openxlsx.

Schoening, T. *et al.* (2012) Semi-automated image analysis for the assessment of megafaunal densities at the Arctic deep-sea observatory HAUSGARTEN, *PLoS One*, 7(6), pp. e38179. doi: 10.1371/journal.pone.0038179.

Selvaraj, S., Case, B. S. and White, W. L. (2021) Effects of Location and Season on Seaweed Spectral Signatures, *Frontiers in Ecology and Evolution*, 9. doi: 10.3389/fevo.2021.581852.

Shao, H. M. *et al.* (2021) Classification of various algae canopy, algae turf, and barren seafloor types using a scientific echosounder and machine learning analysis, *Estuarine Coastal and Shelf Science*, 255. doi: 10.1016/j.ecss.2021.107362.

Sheehan, E. V., Stevens, T. F. and Attrill, M. J. (2010) A quantitative, non-destructive methodology for habitat characterisation and benthic monitoring at offshore renewable energy developments, *PLoS One*, 5(12), pp. 14461. doi: 10.1371/journal.pone.0014461.

Short, F. *et al.* (2007) Global seagrass distribution and diversity: a bioregional model, *Journal of Experimental Marine Biology and Ecology*, 350(1-2), pp. 3-20. doi: 10.1016/j.jembe.2007.06.012.

Short, F. T. and Coles, R. G. (2001) *Global seagrass research methods*. Elsevier. doi: 10.1016/S0044-8486(02)00307-1.

Short, F. T. *et al.* (2011) Extinction risk assessment of the world's seagrass species, *Biological Conservation*, 144(7), pp. 1961-1971. doi: 10.1016/j.biocon.2011.04.010.

Solstad, H. *et al.* (2021) Karplanter: Vurdering av dvergålegras Zostera noltei for Norge. *Rødlista for arter 2021. Artsdatabanken*. Available at: https://www.artsdatabanken.no/lister/rodlisteforarter/2021/32494 (Accessed: 10.05.2022).

Specht, C., Switalski, E. and Specht, M. (2017) Application of an autonomous/unmanned survey vessel (ASV/USV)in bathymetric measurements, *Polish Maritime Research*, 24(3), pp. 36-44. doi: 10.1515/pomr-2017-0088.

Standards Norway (2013) *NS-EN 16260:2012 Water quality-Visual seabed surveys using remotely operated and towed observation gear for collection of environmental data.* Available at: https://www.standard.no/no/nettbutikk/produktkatalogen/Produktpresentasjon/?ProductID=606849 (Accessed: 10.05.2022).

Sture, Ø. *et al.* (2017) Autonomous underwater vehicles as a platform for underwater hyperspectral imaging, *Oceans Aberdeen*, *Aberdeen*, *19-22 June 2017*. pp. 1-8.

Sture, Ø. *et al.* (2018) Recognition of cold-water corals in synthetic aperture sonar imagery, *2018 IEEE/OES Autonomous Underwater Vehicle Workshop (AUV)*, *Porto, Portugal*. IEEE, pp. 1-6.

Sture, Ø., Snook, B. and Ludvigsen, M. (2019) Obtaining Hyperspectral Signatures for Seafloor Massive Sulphide Exploration, *Minerals*, 9(11), pp. 694. Available at: https://www.mdpi.com/2075-163X/9/11/694.

Summers, N. *et al.* (2022) Underwater Hyperspectral Imaging of Arctic Macroalgal Habitats during the Polar Night Using a Novel Mini-ROV-UHI Portable System, *Remote sensing*, 14(6), pp. 1325. doi: 10.3390/rs14061325.

Sørensen, A. J. *et al.* (2020) Sensor-Carrying Platforms, in Berge, J., Johnsen, G. and Cohen, J. H. (ed.) *POLAR NIGHT Marine Ecology: Life and Light in the Dead of Night.* Springer International Publishing, pp. 241-275. doi: 10.1007/978-3-030-33208-2_9.

Tan, Y. M. *et al.* (2020) Seagrass restoration is possible: Insights and lessons from Australia and New Zealand, *Frontiers in Marine Science*, 7, pp. 617. doi: 10.3389/fmars.2020.00617.

Teacă, A., Ungureanu, C. and Mureșan, M. (2017) Assessment of diversity and distribution of benthic communities in Hopavågen bay, Sletvik area (Norway), *Geo-eco-marina*, 2017(23), pp. 103-120. Available at: https://www.proquest.com/scholarly-journals/assessment-diversity-distribution-benthic/docview/2070893004/se-2?accountid=12870 (Accessed: 10.05.2022).

Thiele, C. and Hirschfeld, G. (2021) cutpointr: Improved Estimation and Validation of Optimal Cutpoints in R (98(11), 1-27 edn.): Journal of Statistical Software. doi: 10.18637/jss.v098.i11.

Thorhaug, A., Richardson, A. D. and Berlyn, G. P. (2007) Spectral reflectance of the seagrasses: Thalassia testudinum, Halodule wrightii, Syringodium filiforme and five marine algae, *International journal of remote sensing*, 28(7), pp. 1487-1501. doi: 10.1080/01431160600954662.

Thu, M. (2022) *Phytoplankton spring bloom mapping in coastal areas using Autonomous Underwater Vehicle (AUV) and optical approaches*. Master thesis, Norwegian University of Science and Technology.
Tucker, C. J. (1979) Red and photographic infrared linear combinations for monitoring vegetation, *Remote Sensing of Environment*, 8(2), pp. 127-150. doi: 10.1016/0034-4257(79)90013-0.
United Nations Environment Programme (2009) *Blue carbon: the role of healthy oceans in binding carbon*. Available at: https://wedocs.unep.org/20.500.11822/7772 (Accessed: 15.05.2022).
Unsworth, R. K. F. *et al.* (2018) Global challenges for seagrass conservation, *Ambio*, 48(8), pp. 801-815. doi: 10.1007/s13280-018-1115-y.
Unsworth, R. K. F. *et al.* (2019) Global challenges for seagrass conservation, *Ambio*, 48(8), pp. 801-815. doi: 10.1007/s13280-018-1115-y.
Vahtmäe, E. *et al.* (2006) Feasibility of hyperspectral remote sensing for mapping benthic macroalgal cover in turbid coastal waters—a Baltic Sea case study, *Remote Sensing of Environment*, 101(3), pp. 342-351. doi: 10.1016/j.rse.2006.01.009.
van Marion, P. (1996) *Ecological studies in Hopavågen, a landlocked bay at Agdenes, Sør-Trøndelag, Norway*. Trondheim: Norges teknisk-naturvitenskapelige universitet, Vitenskapsmuseet.
Veettil, B. K. *et al.* (2020) Opportunities for seagrass research derived from remote sensing: A review of current methods, *Ecological Indicators*, 117, pp. 106560. doi: 10.1016/j.ecolind.2020.106560.
Velez-Reyes, M. *et al.* (2006) Benthic habitat mapping using hyperspectral remote sensing, in Bostater, C. R.*, et al.* (ed.) *Remote Sensing of the Ocean, Sea Ice, and Large Water Regions 2006.* doi: 10.1117/12.692996.
Volent, Z., Johnsen, G. and Sigernes, F. (2007) Kelp forest mapping by use of airborne hyperspectral imager, *Journal of Applied Remote Sensing*, 1(1), pp. 011503. doi: 10.1117/1.2822611.
Volent, Z., Johnsen, G. and Sigernes, F. (2009) Microscopic hyperspectral imaging used as a bio-optical taxonomic tool for micro- and macroalgae, *Applied Optics*, 48(21), pp. 4170-4176. doi: 10.1364/AO.48.004170.
Wang, H. *et al.* (2012) Improvement in Real-time Obstacle Detection System for USV, *12th International Conference on Control, Automation, Robotics and Vision (ICARCV)*, *Guangzhou, PEOPLES R CHINA*, *Dec 05-07*. pp. 1317-1322.
Wang, X. J. *et al.* (2015) Evaluation of positioning error-induced pixel shifts on satellite linear push-broom imagery, *Journal of Applied Remote Sensing*, 9(1). doi: 10.1117/1.Jrs.9.095061.
Wang, Y. (2009) *Remote sensing of coastal environments*. CRC Press. doi: 10.1201/9781420094428.
Waycott, M. *et al.* (2009) Accelerating loss of seagrasses across the globe threatens coastal ecosystems, *Proceedings of the national academy of sciences*, 106(30), pp. 12377-12381. doi: 10.1073/pnas.0905620106.
Wickham, H. (2016) ggplot2: Elegant Graphics for Data Analysis: Springer-Verlag New York. Available at: https://ggplot2.tidyverse.org.
Wickham, H. and Bryan, J. (2019) readxl: Read Excel Files (R package version 1.3.1 edn.). Available at: https://CRAN.R-project.org/package=readxl.
World Register of Marine Species (2022) Tracheophyta. Available at: https://www.marinespecies.org/aphia.php?p=taxdetails&id=596326.
Wu, X. *et al.* (2008) Top 10 algorithms in data mining, *Knowledge and Information Systems*, 14(1), pp. 1-37. doi: 10.1007/s10115-007-0114-2.

Zimmerman, R. C. (2006) Light and Photosynthesis in Seagrass Meadows, in Larkum, A. W. D., Orth, R. J. and Duarte, C. M. (ed.) *Seagrasses: Biology, Ecology and Conservation.* Dordrecht: Springer Netherlands, pp. 303-321. doi: 10.1007/978-1-4020-2983-7_13.

Öztürk, M., Vadstein, O. and Sakshaug, E. (2003) The effects of enhanced phytoplankton production on iron speciation and removal in mesocosm experiments in a landlocked basin of Hopavågen, Norway, *Marine chemistry*, 84(1), pp. 3-17. doi: 10.1016/S0304-4203(03)00087-2.

Appendix

Appendix 1: Navigation of the Otter Pro

Appendix 2: *In vivo* vs. *In situ* Maximum Reflectance of Groups of Interest

Appendix 3: Species from the *Zostera* habitat in Hopavågen

Appendix 4: Pictures of Species from the *Zostera* habitat in Hopavågen

Appendix 5: R scrips

Appendix 1: Navigation of the Otter Pro

Positioning system

Positioning data of the USV was logged using 2x Ublox F9P-ZED GNSS – receiver with each Harxon GPS1000 survey GNSS antenna for position, speed and heading, a ADIS 16495 IMU logging acceleration, angular velocity at 125 Hz and a Sentiboard (NTNU/Senti Systems, Trondheim, Norway) for connecting and synchronizing the measurements regarding to time stamp. The measurements were integrated through a custom made Kalman filter (Senti Systems, NTNU, Trondheim, Norway) that estimates position, speed and orientation (attitude = roll, pitch, yaw) of the USV.

Georeferencing precision

The difference in position of frame F2 to the right between each transect subset (T2, T3, T4; Figure A.1), and the difference between the stone to the left are estimated and given in Table A.1. The numbers in the table are the difference between the stone/frame in each transect given by the column and row.

Table A.1: Offset from corner of frame F2 and top right tip of stone in the subsetted transects (T2, T3 and T4).

Stone / F2	T2	T3	T4
T2		0.717 m	1.2510 m
T3	0.616 m		1.8322 m
T4	0.556 m	0.8615 m	

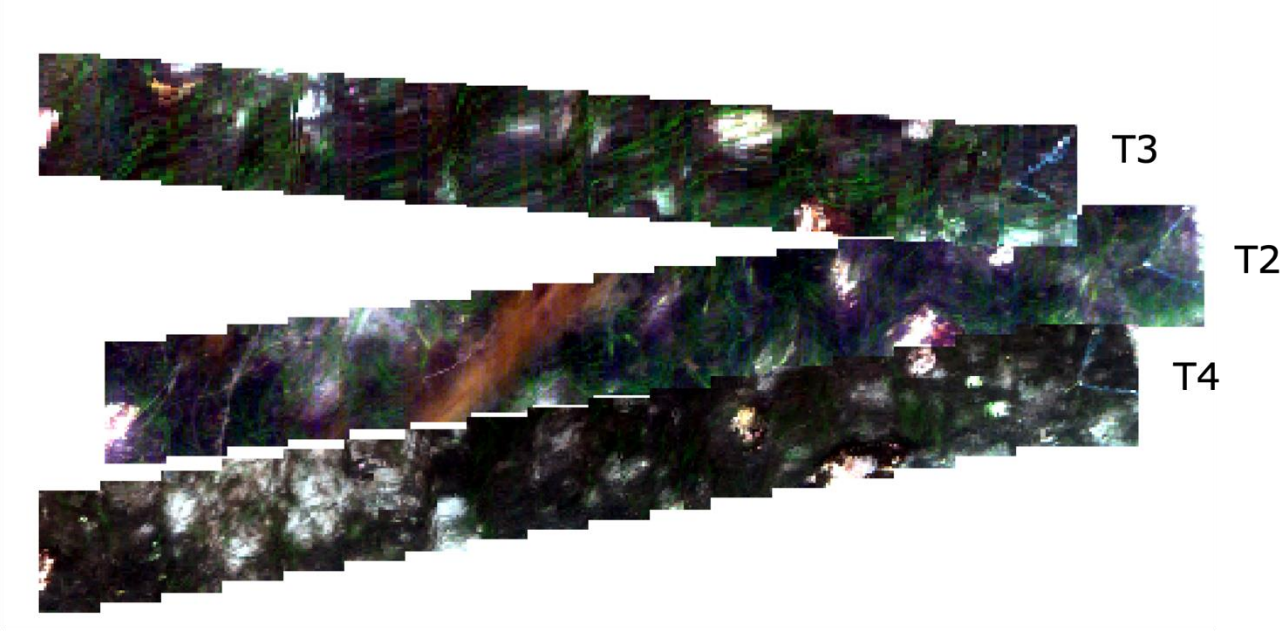

Figure A.1: The georeferenced position of the subsetted RGB photomosaics from September (T2), December (T3) and February (T4) viewed in ENVI.

Appendix 2: *In vivo* vs. *In situ* Spectral Reflectance Maxima

Table A.2: Maximum reflectance at the respective wavelength (nm and corresponding relative reflectance value in brackets) for each group of interest from *in vivo* (Reference) and *in situ* (T2, T3, T4) spectral reflectance data.

Data Source	Brown algae	Red algae	Seagrass	Invertebrates	Sediment	Green algae	Withered
Reference	597	600	550	-	-	559	599
In vivo	[0.0575]	[0.133]	[0.128]			[0.137]	[0.0867]
T2	603	603	557	681	603	-	-
In situ	[0.136]	[0.256]	[0.0993]	[0.269]	[0.171]		
T3	603	645	557	685	599	-	-
In situ	[0.0712]	[0.231]	[0.0688]	[0.329]	[0.199]		
T4	603	603	557	681	603	-	-
In situ	[0.0548]	[0.194]	[0.0502]	[0.180]	[0.128]		

Appendix 3: Species in the *Zostera* habitat in Hopavågen

Species from the *Zostera* habitat and UHI study area collected 06.05.2021, 07.09.2021 and 10.09.2021 by snorkeling and grab samples (noted with "ZH" in Table A.3). Species noted with "RL" are measured by the QE Pro Spectrometer (Ocean Insight Inc., Orlando, USA), but some of these specimens are not collected from an area delimited by the transect line.

Scientific names and authors are retrieved from the World Register of Marine Species (www.marinespecies.org) on 01.05.2022, and the nomenclature has followed the guidelines from (Horton *et al.*, 2021). Norwegian names are retrieved from "Artsnavnebasen" hosted by the Norwegian Biodiversity Information Centre (www.artsdatabasen.no). Algae are identified mainly using *Alger i farger* (Rueness, 1998).

Table A.3: Species identified from the *Zostera* habitat at the southeastern shoreline in Hopavågen by field observations and samples in May and September 2021.

Phylum	Scientific name	Norwegian name	Author	Note
PLANT				
Tracheophyta				
	Zostera marina	Vanlig ålegras	Linnaeus, 1753	ZH, RL
	Zostera marina, withered	Vanlig ålegras	Linnaeus, 1753	ZH, RL
ALGAE				
Chlorophyta				
	Chlorophyta indet		Pascher, 1914	ZH, RL
	Cladophora rupestris	Vanlig grønndusk	(Linnaeus) Kützing, 1843	RL
	Codium fragile	Pollpryd	(Suringar) Hariot, 1889	ZH, RL
	Rhizoclonium tortuosum inc.	Viklesnøre	(Dillwyn) Kützig, 1845	RL
	Ulva intestinalis	Tarmgrønske	Linnaeus, 1753	RL
	Ulva sp.		Linnaeus, 1753	RL
Phaeophyceae				
(Class)				
	Ascophyllum nodosum	Grisetang	(Linnaeus) Le Jolis, 1863	RL
	Chorda filum	Martaum, åletang	(Linnaeus) Stackhouse, 1797	ZH, RL
	Dictyosiphon foeniculaceus inc.	Finsveig	(Hudson) Greville, 1830	RL
	Ectocarpus inc.		Lyngbye, 1819	ZH, RL
	Fucus serratus	Sagtang	Linnaeus, 1753	ZH, RL
	Fucus spiralis	Kaurtang	Linnaeus, 1753	ZH, RL
	Fucus vesiculosus	Blæretang	Linnaeus, 1753	ZH, RL
	Mesogloia vermiculata	Bruntrevl	(Smith) S.F Gray, 1821	RL
	Scytosiphon lomentaria	Fjæreslo	(Lyngbye) Link, 1833	ZH, RL
	Phaeophyceae indet		Kjellman, 1891	ZH, RL
Rhodophyta				
	Corallina officinalis	Krasing	Linnaeus, 1758	ZL, RL
	Hildenbrandia rubra	Fjæreblod	(Sommerfelt) Meneghini, 1841	RL

	Lithothamnion glaciale	Vorterugl	Kjellmann, 1883	ZH, RL
	Mastocarpus stellatus	Vorteflik	(Stackhouse) Guiry, 1984	ZH, RL
	Phymatolithon lenormandii	Slettrugl	(Areschoug) W.H.Adey, 1966	ZH, RL
ANIMALS				
Annelida				
	Hesionidae indet.		Grube, 1850	ZH
	Nereimyra punctata inc.		Müller, 1776	ZH
	Pherusa plumosa inc.	Skjeggbørstemark	Müller, 1776	ZH
	Pryonospio cirrifera		Wirén, 1883	ZH
	Scalibregna inflatum			ZH
	Spirobranchus triqueter	Trekantmark	Linnaeus, 1758	
	Terrebellidae sp.			
Arthropoda				
	Balanus balanus	Steinrur	Linnaeus, 1758	ZH, RL
	Carsinus maenas	Strandkrabbe	Linnaeus, 1758	ZH, RL
	Liocarcinus sp.	Svømmekrabbe	Stimpson, 1871	ZH
	Pagurus bernhardus	Bernakeremittkreps	Linnaeus, 1758	ZH, RL
Chordata				
	Stiela rustica	Tornsekkdyr		ZH, RL
Cnidaria				
	Metridium senile	Sjønellik	Linnaeus, 1761	ZH, RL
Echinodermata				
	Asterias rubens	Vanlig korstroll	Linnaeus, 1758	ZH, RL
	Echinus esculentus	Svabergsjøpiggsvin	Linnaeus, 1758	ZH, RL
	Ophiocomina nigra	Svartslangestjerne	Abildgaard, 1789	ZH, RL
	Ophiopholis aculeata	Kameleonslangestjerne	Linnaeus, 1767	ZH
	Ophiothrix fragilis	Skjørslangestjerne	Abildgaard in O.F. Müller, 1789	ZH
	Strongylocentrotus droebachiensis	Drøbakksjøpiggsvin	O.F. Müller, 1776	ZH, RL
Mollusca				
	Callochiton septemvalis inc.	Flekkleddsnegl	Montagu, 1803	ZH, RL
	Gibbula sp.			ZH
	Heteranomia squamula	Sadelskjell	Linnaeus, 1758	ZH
	Peringia ulvae inc.	mudderfjæresnegl	Pennant, 1777	ZH
	Lacuna sp.		W. Turton, 1827	ZH
	Littorina littorea	Storstrandsnegl	Linnaeus, 1758	ZH, RL
	Macoma calcarea		Gmelin, 1791	ZH
	Mimachlamys varia	Urskjell	Linnaeus, 1758	ZH, RL
	Mya truncata	Butt sandskjell	Linnaeus, 1758	ZH, RL
	Pododesmus patelliformis	Sadelskjell	Linnaeus, 1761	ZH, RL
	Rissoa parva		da Costa, 1778	ZH
	Rissoidae indet	Tangsnegl	Gray, 1847	ZH
	Steromphala cineraria	Glatt kjeglesnegl	Linnaeus, 1758	ZH, RL

Appendix 4: Pictures of Species from the *Zostera* habitat in Hopavågen

Figure A.4.1: *Zostera marina* specimens collected 06.05.2021 (top row) compared to 09.09.2021 (bottom row). Photo: M. Søreng

Figure A.4.4: Macroalgae species collected from the *Zostera* habitat, measured *in vivo* with the QE Pro Sprectrometer. *Ascophyllum nodosum* (a; 07.09.2021), *Fucus spiralis* (b; 09.09.2021) and *Codium fragile* (c; 09.09.2021). Photo: M. Søreng

Figure A.4.2: From top left: *Zostera marina* with turf algae covering the canopy (a), Ascidiacea stet. (b), *Echinus esculenta* and *Littorina littorea* (c) and *Metridium senile* (d). Photo: M. Søreng, G. Johnsen.

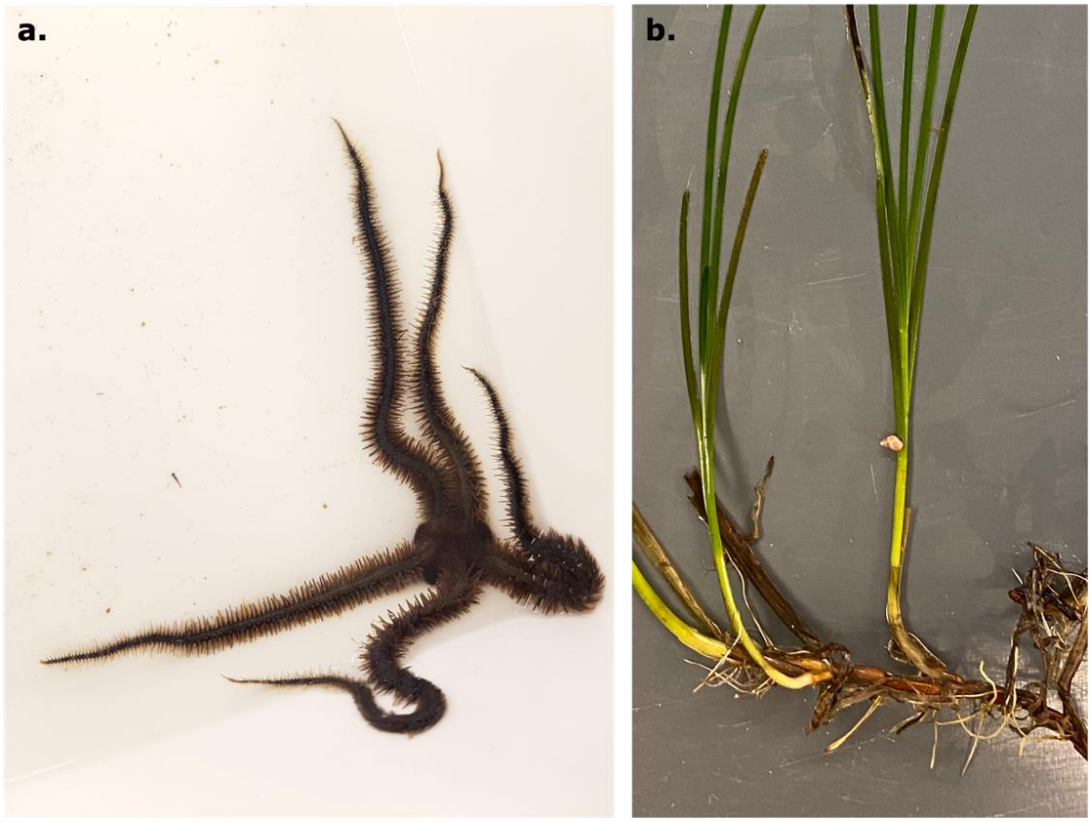

Figure A.4.3: *Ophiocomina nigra* (a; 07.09.2021) and *Zostera marina* with *Rissoidae* indet (b; 09.09.2021). Photo: C. Marnor, M. Søreng

Appendix 5: R Scripts

SVM tuning

```
library("openxlsx")
library("e1071")
library("caret")
df = read.xlsx("ROISept.xlsx", sheet = 3)
dat = df
dat$Class = factor(dat$Class)
svm_tune = tune(svm, Class ~ ., data = dat, kernel = «radial»,
                ranges = list(cost = 10^(-3:6), gamma = 10^(-6:3)),
                scale = FALSE)
plot(svm_tune, transform.x = log10, transform.y = log10, xlab = «log(C)»,
ylab = «log(gamma)»,
     main = "SVM grid search cross-validation (classification error)")
dev.off()
print(svm_tune)
svm_tune$performances
```

DT-thresholds

```
### Example of September data and seagrass index
install.packages("cutpointr")
library(ggplot2)
library(cutpointr)
library(openxlsx)

### Seagrass threshold ###
df_seagrass = read.xlsx("September.xlsx", sheet = 1)
cp = cutpointr(data = df_seagrass, x = Value, class = Class,
               method = maximize_metric, metric = acc_constrain,
constrain_metric = ppv, min_constrain = 0.99,
               use_midpoints = TRUE, break_ties = mean)
g = ggplot(df_seagrass, aes(x = Value, fill = Class)) +
  scale_fill_manual(values = c("white", "gray"),
                    labels = c("Other", "Seagrass")) +
  geom_density(aes(y = ..scaled..), alpha = .3) +
  labs(fill = "Seafloor class") + geom_vline(xintercept = 1.39197) +
  ylab("Scaled probability density") + xlab("Seagrass index")
ggsave(plot = g, filename = "Seagrass_index.jpg", units = "in", height = 9,
width = 12, dpi = 1000)
```

Creating *in vivo* spectral reflectance curves

```
install.packages("pavo")
library(pavo)
library(readxl)
library(openxlsx)
TotalReference <- read_excel("Reference4groups.xlsx")
rspecdata <- as.rspec(TotalReference, whichwl="WL", interp = FALSE)
spp <- gsub("\\.[0-9].*$", "", names(rspecdata))[-1]
table(spp)
```

Average spectra for each class and round numbers

```
sppspec <- aggspec(rspecdata, by = spp, FUN = mean)
round(sppspec[1:7, ],5)
```

Plot using mean and standard error, in colors

```
par(mfrow=c(1,2))
colClass <- c("darkorange4","mediumseagreen","hotpink3","yellowgreen")
colMeanSd <- aggplot(rspecdata[-1:-4,], spp,
```

```
                    ylim = c(0, 0.20),
                    FUN.error = function(x) sd(x) / sqrt(length(x)),
                    lcol = colClass, shadecol = colClass,
                    alpha = 0.3, legend=FALSE)
legend("topleft", legend=c("Brown algae",  "Seagrass", "Red algae","Green
algae"),col=colClass, lty=1, cex=0.8,box.lty=0)
```

Find reflectance peak and wavelength

```
spec.sm <- procspec(sppspec, opt = "smooth", span = 0.2)
peakshape(spec.sm, select = 2, lim = c(400, 600), plot = TRUE)
peakshape(spec.sm, select = 3, lim = c(400, 600), plot = TRUE)
peakshape(spec.sm, select = 4, lim = c(400, 600), plot = TRUE)
peakshape(spec.sm, select = 5, lim = c(400, 600), plot = TRUE)
```

Plot brown algae and withered seagrass

```
TotalReference <- read_excel("Reference4groups.xlsx", sheet = 2)
rspecdat <- as.rspec(TotalReference, whichwl="WL", interp = FALSE)
sPP <- gsub("\\.[0-9].*$", "", names(rspecdat))[-1]
table(sPP)
```

Average spectra for each class and round numbers

```
sppspec <- aggspec(rspecdat, by = sPP, FUN = mean)
colCla <- c("darkorange4","yellow4")
colMeanSd <- aggplot(rspecdat, sPP,
                    ylim = c(0, 0.20),
                    FUN.error = function(x) sd(x) / sqrt(length(x)),
                    lcol = colCla, shadecol = colCla,
                    alpha = 0.3, legend=FALSE)
legend("topleft", legend=c("Brown algae", "Withered seagrass"),
       col=colCla, lty=1, cex=0.8,
       box.lty=0) #, title = "", title.adj=0.6)
```

Find reflectance peak and wavelength

```
spec.sm <- procspec(sppspec, opt = "smooth", span = 0.2)
peakshape(spec.sm, select = 3, lim = c(400, 600), plot = TRUE)
```

In situ **reflectance data**

Example from September data

```
library(pavo)
library(readxl)
TotalReference <- read_excel("ROISpectraSept.xlsx")
rspecdata <- as.rspec(TotalReference, whichwl="WL", interp = FALSE)
spp <- gsub("\\.[0-9].*$", "", names(rspecdata))[-1]
table(spp)
```

Graph with different colors and standard error

```
colClass2 <-
c("darkorange4","indianred1","lightcyan4","mediumseagreen","hotpink3")
aggplot(rspecdata, spp,
        ylim = c(0, 0.3),
        FUN.error = function(x) sd(x) / sqrt(length(x)),
        lcol = colClass2, shadecol = "grey",
        alpha = 0.5, lwd= 2, legend=FALSE, xaxt = "n")
axis(1, at = c(1, 15, 29, 45, 58),
     labels = c("490", "540", "590","640", "690"))
legend("topleft", legend=c("Brown algae", "Invertebrates", "Red algae",
"Seagrass", "Sediment"),col=colClass2, lty=1, cex=0.8,
       box.lty=0, title = "September", title.adj=0.7)
```

Find reflectance peak and wavelength

```
spec.sm <- procspec(sppspec, opt = "smooth", span = 0.2)
peakshape(spec.sm, select = 2, lim = c(1, 55), plot = TRUE)
peakshape(spec.sm, select = 3, lim = c(1, 55), plot = TRUE)
peakshape(spec.sm, select = 4, lim = c(1, 55), plot = TRUE)
peakshape(spec.sm, select = 5, lim = c(1, 55), plot = TRUE)
peakshape(spec.sm, select = 6, lim = c(1, 55), plot = TRUE)
```

Bar plot of percent coverage

```
library(RcolorBrewer)
library(readxl)
data <- read_excel("Percent.xlsx")
DF2 <- data.matrix(data)
coul <- brewer.pal(4, "Pastel2")
colClass4 <- c("mediumseagreen","lightsalmon4","hotpink3","lightcyan4")
barplot(DF2[-4,-1], width=c(0.5,0.5,0.5), col=colClass4 , border="white",
xlab="Transect", ylab="Percent coverage", ylim=c(0,100))
legend("topleft", legend=c("Seagrass", "Brown algae", "Sediment", "Red
algae"),bty = "n", pch=15 , pt.cex = 1, pt.bg = 1, pt.lwd = 5, cex = 0.8,
horiz = FALSE, inset = c(0.05, 0.05), col= colClass4)
```

Downwelling spectral irradiance curves

Same code is used for 24h curves, only changed the scale_x_continuous to include wanted time

```
library(readxl)
library(ggplot2)
Average <- read_excel("Mooring Average Epar Modified.xlsx", sheet = 4)
### Plot three months, from 10:00 to 15:00 ###
figure <- ggplot(data = Average, aes(x = time…1)) +
  geom_line(aes(y = Epar…2, colour = "May")) +
  geom_line(aes(y = Epar…4, colour = "September")) +
  geom_line(aes(y = Epar…6, colour = "March")) +
  xlab("Time") + ylab("Epar [W/m2]") + labs(colour=NULL) +
  scale_color_brewer(palette = 'Set1') +
  scale_x_continuous(breaks = c(0,100,200,300),labels = c("10:00", "11:40",
"13:20","15:00")) +
  theme(panel.grid.major.y = element_line(color = "grey", size = 0.5,
linetype = 2),
        panel.grid.major.x = element_blank(),
        panel.background = element_blank(),
        axis.line = element_line(colour = "black"),
        axis.text.x = element_text(color = "grey20", size = 15, angle = 0),
        axis.text.y = element_text(color = "grey20", size = 15, angle = 0),
        axis.title.x = element_text(margin = margin(t=10), color = "black",
size = 18, angle = 0),
        axis.title.y = element_text(margin = margin(r=10), color = "black",
size = 18, angle = 90),
        legend.key = element_blank(),
        legend.position = c(.05, 1.02),
        legend.justification = c("left", "top"),
        legend.box.just = "left",
        legend.margin = margin(2, 2, 2, 2),
        legend.key.size = unit(5, 'line'),
        legend.key.height = unit(1, 'cm'),
        legend.key.width = unit(1, 'cm'),
        legend.title = element_text(size=16),
        legend.text = element_text(size=14)) +
  guides(color = guide_legend(override.aes = list(size=1.5)))
```

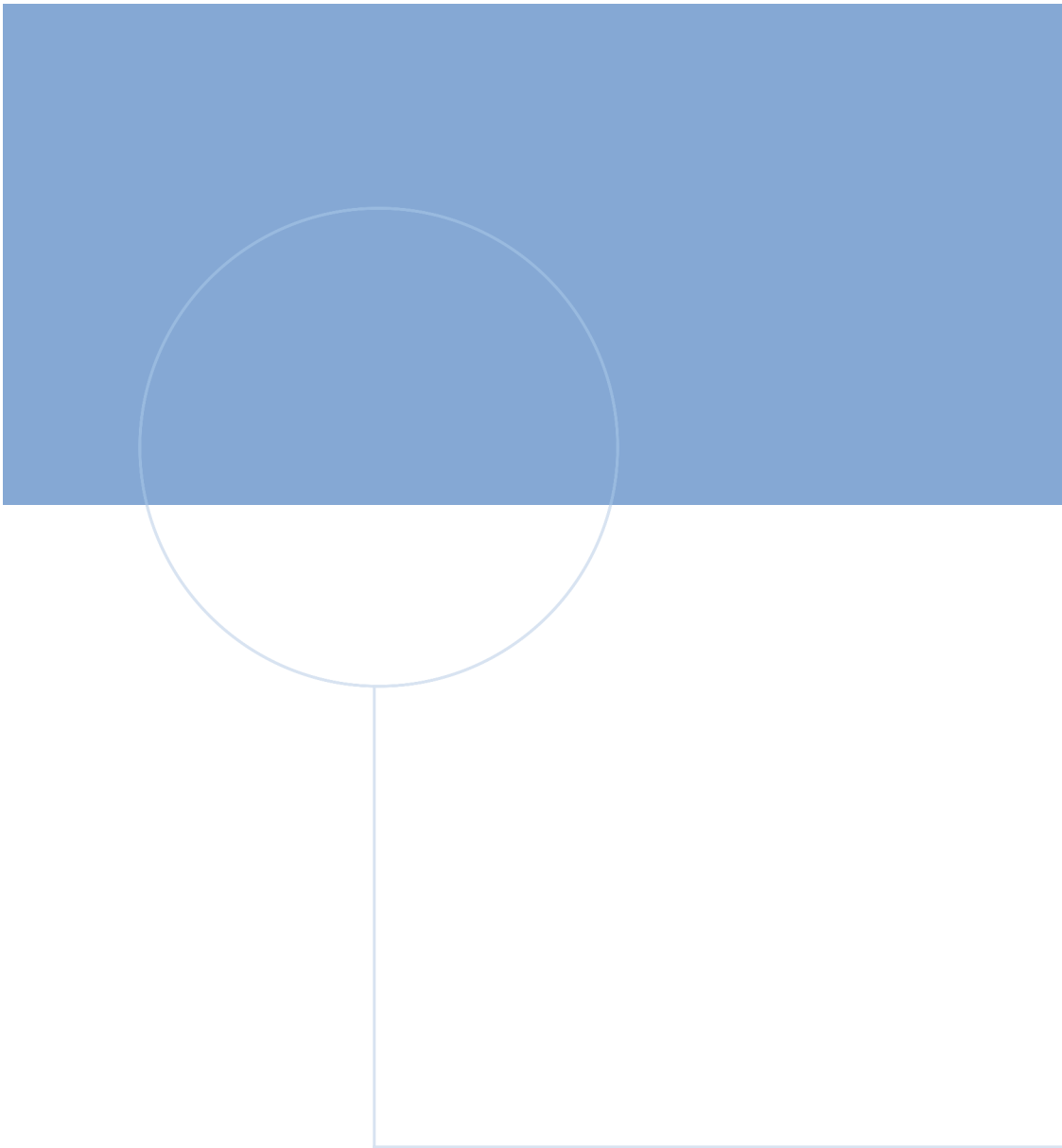

NTNU

Kunnskap for en bedre verden